Interacting populations: hosts and pathogens, prey and predators

by

Petra Klepac

Dipl. Ing. Biology - Ecology, University of Zagreb, Croatia

Submitted in partial fulfillment of the requirements for the degree of

Doctor of Philosophy

at the

MASSACHUSETTS INSTITUTE OF TECHNOLOGY

and the

WOODS HOLE OCEANOGRAPHIC INSTITUTION

June 2007

Author .....
Department of Biology
Massachusetts Institute of Technology
and Woods Hole Oceanographic Institution
March 22, 2007

Certified by .....
Michael G. Neubert
Associate Scientist, Woods Hole Oceanographic Institution
Thesis Supervisor

Accepted by .....
Edward DeLong
Chair, Joint Committee for Biological Oceanography
Massachusetts Institute of Technology
and Woods Hole Oceanographic Institution

Interacting populations:
hosts and pathogens, prey and predators

by

Petra Klepac

Submitted to the Department of Biology
in partial fulfillment of the requirements for the degree of

Doctor of Philosophy in Biological Oceanography

Abstract

The interactions between populations can be positive, neutral or negative. Predation and parasitism are both relationships where one species benefits from the interaction at the expense of the other. Predators kill their prey instantly and use it only for food, whereas parasites use their hosts both as their habitat and their food. I am particularly interested in microbial parasites (including bacteria, fungi, viri, and some protozoans) since they cause many infectious diseases.

This thesis considers two different points in the population-interaction spectrum and focuses on modeling host-pathogen and predator-prey interactions. The first part focuses on epidemiology, *i. e.*, the dynamics of infectious diseases, and the estimation of parameters using the epidemiological data from two different diseases, phocine distemper virus that affects harbor seals in Europe, and the outbreak of HIV/AIDS in Cuba. The second part analyzes the stability of the predator-prey populations that are spatially organized into discrete units or patches. Patches are connected by dispersing individuals that may, or may not differ in the duration of their trip. This travel time is incorporated via a dispersal delay in the interpatch migration term, and has a stabilizing effect on predator-prey dynamics.

Thesis supervisor: Michael G. Neubert

Title: Associate Scientist, Woods Hole Oceanographic Institution

Acknowledgments

I was very fortunate to have a mentor, Michael G. Neubert, who is both an excellent scientist and a wonderful person. I am very grateful for everything he has taught me, for all the invaluable advice and guidance, for continual support and understanding, and for his endless patience. Hal Caswell has been much more than just a committee member, and due to his willingness to give me advice, feedback, and encouragement, and I've come to consider him as my second advisor. I also wish to thank other members of my committee: Ottar Bjørnstad, Glenn Flierl, Karin Harding, and Andy Solow.

Many thanks to Ottar and the rest of the group from the Center for Infectious Disease Dynamics for their incredible hospitality over my several visits there. I am very grateful to Karin Harding and Tero Härkönen for their hospitality during my two-month visit to Göteborg University, and for making the data on phocine distemper virus readily available to me. I also want to thank many other people involved in the Seal Project that have collected the data used in this thesis.

The Academic Programs Office, especially Marsha Gomes and Julia Westwater, have been extremely helpful since my first day at WHOI, and I am grateful for all the problems they have solved and for their friendship.

I thank the past and present members of the math ecology lab – Christine Hunter, Masami Fujiwara, Stéphanie Jenouvrier, Tin Klanjšček, Richard Lawler, Amanda McDonald, Lori Thomas, and our adopted member Carly Strasser – on their helpful discussions, support, perspective, and many friendly moments. I am also greatly indebted to my collaborators Pauline van den Driessche, Tero Härkönen, Brandy Rapatski, Leda Ivić Weiss, Laura Pomeroy and Jolianne Rijks for making my scientific pursuits more fruitful, and for always being selfless in sharing their data and knowledge.

Slaven Smojver, Ana Širović and Vlatka Nimac have been my closest friends for over half of my lifetime, regardless of the continents we're scattered on. They have helped me grow as a person, and kept me somewhat sane over the years. My friends here, Diane Adams, Claudia Martins, Anna Michel, Rachel Stanley, Jessica Warren, Clare Williams, have made this place feel more like home and I wish to thank them on all the joyful moments and laughs, for providing a fun balance to work.

And, at last, the biggest gratitude I express to my family: my mother, my father, all my grandparents, my sister Vanja, my brother-in-law Ivan (thanks for all the processing power!), and my niece Zara, who always manages to put a smile on my face. Thank you for being one constant in my life I can always count on, for being my rock through all of the stages of my life.

This work has been supported by the US National Science Foundation (DEB-0235692), the US Environmental Protection Agency (R-82908901), the Ocean Ventures Fund, and the Academic Programs Office.

Contents

List of Figures

List of Tables

Chapter 1

Introduction

1.1 Interactions between populations

Populations interact in different ways. Their interactions can be positive, neutral or negative. Predation and parasitism are both antagonistic relationships where one species benefits from the interaction at the expense of the other. Predators kill their prey instantly and use it only for food, whereas parasites use their hosts both as their habitat and their food. Some parasites, including bacteria, fungi, viri, and some protozoans, are microbial and replicate within the host (microparasites). Other pathogens, such as ticks, nematodes, and tapeworms, have no within host replication and are known as macroparasites. I am particularly interested in microparasites since they are pathogenic agents that cause many infectious diseases.

Most models for predator-prey relationships assume prey and predators have relatively equivalent sizes and life history characteristics. This approach is applicable to a variety of organisms, from rabbits and foxes, to various macroparasites. But, when the host is very large with relatively slow dynamics, and the pathogen is small and multiplies rapidly inside the host, the traditional predator-prey approach is not very useful. Here the dynamics of such host-pathogen interactions, typical for infectious diseases, is studied using a different mathematical approach. Given the fast dynamics of the pathogen, and the slow dynamics of the host, we assume that the host population is constant and we ask questions about the spread of the pathogen between infected and not-infected segments of the host population.

In this thesis, I focus on two extremes along this consumer resource sprectrum and contrast host-pathogen and predator-prey interactions.

The first part (Chapters 2 - 4) focuses on the host-pathogen end of the spectrum with Chapters 2 and 3 studying the Phocine Distemper Virus that affects harbor seals in Europe, and Chapters 4 focusing on the outbreak of HIV/AIDS in Cuba. The second part (Chapters 5 and 6) studies theoretical models for spatially-extended predator–prey populations.

In this introductory chapter I discuss the basic biology of Phocine Distemper Virus outbreaks, the pathology of the virus, the population biology of harbor seals, the available data set, and the motivation for the spatial predator–prey.

1.2 Epidemiology

An outbreak of a disease that spreads rapidly and infects a substantial portion of the population in a region over a short period of time is known as an epidemic. Major epidemics in the past include the bubonic plague ("Black Death") that spread from Asia throughout Europe in 14-th century. It is estimated that bubonic plague has killed to one third of Europeans between 1346 and 1350. Another example is smallpox, which was brought to North America by invading Spaniards and in some cases reduced indigenous population to one tenth of its preepidemic size — the Indian population of Mexico is thought to have been reduced from 30 million in 1519 to only 3 million in 1530. The "Spanish flu" H1N1 influenza epidemic of 1918-1919 caused 10-20 millions of deaths worldwide.

Major epidemics today include malaria, tuberculosis and HIV/AIDS, which combined kill over 6 million people each year. At the end of 2004, there were 40 million people infected with HIV, 5 million infected in 2004 alone (UNAIDS, 2004).

When an epidemic affects an animal population, it is called an epizootic. An example of a recent major epizootics is Phocine Distemper Virus that caused the death of up to 60% of harbor seals (*Phoca vitulina*) in certain locations in the North Sea in 1988 and 2002 (Reineking, 2002, 2003; Härkönen *et al.*, 2006). Other species within the morbilliviridae have been implicated in mass mortalities of bottlenose dolphins (*Tursiops truncatus*) along the U.S. Atlantic coast (1987-88) and Gulf of Mexico (1993-94), striped dolphins (*Stenella coeruleoalba*) in the Mediterranean Sea (1990-92) and common dolphins (*Delphinus delphis*) in the Black Sea (1994) (Osterhaus, 1988; Dietz *et al.*, 1989; Domingo *et al.*, 1990; Kennedy, 1998).

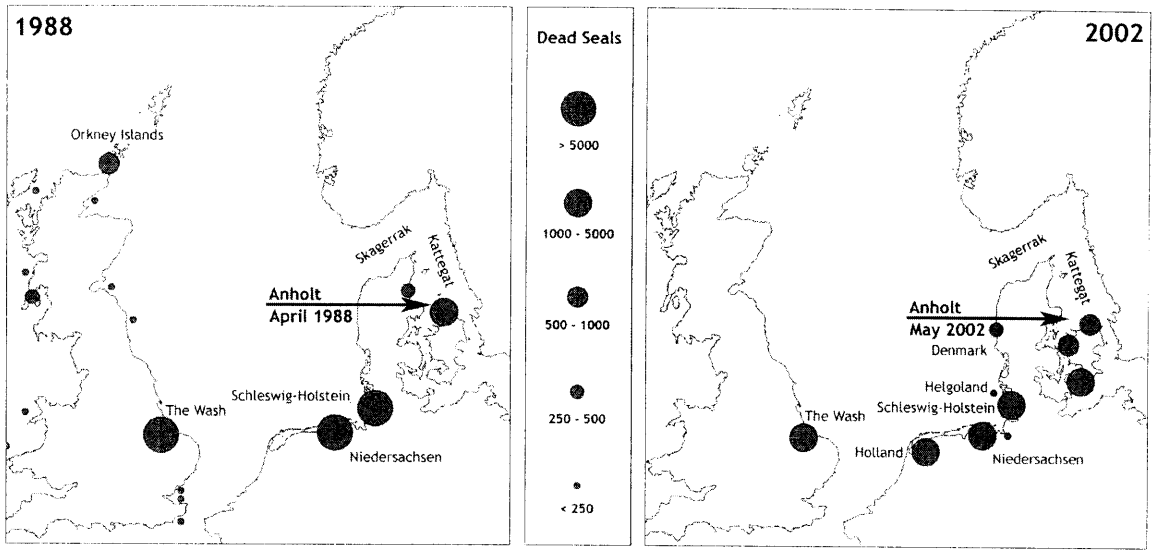

Figure 1-1: Maps of 1988 and 2002 PDV outbreaks in northern Europe. Circles indicate how many seals died in a particular region. After Markon *et al.* (2003).

1.2.1 Phocine distemper virus

Phocine distemper virus (PDV) was first described in 1988, when it killed over 23,000 harbor seals (*Phoca vitulina*) in northern Europe (Härkönen *et al.*, 2006). The 'seal plague' started at the Danish island of Anholt (see Figure 1-1) and the virus quickly spread to populations in Sweden, Netherlands, England, Scotland and Ireland (Dietz *et al.*, 1989). It resulted in the largest recorded epizootic of any marine mammal population with an estimated mortality of $56-58\%$ in large regions (Dietz *et al.*, 1989; Heide-Jørgensen & Härkönen, 1992; Härkönen *et al.*, 2002; Harding *et al.*, 2002).

PDV caused another outbreak in 2002 (see Figure 1-1), killing 33,000 harbor seals in Baltic, Wadden and North Seas between May and October (Reineking, 2002; Härkönen *et al.*, 2006). Both epizootics originated at the same location, the island of Anholt, but it appeared 23 days later in 2002. The population size on the European continent in 2002 was about twice that of 1988, where in the UK it was at comparable levels both years. On the percent basis, the two outbreaks had comparable mortality.

1.2.2 Population biology of harbor seals

The dynamics of an infectious disease is determined by the size and structure of the host population, its life history, and the behavior of individuals. All of these factors affect the transmission of the virus, and influence the dynamics of the disease.

Figure 1-2: Harbor seal, *Phoca vitulina*. http://www.wildlife.shetland.co.uk/.

Table 1.1: Harbor seal population sizes before and after the 1988 and 2002 epizootics in Europe.

Location	Pre-1988	Post-1988	Pre-2002	Post-2002
Kattegat-Skagerrak	12,700	5,600	23,000	11,750
Wadden Sea	16,840	7,000	35,660	18,980
European continent	36,800	18,770	62,070	33,490
UK	53,000	48,000	53,000	50,000
Grand total	82,000	59,500	116,000	82,800

Population size

There are five recognized subspecies of harbor seal distributed widely over the northern hemisphere. Current estimates of population sizes are imperfect and often outdated, so it is hard to say how many harbor seals there are in the region. In the eastern Atlantic region there were about $80,000$ before the 1988 epizootic, of which $36,800$ were estimated to be on the European continent (Härkönen *et al.*, 2006). Areas of greatest abundances were Great Britain ($53,000$), the Wadden Sea ($16,840$) and Kattegat-Skagerrak ($12,700$) (Härkönen *et al.*, 2006). After the PDV outbreak, European harbor seal population dropped to an estimated $59,500$ (see Table 1.1 for more details). During the next 14 years the population recovered, and reached a size double that of pre-1988 epizootic on the continent ($62,000$ in 2002), and comparable levels to the pre-1988 epizootic in the UK (see Table 1.1). The estimated total population size in 2002 was $116,000$ seals (which was reduced to about $83,000$ after the second PDV outbreak).

Demography

Common seals have a yearly pupping season that runs from late May to early August, and peaks in late June/early July in Europe. Females mature at 3 to 4 years; males mature a year later. Mothers suckle their pups during a 4-week nursing period, after which the pups undergo a post-weaning fast lasting $3-6$ weeks, when they start to catch their own food. After the pups are weaned, seals mate in water. Fertilization is followed by embryonic diapause (prolonged period of delayed implantation) that lasts about 2.5 months. The total gestation period is around 10.5 months. Pregnancy rates exceed 85% (Burns, 2002) and $80-97\%$ of the mature females bear a pup each year (Härkönen & Heide-Jørgensen, 1990). The single pup per female per year poses a major constraint on population growth. Heide-Jørgensen *et al.* (1992a) constructed a matrix population model and calculated that in the stable age distribution the asymptotic growth rate λ was 1.112. Annual survivorship of adult harbor seals in the absence of PDV is around 90% for males (data for females suggest 95% survival) (Härkönen & Heide-Jørgensen, 1990).

Dispersal

For determining epidemic behavior, besides knowing the total population size, it is also important to know the population structure, mixing of individuals, as well as the mixing of subpopulations. Telemetry studies (Thompson & Harwood, 1990) and long-term study of freeze-branded animals (Härkönen & Harding, 2001) suggest a high degree of site fidelity among adult harbor seals. None of 163 branded seals were observed to haul out beyond a 32-km radius from the site where they were branded as pups, (Härkönen & Harding, 2001). On the smaller scale, there is a strong spatial segregation by age and sex, as well as different migration tendencies between sexes and ages. A genetic study of micro-satellite polymorphism (Goodman, 1998) suggests six distinct population units: Ireland-Scotland, English east coast, Wadden Sea, Western Scandinavia, East Baltic and Iceland.

Haul-out behavior

Seals give birth, rear their offspring and molt on land. That introduces seasonality to the seal haul-out behavior, which peaks during the pupping and molting seasons in late spring and summer. The molt occurs during midsummer to early fall, after

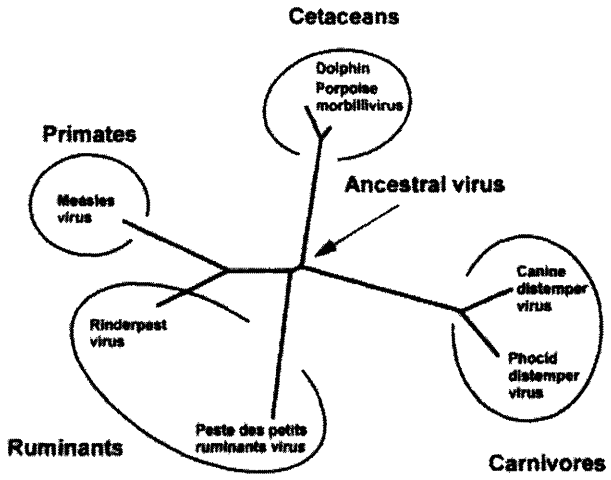

Figure 1-3: Phylogenetic tree showing the relationships between the different morbilliviri based on partial sequence of one of the protein coding genes (the P gene). The branch lengths are proportional to the mutational differences between the viruses and the hypothetical common ancestor that existed at the nodes in the tree. Source: Barrett (1999).

cessation of the breeding season. At that time up to 57% of a colony can be found on land (Heide-Jørgensen & Härkönen, 1992). There are differences in haul-out timing among age and sex cohorts. Yearlings usually molt earliest, followed by subadults, then adult females and adult males molt last (Burns, 2002). Therefore, the number of animals on land depends on age, sex, and the time of year (Thompson, 1989; Härkönen *et al.*, 1999, 2002). Seals also haul out throughout the year but less frequently and in smaller numbers than in the summer.

1.2.3 Phocine distemper pathology

The agent responsible for mass die-offs of seals, phocine distemper virus (Cosby *et al.*, 1988; Mahy *et al.*, 1988; Osterhaus *et al.*, 1989), belongs to the Morbilliviridae genus (see Figure 1-3); a group of RNA viruses that cause infectious diseases in mammals (Barrett *et al.*, 1993; Forsyth *et al.*, 1998; Barrett, 1999) and measles in humans (Barrett, 1987). PDV is most closely related to the canine distemper virus (CDV) (Osterhaus *et al.*, 1988; Kennedy *et al.*, 1988; Rima *et al.*, 1992) that can cause similar infections in other seal species (Grachev *et al.*, 1989; Kennedy *et al.*, 2000). PDV is thought to be endemic in arctic harp seals (*Phoca groenlandica*) (Markussen & Have, 1992). In 1987 and 1988 harp seals were observed to migrate as far south as Danish waters, and are thought to have spread the virus to the previously unexposed harbor seal population (Goodhart, 1988).

The disease transmits between animals in close contact in the same way a cold spreads in humans - by inhalation when an infected individual coughs or sneezes

(Kennedy, 1990, 1998). Once in the host, the virus spreads through macrophages, lymphocytes and thrombocytes and infects various tissues. Since the virus is spread in air, an infected animal can only spread the disease to its neighbors during haul outs.

Symptoms of the PDV infection in seals include fever, respiratory problems such as coughing, nasal discharge, as well as discharge from the eyes, conjunctivitis. Infected pregnant females abort their pups, and elevated numbers of aborted pups in a certain area can be an indicator of the presence of PDV. A pup that is orphaned or abandoned before weaning will die. If the virus enters the central nervous system, infected seals become disoriented and will be disinclined to move which can cause them to spend more time on land, and less time in water searching for food. Postmortem findings include subcutaneous emphysema (air bubbles under the skin) of the head and neck (Bergman *et al.*, 1990; Munro *et al.*, 1992; Baker, 1992) due to which dead animals float for a long time before being washed up on land. The disease is confirmed by blood testing diseased animals or tissue sampling dead animals (Barrett, 1999). Morbilliviri are known to suppress their host's immune system, thus increasing the risk of secondary infection by a wide range of agents. Autopsies of dead seals have shown that the main proximate cause of death is a secondary infection, bacterial pneumonia caused by *Bordetella bronchiseptica* (Baker & Ross, 1992; Kennedy, 1998).

In 1988 the disease quickly spread from central Kattegat (see Figure 2-7), where it appeared in April, to Danish and Dutch Wadden Sea (May), and then to Skagerrak and German Wadden Sea (June). By mid July seal herds in the Oslo Fjord and the Baltic were affected. British haul-outs were the last to be hit by disease in August and September (Dietz *et al.*, 1989). The estimated rate of spread was $3,970$ km/year (McCallum *et al.*, 2003). In each location the epidemic lasted 70-100 days; longer when haul-outs were less discrete as in the Wadden Sea (Dietz *et al.*, 1989).

1.2.4 Data on haul-out behavior

Harbor seals have been studied at their haul-out sites for decades. During 1978-1998 aerial surveys were conducted for Swedish and Danish haul-out locations, which were photographed in the peak haul-out season and seals were later counted from photographs (Heide-Jørgensen *et al.*, 1992b; Härkönen *et al.*, 1999, 2002). The sex-related and age-specific seasonal behavior of seals has been inferred by studying 163 freeze-branded animals during 1985-1997 (Härkönen *et al.*, 1999) and 8 VHF-tagged

seals during 1984-1986 (Thompson, 1989).

1.2.5 Epizootic data

Major haul-out locations in the Kattegat-Skagerrak were regularly surveyed for seal carcasses by biologists and other trained personnel during both epizootic periods (Härkönen & Heide-Jørgensen, 1990). In the UK, most of the dead seals were reported by the general public via a "hotline" number (http://www.defra.gov.uk/). The number of reported stranded seals are treated as the 'number of dead seals per day' which form the epizootic curves (cumulative numbers of dead seals). By comparing the number of seals found dead to numbers of seals in population surveys before and after the epizootic we can estimate the mortality in each location (Dietz *et al.*, 1989; Reineking, 2002). For most locations the day that first dead seal appeared is also known.

This data-set is vulnerable to several sources of observational error. The number of stranded carcasses depends on wind directions and reporting effort. Carcasses may float for a while before finally getting washed ashore, so the seals may be lost or washed up on shores far away from their actual territory and dead seals might be reported several times (Thompson & Miller, 1992).

The epidemic curves are the only epidemic data available for PDV outbreaks, and they form a link between the data and the models.

1.2.6 PDV modeling

Chapter 2 presents a model for PDV outbreaks, that includes the information on the life history of seals, and the transmission of the virus. Using the model, I develop a way to estimate epidemiological parameters based on the available epizootic data. Seasonal haul-out behavior influences the mixing between seals and the transmission of the virus. The process of transmission in Chapter 3 incorporates the haul-out behavior, and I use this model to investigate differences in mortality between locations.

1.3 Prey–predator interactions

The most basic models (Lotka, 1926; Volterra, 1931; Nicholson & Bailey, 1935) and experiments (Gause, 1934) predict instability of predator–prey systems. How do then

predator–prey systems persist stably in nature? The answer most often given is that the models and experiments omit processes that affect stability in natural systems (for examples see May, 1973; Hassell, 1978; Crawley, 1992; Mueller & Joshi, 2000).

Natural systems are spatially structured. Populations are often organized into discrete spatial units or patches that are connected by dispersal (metapopulation structure). In the traditional approach, dispersal is assumed to occur instantaneously, leaving the dynamics of the model often unchanged. In reality, individuals spend a finite amount of time in transit from one patch to another. This travel time can be incorporated in predator–prey models via a delay in the inter-patch dispersal term.

What are the effects of dispersal delays on the dynamics of the predator–prey models? To find out, I developed predator–prey models that include dispersal delays. These models have the form of a system of delayed differential equations. I study the dynamics of these systems analytically and numerically.

To determine whether the dispersal delays have a stabilizing effect on the predator–prey equilibrium point, I incorporated dispersal delays into the Lotka–Volterra model. The equilibrium point of the non-spatial predator–prey Lotka–Volterra model is a center, *i. e.*, a "neutrally stable" equilibrium surrounded by a family of periodic solutions whose amplitudes depend on the initial conditions. The slightest change to the model's structure typically results in qualitatively different behavior. For example, if the growth rate of prey decreases linearly with prey density the equilibrium point is stable; on the other hand, introducing a saturating (Type II) functional response turns the equilibrium into an unstable spiral point (Gotelli, 1995). In Chapter 5, I use this structural instability of the Lotka–Volterra model to show that dispersal delays stabilize the equilibrium point of the spatially structured Lotka–Volterra model.

However, the the Lotka–Volterra model is considered oversimplified for two reasons. First, in the absence of the predators, the prey grow exponentially without bound. Second, the per capita rate of consumption of prey by predators grows in proportion to the prey population size, implying that individual predators can process prey items infinitely fast. These faults are eliminated in the Rosenzweig–MacArthur model, which includes a carrying capacity for the prey and a finite prey handling time for the predators that results in a saturating functional response.

The Rosenzweig–MacArthur model has a more complicated dynamics than the Lotka–Volterra model. For small values of carrying capacity, the coexistence equilibrium point is locally asymptotically stable. As the carrying capacity increases beyond

some threshold value, a Hopf bifurcation occurs, the equilibrium point becomes unstable, and trajectories are drawn onto a single stable limit cycle. This destabilization by increasing prey carrying capacity is known as the 'paradox of enrichment' (Rosenzweig, 1971; May, 1972; Gilpin, 1972).

Dispersal delays are strong enough to overcome the destabilizing effect of the Type II response and can stabilize the coexistence equilibrium of the Rosenzweig–MacArthur model. For many parameter values, stability persists even in the limit of infinite carrying capacity. Dispersal delays also help resolve the paradox of enrichment by reducing the amplitude of oscillations when the equilibrium is unstable.

References

Baker, J. R. 1992. The pathology of phocine distemper. *Sci. Tot. Environ.*, **115**, 1–7.

Baker, J. R., & Ross, H. M. 1992. The role of bacteria in phocine distemper. *Sci. Tot. Environ.*, **115**, 9–14.

Barrett, T. 1987. The molecular biology of the morbillivirus (measles) group. *Biochem Soc Symp*, **53**, 25–37.

Barrett, T. 1999. Morbillivirus infections, with special emphasis on mobilliviruses of carnivores. *Veterinary Microbiology*, **69**, 3–13.

Barrett, T., Visser, I. K. G., Mamaev, L., Goatley, L., van Bressem, M.-F., & Osterhaus, A. D. M. E. 1993. Dolphin and porpoise morbilliviruses are genetically distinct from phocine distemper virus. *Virology*, **193**, 1010–1012.

Bergman, A., Järplid, B., & Svensson, B.M. 1990. Pathological findings indicative of distemper in European seals. *Vet. Microbiol.*, **23**, 331–341.

Burns, J. J. 2002. *Ecyclopedia of Marine Mammals.* Academic Press. Chap. Harbor seal and spotted seal, pages 552–560.

Cosby, S. L., McQuaid, S., Duffy, N., Lyons, C., Rima, B.K., Allan, G.M., McCullough, S. J., & Kennedy, S. 1988. Characterization of a seal morbillivirus. *Nature*, **336**, 115–116.

Crawley, M. J. 1992. *Natural Enemies: The Population Biology of Predators, Parasites and Diseases.* London: Blackwell Scientific.

Dietz, R., Heide-Jørgensen, M.P., & Härkönen, T. 1989. Mass deaths of harbour seals (*Phoca vitulina*) in Europe. *Ambio*, **18**, 258–264.

Domingo, M., Ferrer, L., Pumarola, M., Marco, A., Plana, J., Kennedy, S., & McAliskey, M. 1990. Morbillivirus in dolphins. *Nature*, **348**, 21.

Forsyth, M. A., Kennedy, S., Wilson, S., Eybatov, T., & Barrett, T. 1998. Canine distemper virus in a Caspian seal. *Vet Rec.*, **143**, 662–4.

Gause, G. F. 1934. *The Struggle fo Existence.* Williams and Wilkins, Baltimore.

Gilpin, M. E. 1972. Enriched predator–prey systems: Theoretical stability. *Science*, **177**, 902–904.

Goodhart, C. B. 1988. Did virus transfer from harp seals to common seals? *Nature*, **336**, 21.

Goodman, S. J. 1998. Patterns of extensive genetic differentiation and variation among European harbour seals (*Phoca vitulina vitulina*) revealed using microsatellite DNA polymorphisms. *Mol. Biol. Evol.*, **15**, 104–118.

Gotelli, N. J. 1995. *A Primer of Ecology.* Sunderland: Sinauer Associates, Inc.

Grachev, M. A., Kumarev, V. P., Mamaev, L. V., Zorin, V. L., Baranova, L. V., Denikina, N. N., Belikov, S. I., Petrov, E. A., Kolesnik, V. S., Kolesnik, R. S., Dorofeev, V. M., Beim, A. M., Kudelin, V. N., Nagieva, F. G., & Sidorov, V. N. 1989. Distemper virus in Baikal seals. *Nature*, **338**, 209.

Harding, K. C., Härkönen, T., & Caswell, H. 2002. The 2002 European seal plague: epidemiology and population consequences. *Ecol. Letters*, **5**(6), 727–727.

Härkönen, T., & Harding, K. C. 2001. Spatial structure of harbour seal populations and the implications thereof. *Can. J. Zool.*, **79**, 2115–2127.

Härkönen, T., & Heide-Jørgensen, M. P. 1990. Comparative life histories of East Atlantic and other harbour seal populations. *Ophelia*, **32**, 211–235.

Härkönen, T., Harding, K. C., & Heide-Jørgensen, M. P. 2002. Rates of increase in age-structured populations: a lesson from the European harbour seals. *Can. J. Zool.*, **80**, 1498–1510.

Härkönen, T., Dietz, R., Reijnders, P., Teilmann, J., Harding, K., Hall, A., Brasseur, S., Siebert, U., Goodman, S.J., Jepson, P.D., Rasmussen, T.D., & Thompson, P. 2006. A review of the 1988 and 2002 phocine distemper virus epidemics in European harbour seals. *Dis. Aquat. Org.*, **68**, 115–130.

Härkönen, Tero, Harding, Karin C., & Lunneryd, Sven Gunnar. 1999. Age- and sex-specific behaviour in harbour seals *Phoca vitulina* leads to biased estimates of vital population parameters. *J. Appl. Ecology*, **36**(5), 825–825.

Hassell, M. P. 1978. *The Dynamics of Arthropod Predator–Prey Systems.* Princeton, NJ: Princeton University Press.

Heide-Jørgensen, M. P., & Härkönen, T. 1992. Epizootiology of the seal disease in the eastern North Sea. *Journal of Applied Ecology*, **29**, 99–107.

Heide-Jørgensen, M. P., Härkönen, T., & Åberg, P. 1992a. Long-term effects of epizootic in harbor seals in the Kattegat-Skagerrak and adjacent areas. *Ambio*, **21**, 511–516.

Heide-Jørgensen, M. P., Härkönen, T., Dietz, R., & Thompson, P. M. 1992b. Retrospective of the 1988 European seal epizootic. *Diseases of Aquatic Animals*, **13**, 37–62.

Kennedy, S. 1990. A review of the 1988 European seal morbillivirus epizootic. *Vet. Rec.*, **127**, 563–567.

Kennedy, S. 1998. Morbillivirus infections in aquatic mammals. *J. Comp. Path.*, **119**, 210–205.

Kennedy, S., Smyth, J.A., McCullough, S.J., Allan, G.M., McNeilly, F., & McQuaid, S. 1988. Confirmation of cause of recent seal deaths. *Nature*, **335**, 404.

Kennedy, S., Kuiken, T., Jepson, P.D., Deaville, R., Forsyth, M., Barrett, T., van de Bildt, M.W.G., Osterhaus, A.D.M.E., Eybatov, T., Duck, C., Kydyrmanov, A., Mitrofanov, I., & Wilson, S. 2000. Mass die-off of Caspian seals caused by canine distemper virus. *Emerg. Infect. Dis.*, **6**, 637–639.

Lotka, A. J. 1926. *Elements of Physical Biology.* Williams and Wilkins, Baltimore.

Mahy, B. W. J., Barret, T., Evans, S., Anderson, E. C., & Bostock, C. J. 1988. Characterization of a seal morbillivirus. *Nature*, **336**, 115.

Markon, K., Linsbichler, B., Strele, C., Hois, A., Rubel, F., & Windischbauer, G. 2003. *Computersimulation der Seehundstaupeepidemien 1988 und 2002.* Poster.

Markussen, Nina Hedlund, & Have, Per. 1992. Phocine distemper virus infection in harp seals (*Phoca groenlandica*). *Marine Mammal Science*, **8**(1), 19–26.

May, R. M. 1972. Limit cycles in predator–prey communities. *Science*, **177**, 900–902.

May, R. M. 1973. *Stability and Complexity in Model Ecosystems.* Princeton, NJ: Princeton University Press.

McCallum, H., Harvell, D., & Dobson, A. 2003. Rates of spread of marine pathogens. *Ecol. Letters*, **6**, 1062–1067.

Mueller, L. D., & Joshi, A. 2000. *Stability in Model Populations.* Princeton, NJ: Princeton University Press.

Munro, R., Ross, H. M., Cornwell, H. J. C., & Gilmour, J. 1992. Disease conditions affecting common seals (*Phoca vitulina*) around the Scottish mainland, September-November 1988. *Sci. Tot. Environ.*, **115**, 67–82.

Nicholson, A. J., & Bailey, V. A. 1935. The balance of animal populations. *Proceedins of the Zoological Society of London*, **1**, 551–598.

Osterhaus, A. D. M. E. 1988. Seal death. *Nature*, **334**, 301–302.

Osterhaus, A. D. M. E., Groen, J., De Vries, P., & UytdeHaag, F. G. C. M. 1988. Canine distemper virus in seals. *Nature*, **335**, 403–404.

Osterhaus, A. D. M. E., UytdeHaag, F. G. C. M., Visser, I. K. G., Vedder, E. J., Reijnders, P. J. H., Kuiper, J., & Brugge, H. N. 1989. Seal vaccination success. *Nature*, **337**, 21.

Reineking, B. 2002. Seal Distemper Epidemic amongst Seals in 2002. *Wadden Sea Newsletter*, **2**.

Reineking, B. 2003. Phocine Distemper Epidemic Amongst Seals in 2002. *In: Management of North Sea Harbour and Grey Seal Populations. Proceedings of the International Symposium at EcoMare, Texel, The Netherlands, November 29 - 30, 2002. Wadden Sea Ecosystem No. 17.* Common Wadden Sea Secretariat, Wilhelmshaven, Germany.

Rima, B. K., Curran, M. D., & Kennedy, S. 1992. Phocine distemper virus, the agent responsible for the 1988 mass mortality of seals. *Sci. Tot. Environ.*, **115**, 45–55.

Rosenzweig, M. L. 1971. Paradox of enrichment: destabilization of exploitation ecosystems in ecological time. *Science*, **171**, 285–387.

Thompson, P. M. 1989. Seasonal changes in distribution and composition of common seal (*Phoca vitulina*) haul-out groups. *J. of Zoology*, **217**, 281–294.

Thompson, P. M., & Harwood, J. 1990. Methods for estimating the population size of common seals (*Phoca vitulina*). *J. Appl. Ecol.*, **27**, 924–938.

Thompson, P. M., & Miller, D. 1992. Phocine distemper virus outbreak in the Moray Firth common seal population: an estimate of mortality. *Sci. Tot. Environ.*, **115**, 57–65.

UNAIDS. 2004 (December). *UNAIDS/WHO AIDS epidemic update.* Available online at http://www.unaids.org/wad2004/report.html.

Volterra, V. 1931. *Leçons sur la Théorie Mathématique de la Lutte Pour la Vie.* Gauthier-Villars, Paris.

Chapter 2

Estimation of the basic reproductive number, $\mathcal{R}_0$

2.1 Introduction

Phocine distemper virus (PDV) caused mass die-offs of European harbor seals (*Phoca vitulina*) in 1988 and 2002 (Osterhaus *et al.*, 1988; Mahy *et al.*, 1988; Cosby *et al.*, 1988; Rima *et al.*, 1992). Both outbreaks started at the Danish island of Anholt in the spring, and in the following months spread throughout the entire European harbor seal population, killing more than 23,000 seals in 1988 and 30,000 in 2002 (Härkönen *et al.*, 2006). These are the largest epizootics ever reported for any marine mammal population with estimated mortality of 56 - 58% in large regions (Dietz *et al.*, 1989; Heide-Jørgensen & Härkönen, 1992; Härkönen *et al.*, 2002; Harding *et al.*, 2002).

It is likely that PDV will revisit the harbor seals of Europe. How many seals will eventually become infected? How fast will the epidemic spread? How long will it last? What measures should be taken to control or prevent the outbreak? These quantities are related to the epidemiological parameter known as the *basic reproductive number*, $\mathcal{R}_0$.

$\mathcal{R}_0$ is defined as the expected number of new infections caused by a single infected individual in an entirely susceptible population (Dietz, 1975). As a result, $\mathcal{R}_0$ provides a threshold for whether or not an epidemic will occur. If $\mathcal{R}_0 > 1$, the number of infections increases, leading to an epidemic; if $\mathcal{R}_0 < 1$, the infection dies out (no epidemic). $\mathcal{R}_0$ also determines the duration of a closed epidemic (Anderson, 1996) as well as its final size (Kermack & McKendrick, 1927; Heesterbeek & Roberts,

1995; Anderson, 1996). The quantity $\mathcal{R}_0$ also has applications in developing control strategies. In order to prevent or contain an epidemic, the proportion of individuals that needs to be removed from the susceptible pool, either by vaccination or by culling, is $1 - 1/\mathcal{R}_0$ (Anderson, 1996).

The concept of a critical threshold arose from the analysis of mathematical models for vector borne diseases (Ross, 1911), and directly transmitted diseases (Kermack & McKendrick, 1927) at the beginning of the last century. But, it was not until the 1980s that the potential of use of $\mathcal{R}_0$ in epidemiology and in the control of infections diseases was fully recognized (Dietz, 1975; Diekmann *et al.*, 1990; Anderson, 1996; Dietz, 1993; Heesterbeek, 2002). This is surprising, as the analogous concept known as the "net reproductive rate" (denoted by $\mathcal{R}_0$ by Dublin & Lotka (1925)) was fully developed for the study of demography and ecology about fifty years before its widespread application in epidemiology (Sharpe & Lotka, 1911; Dublin & Lotka, 1925). In population biology, $\mathcal{R}_0$ is defined as the expected number of offspring that an individual will produce during its lifetime, or the population growth rate from one generation to the next (Caswell, 2001).

In this chapter, I focus on $\mathcal{R}_0$ in two ways; (i) given a model, how does one calculate $\mathcal{R}_0$, and (ii) given data, can $\mathcal{R}_0$ be estimated directly, or how does one estimate individual parameters in the model to determine $\mathcal{R}_0$. In order to estimate $\mathcal{R}_0$ for a particular disease, one needs some form of data on the number of cases that suffer infection from this disease. Epidemic data from naturally occurring wildlife diseases is often lacking in detail and estimating epidemic parameters is challenging. In the case of the 1988 and 2002 phocine distemper virus outbreaks, only the number of stranded seal carcasses were observed. Extensive efforts were made during both the 1988 and 2002 epizootics to count the seals that died. Time series of stranded carcasses collected by teams of biologists and other trained personnel in each region were used to construct cumulative curves (also called epidemic or epizootic curves). These curves form a link between the data and the models. These epizootic curves, and a review of both PDV outbreaks can be found in Härkönen *et al.* (2006).

In the next section I present a short review of different calculations of $\mathcal{R}_0$, and of common ways to estimate $\mathcal{R}_0$ from data. Based on a model for PDV dynamics, I develop a new likelihood-based method for estimating $\mathcal{R}_0$ from epidemic curves. I will use simulation results to evaluate accuracy, precision, and the bias of the method. Using this method, I estimate $\mathcal{R}_0$ values for different regions, and show that regional

differences in $\mathcal{R}_0$ are significant. Further, I investigate the relationship of $\mathcal{R}_0$ with variables that most commonly influence it, such as population size, spatial structure, timing of infection, and the level of immunity.

2.2 Calculation of $\mathcal{R}_0$

Consider a simple deterministic model where a population of size N is divided into three epidemic compartments: susceptible individuals S, infective individuals I (*i. e.*, individuals that are infectious), and a removed class R that consists of individuals that were infected but are no longer infectious or susceptible to reinfection. Such models are often called SIR models. Contacts between individuals are assumed to be made at random. The disease spreads when an infectious individual contacts and infects a susceptible. The force of infection λ, defined as the probability per unit time for a susceptible to become infected (Diekmann & Heesterbeek, 2000), is a product of three parameters: (i) the contact rate $c(N)$, (ii) the probability that the contact is with an infective, usually assumed to be I/N, and (iii) the probability p that the contact between susceptible and infective individuals in fact leads to transmission of the pathogen, *i. e.*, the probability that the contact is 'successful',

$$\lambda = \frac{c(N)Ip}{N} \tag{2.1}$$

The per contact probability of successful transmission p is usually assumed to be constant.

If the rate of contacts for a given susceptible individual is proportional to the population size N, $c(N) = c_1 N$, the force of infection is proportional to the number of infectives I

$$\lambda = c_1 pI = \beta I. \tag{2.2}$$

The proportionality constant, β, is called the transmission rate; it consists of both the contact rate and the probability that the contact is successful. The rate at which new infections occur is assumed proportional to the number of susceptibles S, and is given by the product $\lambda S = \beta SI$.

If individuals recover from infection and become immune at a rate γ, we obtain

the standard SIR model

$$\frac{dS}{dt} = -\beta SI, \tag{2.3a}$$

$$\frac{dI}{dt} = \beta SI - \gamma I, \tag{2.3b}$$

$$\frac{dR}{dt} = \gamma I \tag{2.3c}$$

first studied by Kermack & McKendrick (1927). (A detailed analysis of this model can be found in, *e. g.*, Heesterbeek & Roberts (1995); Diekmann & Heesterbeek (2000) or Brauer & Castillo-Chávez (2001).)

Under model (2.3) a typical infective individual meets and infects βS susceptible individuals per unit time, and continues to do so during its expected infective period $1/\gamma$, so the total number of secondary infections that individual produces is $\beta S/\gamma$. If at the beginning of the epidemic there are N susceptible individuals, the basic reproductive number for model (2.3) is

$$\mathcal{R}_0 = \frac{\beta N}{\gamma}. \tag{2.4}$$

This type of transmission, where the rate of contacts for a given susceptible is proportional to the population size N, is known as *mass action* or *density-dependent* transmission (Begon *et al.*, 2002; Brauer, 2006).

When the number of contacts per infective per unit time is constant, $c(N) = c_2$, the process of transmission is known as *pseudo-mass-action* (*e. g.*in Swinton *et al.*, 1998), *standard incidence* (Brauer, 2006), or *frequency-dependent transmission* (Thrall & Antonovics, 1997; Begon *et al.*, 2002). This type of transmission is most commonly used in modeling sexually transmitted diseases. The force of infection for frequency-dependent transmission is

$$\lambda = \frac{c_2 pI}{N} = \frac{\beta I}{N}, \tag{2.5}$$

where β is, again, the transmission rate, but has different units than in equation (2.2). In this case, the basic reproductive number

$$\mathcal{R}_0 = \frac{\beta}{\gamma} \tag{2.6}$$

is independent of population size.

2.2.1 Survival function

A more general formulation of $\mathcal{R}_0$ follows directly from its definition. Let $l(a)$ be the probability that a newly infected individual remains infectious for at least time a, and let $m(a)$ be the rate of infectiousness by an individual that has been infectious for a units of time. The number of secondary infections is then given by

$$\mathcal{R}_0 = \int_0^\infty l(a)\, m(a) da. \tag{2.7}$$

An identical formulation is found in population biology, where $l(a)$ is survivorship, that is, the probability of surviving from birth to age a, and $m(a)$ is the rate of reproduction at age a (*e. g.* Heesterbeek & Roberts, 1995; Keeling & Grenfell, 2000; Caswell, 2001).

For model (2.3), the duration of infection is exponentially distributed with the mean $1/\gamma$, so $l(a) = \exp(-\gamma a)$. As the transmission rate, β, does not depend on how long individuals have been infectious, the rate of infection is the same for all infectious individuals. Overall rate of infection in (2.3) is βSI, or $m(a) = \beta S$ per infective individual, *i. e.*, βS_0 at the beginning of the infection. Substituting for $l(a)$ in $m(a)$ in equation (2.7) gives

$$\mathcal{R}_0 = \int_0^\infty e^{-\gamma a} \beta\, S_0\, da = \frac{\beta S_0}{\gamma} \tag{2.8}$$

This mathematically natural definition of $\mathcal{R}_0$ is not always useful for computations, especially when dealing with more complex models.

2.2.2 Next generation method

In many cases it is useful to distinguish between different classes of infectives. For example, in the model for the HIV/AIDS epidemic in Chapter 4, there are three infective compartments – undiagnosed HIV cases, diagnosed HIV cases, and AIDS cases. In other situations, multiple infective classes can be used to capture the underlying age structure or spatial structure. For this type of model, $\mathcal{R}_0$ can be derived using the next generation method (Diekmann *et al.*, 1990; de Jong *et al.*, 1994; Diekmann & Heesterbeek, 2000; van den Driessche & Watmough, 2002), where $\mathcal{R}_0$ is given by

the spectral radius, ρ, (dominant eigenvalue) of the next generation matrix, FV^{-1}:

$$\mathcal{R}_0 = \rho\left[FV^{-1}\right]. \tag{2.9}$$

There is an analogous expression in discrete time demographic models of the form $\mathbf{n}(t+1) = \mathbf{A}_{\mathbf{n}(t)}\,\mathbf{n}(t)$. The vector $\mathbf{n}(t)$ describes the state of the population at time t, and let the projection matrix $\mathbf{A_n}$ consist of the transition matrix $\mathbf{T_n}$ and reproduction matrix $\mathbf{F_n}$, so that $\mathbf{A_n} = \mathbf{T_n} + \mathbf{F_n}$. Then

$$\mathcal{R}_0 = \rho\left[\mathbf{F_n}(\mathbf{I} - \mathbf{T_n})^{-1}\right]. \tag{2.10}$$

To find the next generation matrix FV^{-1}, first assume there are n compartments of which m are infective. Let $x = x_1, \ldots, x_n$ be the number of individuals in each compartment. Let $\mathcal{F}_i(x)$ be the rate at which newly infected individuals enter compartment i, $\mathcal{V}_i^+(x)$ be the rate of transfer of individuals into compartment i by all other means (including the transfer of infectious individuals from one infective compartment to another), and $\mathcal{V}_i^-(x)$ be the rate at which individuals are leaving compartment i. Define $\mathcal{V}_i(x)$ as $\mathcal{V}_i(x) = \mathcal{V}_i^-(x) - \mathcal{V}_i^+(x)$. The rate of change of compartment i is then $\dot{x}_i = \mathcal{F}_i - \mathcal{V}_i(x)$. We can then form the next generation matrix FV^{-1} by

$$F = \left[\frac{\partial \mathcal{F}_i}{\partial x_j}(x_0)\right] \quad \text{and} \quad V = \left[\frac{\partial \mathcal{V}_i}{\partial x_j}(x_0)\right], \tag{2.11}$$

where $i, j = 1, \ldots, m$ and x_0 is the disease free equilibrium, at which the population remains in the absence of the disease. (A detailed description of assumptions, constraints and proofs of theorems can be found in van den Driessche & Watmough (2002)). The (j,k) entry of V^{-1} is the average amount of time an infective individual that was introduced into compartment k spends in compartment j during its lifetime. The (i,j) entry of F is the rate at which infected individuals in compartment j produce new infections in compartment i. Therefore, the entry (i,k) in the generation matrix FV^{-1} is the expected number of new infections in compartment i produced by an individual originally introduced in compartment k.

To illustrate this approach, imagine a case where the early stage and late stage of infection have different transmission rates, β_1 and β_2. We can model this scenario by

a simple SIR model (or SIIR), with two infectious compartments I_1 and I_2:

$$\frac{dS}{dt} = -(\beta_1 I_1 + \beta_2 I_2)S, \tag{2.12a}$$

$$\frac{dI_1}{dt} = (\beta_1 I_1 + \beta_2 I_2)S - \gamma_1 I_1, \tag{2.12b}$$

$$\frac{dI_2}{dt} = \gamma_1 I_1 - \gamma_2 I_2, \tag{2.12c}$$

$$\frac{dR}{dt} = \gamma_2 I_2. \tag{2.12d}$$

All newly infected individuals enter the compartment I_1 so $\mathcal{F}_1 = (\beta_1 I_1 + \beta_2 I_2)S$, and $\mathcal{F}_2 = 0$. Other movements among the compartments are described by $\mathcal{V}_1 = \gamma_1 I_1$ and $\mathcal{V}_2 = \gamma_2 I_2 - \gamma_1 I_1$, giving

$$F = \begin{bmatrix} \beta_1 S_0 & \beta_2 S_0 \\ 0 & 0 \end{bmatrix} \quad \text{and} \quad V = \begin{bmatrix} \gamma_1 & 0 \\ -\gamma_1 & \gamma_2 \end{bmatrix} \tag{2.13}$$

$$FV^{-1} = \begin{bmatrix} \frac{\beta_1 S_0}{\gamma_1} + \frac{\beta_2 S_0}{\gamma_2} & \frac{\beta_2 S_0}{\gamma_2} \\ 0 & 0 \end{bmatrix} \tag{2.14}$$

and $\mathcal{R}_0 = S_0\left(\frac{\beta_1}{\gamma_1} + \frac{\beta_2}{\gamma_2}\right)$.

2.3 Estimation of $\mathcal{R}_0$ from data

Contact rates and transmission rates are often difficult to determine from observations. As a result, $\mathcal{R}_0$ is difficult to calculate using equations (2.7) or (2.9). In this section, I review some alternative approaches to estimating $\mathcal{R}_0$ from data. These approaches either assume an epidemic in a closed population where the infection leads to immunity or death, or an endemic equilibrium.

2.3.1 Final size equation

In the case of a closed epidemic, there is no influx of susceptible hosts. Unlike the endemic case, where a pathogen becomes established in a host population, in a closed epidemic the number of infections, after an initial increase, eventually drops to zero. The fraction of the individuals that eventually become infected during the epidemic, the *final size* of the epidemic, was first analytically determined by Kermack & McKendrick (1927). For model (2.3) we can calculate the final size by formally dividing

equation (2.3b) by equation (2.3a), and integrating the expression for dI/dS to find the orbits in the (S, I) plane

$$dI = \left(-1 + \frac{\gamma}{\beta S}\right) dS, \tag{2.15a}$$

$$I = -S + \frac{\gamma}{\beta} \ln S + c, \tag{2.15b}$$

where c is the arbitrary constant of the integration. In other words, orbits are defined by

$$V(S, I) = S + I - \frac{\gamma}{\beta} \ln S = c. \tag{2.16}$$

Since none of these orbits reaches the I-axis, $S(t) > 0$ for all times. The part of the population that escapes infection is $S_\infty = \lim_{t\to\infty} S(t)$. At the beginning of the epidemic ($t = 0$), all of the individuals are susceptible ($S(0) = N$), and there are essentially no infected individuals ($I(0) \approx 0$). As the disease disappears from the population after some time, there are no infectious individuals at the end of the epidemic, so $I_\infty = \lim_{t\to\infty} I(t) = 0$. The relation $V(S_0, I_0) = V(S_\infty, I_\infty)$ gives

$$S_0 - \frac{\gamma}{\beta} \ln S_0 = S_\infty - \frac{\gamma}{\beta} \ln S_\infty, \tag{2.17a}$$

$$\ln \frac{S_0}{S_\infty} = \frac{\beta}{\gamma} S_0 \left(1 - \frac{S_\infty}{S_0}\right), \tag{2.17b}$$

$$\ln \frac{S_\infty}{S_0} = \mathcal{R}_0 \left(\frac{S_\infty}{S_0} - 1\right), \tag{2.17c}$$

$$\frac{S_\infty}{S_0} = \exp\left[\mathcal{R}_0 \left(\frac{S_\infty}{S_0} - 1\right)\right]. \tag{2.17d}$$

The final size of the epidemic, f, is simply $f = 1 - S_\infty/S_0 = 1 - s(\infty)$. By rearranging equation (2.17c), we can obtain a relationship for $\mathcal{R}_0$ and f,

$$\mathcal{R}_0 = -\frac{\ln(1-f)}{f}. \tag{2.18}$$

For large values of $\mathcal{R}_0$,

$$f \approx 1 - e^{-\mathcal{R}_0} \tag{2.19}$$

is a useful approximation of the final size (Figure 2-2). For small $\mathcal{R}_0$, the final size is approximated by

$$f \approx 2(\mathcal{R}_0 - 1) \tag{2.20}$$

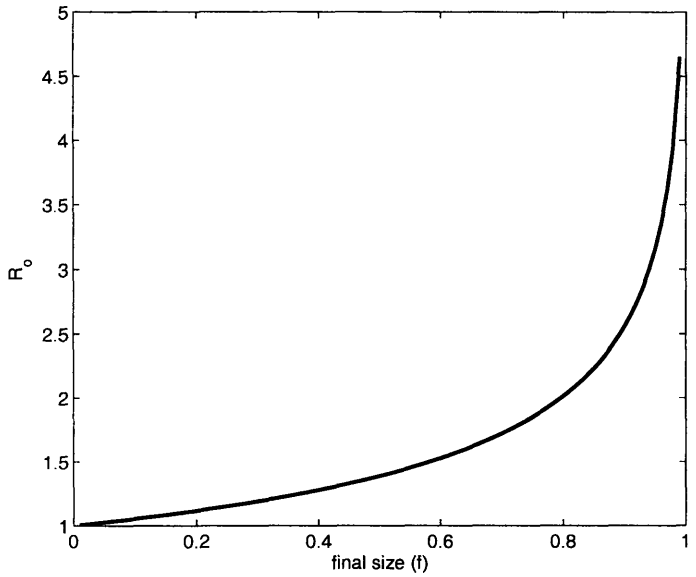

Figure 2-1: Estimates of $\mathcal{R}_0$ using the final size equation (2.18) for different final sizes of the epidemic.

which follows from the Taylor expansion of (2.17c) around $\mathcal{R}_0 = 1$ (or $s(\infty) = 1$) (Diekmann & Heesterbeek, 2000, p182).

The use of the final size equation (2.18) for estimating $\mathcal{R}_0$ requires knowledge of the final size of the epidemic. The proportion of the population that is exposed to the virus during the outbreak can be empirically determined by extensive serological studies. For the PDV outbreak in harbor seals in Europe such studies are rare, although some morbillivirus antibody prevalence studies were done on Scottish populations (e.g. Thompson *et al.*, 1992, 2002; Pomeroy *et al.*, 2005), suggesting that the final size of the 1988 PDV outbreak in Scotland was 0.5-0.7.

Figure 2-1 shows illustrates the relationship given in equation (2.18) over the range of all possible final sizes. Note that for f near 1, small errors in the estimate of f will produce large errors in the estimate or $\mathcal{R}_0$.

2.3.2 Proportion of susceptibles at the endemic equilibrium

When a pathogen invades a host population, the number of susceptible hosts decreases. Eventually the system may arrive at an equilibrium, where the rate at which susceptible individuals are infected is exactly balanced by the rate at which newly susceptible hosts enter the population (either by birth, immigration, or loss of immunity). This is known as an *endemic equilibrium*, where the number of susceptible and

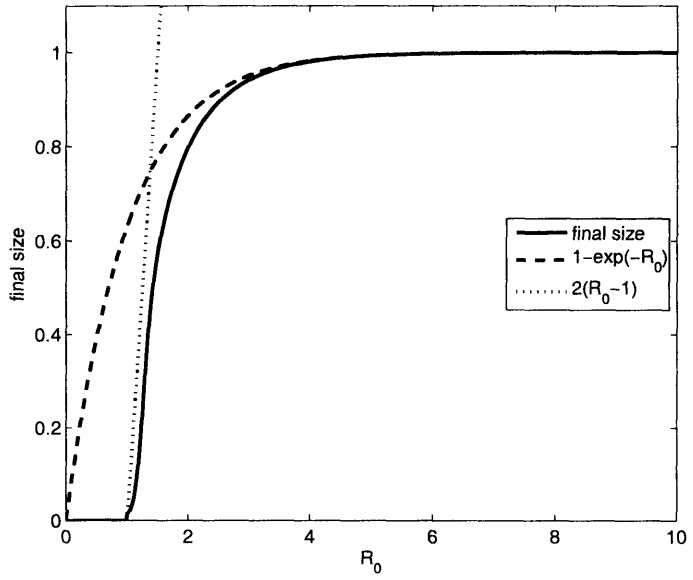

Figure 2-2: Comparison of the true final size and its approximation given with equation (2.19).

infective individuals is given by $(s, i) = (s^*, i^*)$. As the population does not consist entirely of susceptible individuals, $\mathcal{R}_0$ is not directly applicable to this case. Instead, we can use the effective reproductive number, R, which is the number of secondary cases produced in a population not consisting entirely of susceptible individuals (Grenfell & Dobson, 1995). At equilibrium, each infection will on average result in exactly one secondary infection, so the effective reproductive number, R, will be equal to unity. In a homogeneously mixed population, the number of secondary infections will be proportional to the probability that an infectious individual contacts a susceptible. In this case, the effective number R is the basic reproductive number $\mathcal{R}_0$ decreased by a fraction of host population that is still susceptible, s, $R = \mathcal{R}_0 s$ (Dietz, 1975; Anderson, 1996). At equilibrium, $R = 1$ and $s = s^*$, leading to

$$\mathcal{R}_0 = \frac{1}{s^*}. \tag{2.21}$$

2.3.3 Average age at infection

For a homogeneously mixed, stationary population (where births exactly balance deaths), at an endemic equilibrium, $\mathcal{R}_0$ can be estimated as

$$\mathcal{R}_0 \simeq \frac{L}{A}. \tag{2.22}$$

Table 2.1: Summary of $\mathcal{R}_0$ calculations.

$\mathcal{R}_0 =$	description	equation number
$\beta S_0/\gamma$	standard SIR model	(2.4)
$\int_0^\infty l(a)\, m(a) da$	survival function	(2.7)
$\rho(FV^{-1})$	next generation method	(2.9)
$-\frac{\ln(1-f)}{f}$	final size equation	(2.18)
$1/s^*$	endemic equilibrium	(2.21)
L/A	average age at infection	(2.22)

Here L is life expectancy, A is the mean age at infection, and the infection is immunizing (Dietz, 1975; Anderson, 1996). If the net population growth rate is positive, the use of equation (2.22) can lead to overestimation of $\mathcal{R}_0$, as the relevant demographic time-scale, *i. e.*, the reciprocal of the birth rate, is shorter than life expectancy, especially when the birth rate is high. For endemic infections in a growing population, a better approximation is

$$\mathcal{R}_0 \simeq \frac{B}{A}, \tag{2.23}$$

where B is the reciprocal of the average birth rate (Anderson, 1996).

For all approximations in (2.18)-(2.23), one must also assume homogeneous mixing in the population. Therefore, estimates of $\mathcal{R}_0$ obtained from (2.21) or (2.22) would not be reliable in the case where heterogeneity in host demography affects the contact process and the transmission of infection.

Phocine distemper virus is not endemic in harbor seals — the infection seemed to disappear from the seal population following both the 1988 and 2002 outbreaks — so we cannot use equations (2.21)–(2.23) to estimate $\mathcal{R}_0$. PDV outbreaks are short relative to the life-span of this long-lived species, so we can assume that the population did not grow during the outbreak and consider both outbreaks as closed epidemics. In theory, we can use the final size equation (2.18) to roughly estimate $\mathcal{R}_0$. In practice, the data on the fraction of the population that escapes the infection comes from serological surveys. Such surveys are rare for European harbor seals, so there is not enough data to estimate and compare $\mathcal{R}_0$ for phocine distemper for

different locations in Europe. Approximations of $\mathcal{R}_0$ summarized in Table 2.1 do not apply for PDV, so we need to develop a new method to estimate $\mathcal{R}_0$ from the data that is available — the time-series of the number of seals that have died from PDV.

2.4 Phocine distemper virus dynamics

The methods mentioned in Section 2.3 assume that the epidemic process is deterministic. In reality, there are many random perturbations that can influence the transmission of the disease and the final size, and those random effects can be particularly important for small compartmental sizes, or, in the case of seals, for small haul-out units. In those cases, stochastic models are more appropriate. Stochastic, or probabilistic, models allow for the use of more sophisticated estimation procedures, such as maximum-likelihood-type methods that require data on the time-series of the number of individuals in epidemic compartments.

The time-scale of phocine distemper virus outbreaks is much shorter than the demographic time-scale of harbor seals. Therefore, we can assume that seal populations do not grow during an outbreak, and we approximate a single PDV outbreak in a single haul-out location as a closed epidemic. We take a compartmental approach to modeling PDV dynamics, and we divide the population on day t into susceptible seals (S_t), infectious seals (I_t), and a removed class (R_t), which consists of both immune and dead seals.

Let the number of seals that become infected on day t (the incidence) be a random variable X_t. Let x_t be the realization of the random variable X_t, i.e. the actual number of seals infected on that day. After a seal has been infected with PDV, we assume it experiences a latent period of 3 days (Osterhaus *et al.*, 1988, 1989c; Harder *et al.*, 1990), during which it is not infectious. Individuals going through the latent period constitute the exposed class, which is not directly modeled in (2.24). The model accounts for the exposed class by introducing a delay — the newly infected individuals enter the infectious class three days after they got infected. The infectious period lasts 12 days (Osterhaus *et al.*, 1989a,c; Grachev *et al.*, 1989; Harder *et al.*, 1990), after which a seal either becomes immune or dies. Thus, for given initial

conditions we can compute the epidemic trajectory according to

$$S_{t+1} = s_t - X_t, \tag{2.24a}$$

$$I_{t+1} = i_t + x_{t-3} - x_{t-15}, \tag{2.24b}$$

$$R_{t+1} = r_t + x_{t-15}, \tag{2.24c}$$

where x_t is zero for t negative (Heide-Jørgensen & Härkönen, 1992).

An individual that is susceptible at time t remains susceptible at time $t+1$ only if it avoids infectious contact with all i_t infectives. Let p be the probability that a given infectious seal infects a given susceptible during one day. The probability that a susceptible does not get infected upon contact with a given infective is then $1-p$, hence $(1-p)^{i_t}$ is the probability of not getting infected by any of the i_t infectives at time t. The total probability that a susceptible gets infected on day t is then $1-(1-p)^{i_t}$, and this event is independent for each of the s_t susceptible individuals. Thus, the random variable X_t that describes new infections is binomially distributed,

$$X_t \sim \text{Bin}[s_t, 1-(1-p)^{i_t}]. \tag{2.25}$$

This type of formulation dates back to the series of lectures by Reed and Frost in 1928 (first published by Abbey, 1952). The probability of having an epidemic will be a product of a chain of binomial probabilities of the form (2.25). Hence, this type of a model is referred to as a *chain binomial model* (*e. g.* Bailey, 1957; Daley & Gani, 1999; Andersson & Britton, 2000).

We further assume that the number of seals that die each day, Y_t, also is binomially distributed, with constant probability of dying m.

$$Y_t \sim \text{Bin}[x_{t-15}, m]. \tag{2.26}$$

For stochastic epidemics in large communities one of two scenarios can occur. Either a small number of individuals get infected, or there is a major outbreak. If $\mathcal{R}_0 \leq 1$, a small outbreak may occur; major outbreaks are possible if and only if $\mathcal{R}_0 > 1$ (as stated by the threshold theorem Bartlett, 1960). In this case, the asymptotic distribution of final sizes of the epidemic consists of two parts, first one close to zero, and the second one spread around the deterministic final size value (see histogram in Figure 2-3).

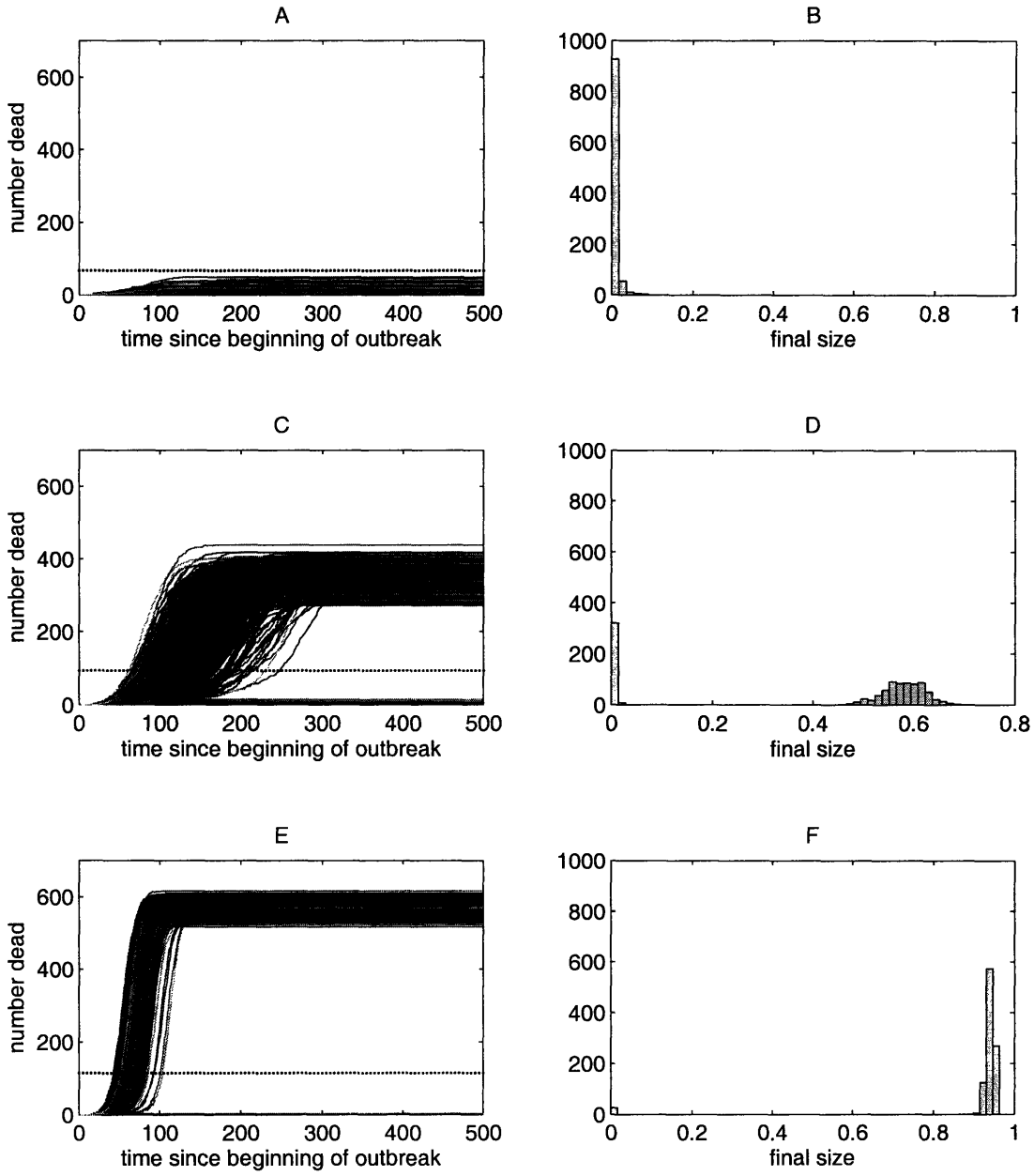

Figure 2-3: Simulated epidemic trajectories and histograms of final sizes of 1000 simulations, for initial susceptible population $s_0 = 1000$, $i_0 = 1$, $m = 0.6$. A) and B) $\mathcal{R}_0 = 0.8$ C) and D) $\mathcal{R}_0 = 1.5$; E) and F) $\mathcal{R}_0 = 3$. Dotted lines represent 20% of the expected deterministic final size approximated by (2.19).

2.4.1 Pseudo-maximum-likelihood method for estimating $\mathcal{R}_0$

For model (2.24) the basic reproductive number is given by

$$\mathcal{R}_0 = 12\, p\, s_0, \tag{2.27}$$

where s_0 is the initial susceptible population size. Estimating $\mathcal{R}_0$ amounts to estimating the parameter p.

The probability of infection p could be estimated by maximum likelihood methods, if we knew the number of seals in each compartment for every day of the epizootic. To see this, let $t = 0$ be the beginning of the disease outbreak, and let $t = T$ indicate the day the outbreak ends. Had we observed the number of seals in each class throughout the outbreak, the likelihood of the observed trajectory would be

$$L(p) = \prod_{k=0}^{T} f\left(x_k | s_k, 1-(1-p)^{i_k}\right), \tag{2.28}$$

where f is the binomial probability density function,

$$f(x \mid s, p) = \binom{s}{x} p^x (1-p)^{s-x}. \tag{2.29}$$

The maximum likelihood estimate of p would then be the value $\hat{p}$ which maximizes $L(p)$.

However, as in most wildlife disease outbreaks, the numbers of susceptibles and newly infected *etc.* were not observed every day. Our only observation is the number of stranded dead seals. Each day a certain number of seals dies from PDV. Out of this total number of victims, a certain proportion strands ashore, and, finally, some proportion of the stranded carcasses gets reported. The daily number of reported stranded carcasses is the only available information on the number of seals that died each day. The number of seals that gets stranded and reported will depend on many factors such as the weather conditions, direction of the wind, stranding location, reporting effort, etc. Therefore, there is inevitably an observational error associated with the daily number of reported carcasses, and the observational error will vary from day to day.

I account for the observation error in a simple way. There are two sources for the information on the total number of seals that have died in the outbreak. One source

is the sum of the daily number of reported strandings. Themore reliable data on the total number of seals that died comes from census data. Since we know the total population size before and after the epizootic, we can use the difference in census data to infer the total death toll. I model the observation error as equal to the ratio of the total number recovered stranded seals to the difference in census data. I further assume that the observation error is constant throughout the outbreak and scale the epidemic curve to match the total number of seals that died according to the population counts. The scaled daily counts of dead seals are then used to construct the estimates of $\hat{s}_t, \hat{x}_t$ and $\hat{i}_t$.

To estimate the series of incidence, we equated the observed mortality with its expectation under (2.26) and find

$$\hat{x_t} = \frac{y_{t+15}}{m}. \tag{2.30}$$

The incidence cases can only have integer values. Rounding of the series to the nearest integer introduces the possibility that the number of the total individuals infected is larger than the initial susceptible population size. Therefore, to keep $\hat{x}$ series in integer form, I round the right-hand side of the equation (2.30) to the nearest integers towards minus infinity using the MATLAB command `floor()`.

With $\hat{x}_t$ in hand we used model (2.24) to reconstruct the series for susceptible seals

$$\hat{s}_{t+1} = \hat{s}_t - \hat{x}_t; \quad \hat{s}_1 = N. \tag{2.31}$$

and the series of infectious seals via

$$\hat{i}_t = \hat{i}_{t+1} - \frac{y_{t+12} - y_t}{m}; \quad \hat{i}_T = 0. \tag{2.32}$$

We then treat estimates $\hat{s}, \hat{x}, \hat{i}$ as though they were actual observations and estimated $\hat{p}$ by minimizing the negative log-likelihood of the estimates

$$\ell(p) = -\sum_{k=0}^{T} \ln \left[f\left(\hat{x}_k, \hat{s}_k, 1 - (1-p)^{\hat{i}_k}\right)\right]. \tag{2.33}$$

over p. The estimate for the basic reproductive ratio is then $\hat{\mathcal{R}}_0 = 12\hat{p}N$.

2.5 Testing the accuracy of the estimation method

Before we use our estimation on the PDV data, it is important to have a sense of the method's accuracy (how close are the estimates to actual, true value), precision (how close are the estimates from one another) and potential bias (how far is the mean of the estimates from the true value). I have tested the method on simulated epidemic trajectories for a fixed infectious period equal to 12 days over the range of initial susceptible population size S_0 and $\mathcal{R}_0$, $S_0 = (100;\ 1,000;\ 10,000;\ 100,000)$, and $\mathcal{R}_0 = (1.5, 3, 6, 12)$. Figure 2-4 shows estimates of $\mathcal{R}_0$ for all the trajectories that resulted in at least one new infection (when there are no new infections, $\ell(p) = 1$ for all values of p so we can't estimate p this way).

Since model (2.24) is a stochastic one, there is some probability not to have an outbreak even when one is expected. As a result, when $\mathcal{R}_0 > 1$, the distribution of final sizes is bimodal (as seen in Figure 2-3), consisting of non-outbreaks and outbreaks. Since the realizations of the model that are non-outbreaks would not observed in the available data set, I'm setting a threshold of what constitutes an outbreak so as to unambiguously distinguish between an outbreak and a non-outbreak. I define this threshold to be 20% of the expected deterministic final size $1 - \exp(-R_0)$, and indicate it with a dotted line in Figure 2-3. Figure 2-5 summarizes the estimates from the set of trajectories shown in Figure 2-4 that exceed this threshold. The level of bias is comparable in both figures, but the discarding of non-outbreak trajectories reduces the number of outliers, particularly for small values of $\mathcal{R}_0$.

Each box plot in Figure 2-5 represents a summary of estimates of $\mathcal{R}_0$ ($\hat{\mathcal{R}}_0$) from 1,000 simulated epidemic trajectories with known parameters. I scaled the value p in each series of simulations with respect to the initial population size S_0, $p = \mathcal{R}_0/(12\,S_0)$, so that $\mathcal{R}_0$ is constant in each graph. (The $\mathcal{R}_0$ used in simulations is shown with horizontal black line.) To eliminate the contributions of the uncertainties of other parameters, I assume all other parameters (except p) are known when estimating p from the epidemic curves.

The accuracy of the pseudo-maximum likelihood method described in Section 2.4.1 depends on the initial size of the population. The method works poorly for small population sizes (under 100 individuals), especially for large values of $\mathcal{R}_0$. Figure 2-5 also shows a negative bias; I consistently underestimate the true value of $\mathcal{R}_0$, which is again most prominent for small population sizes, and large $\mathcal{R}_0$. For example, for a population of 1000 individuals, in 78% cases of $1 < \hat{\mathcal{R}}_0 \leq 1.5$, the real value of $\mathcal{R}_0$

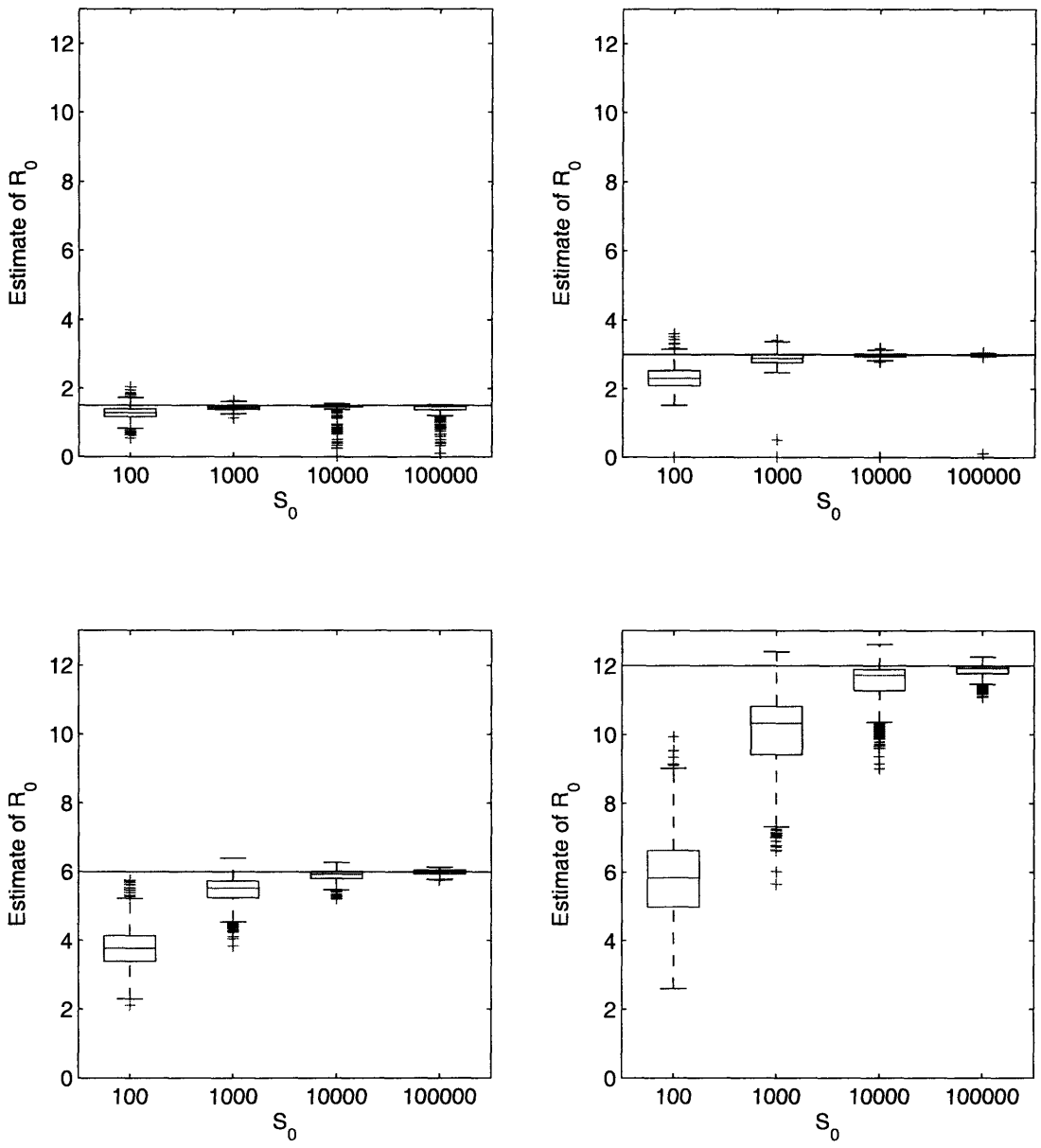

Figure 2-4: Accuracy and precision of the pseudo-maximum-likelihood method for estimating $\mathcal{R}_0$ from epidemic curves, for various values of $\mathcal{R}_0$ and S_0, and fixed infectious period (12 days). Each box plot represents a summary of estimates from 1,000 simulations using the $\mathcal{R}_0$ value indicated by the black horizontal line. The box represents the inter-quartile range of the estimates, and the red line is the median. The whiskers are lines extending from each end of the box to show the extent of the rest of the data; the maximum length of the whiskers is 1.5 times the inter-quartile range. Data that fall beyond the ends of whiskers are are shown with red plus signs.

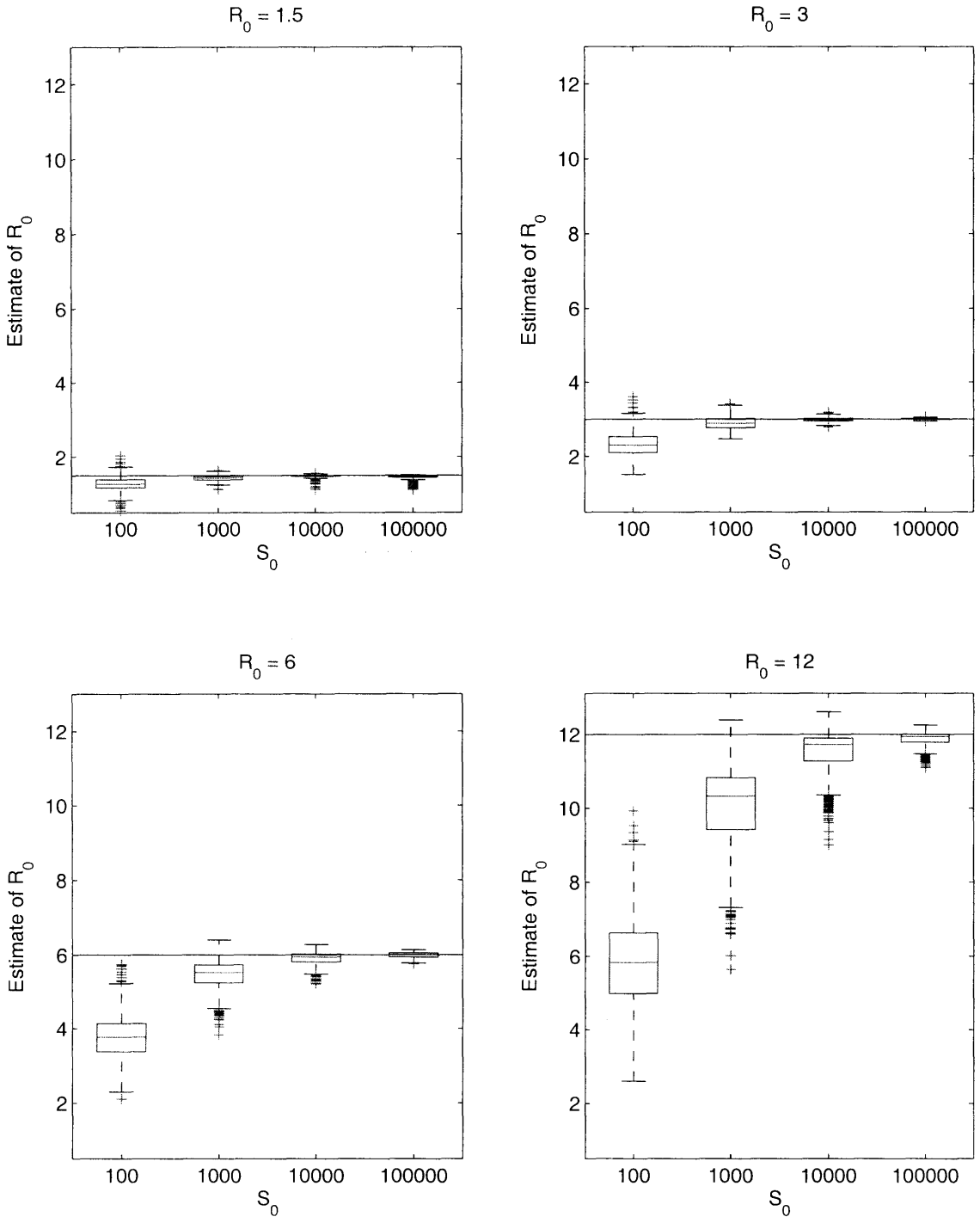

Figure 2-5: Performance of the pseudo-maximum-likelihood method for estimating $\mathcal{R}_0$ from epidemic curves, for various values of $\mathcal{R}_0$ and S_0, and fixed infectious period (12 days). Each box plot represents a summary of estimates from 1,000 simulations using the $\mathcal{R}_0$ value indicated by the black horizontal line. Trajectories that do not exceed the threshold mentioned in the text are discarded. Box plots are constructed as in Figure 2-4.

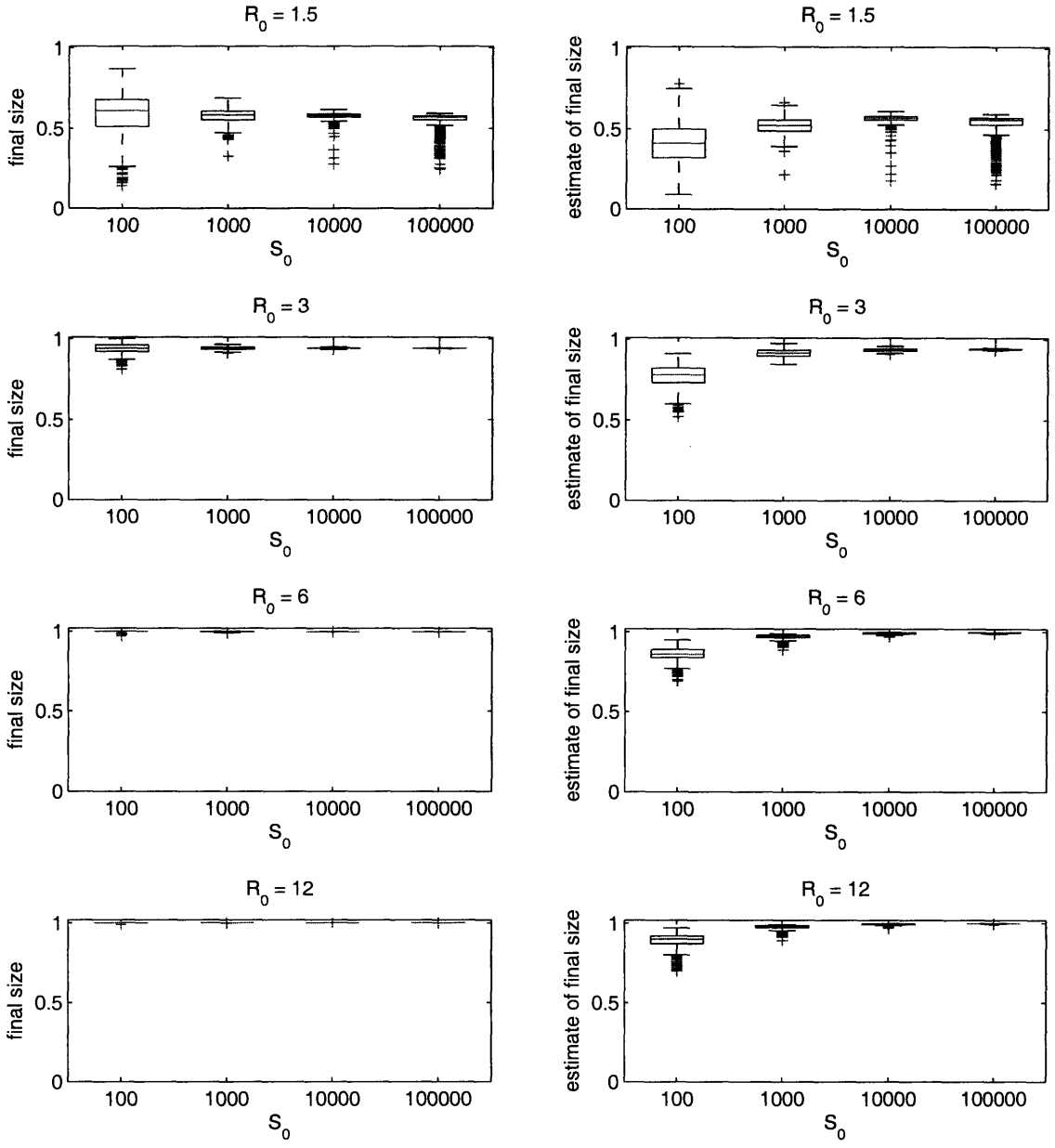

Figure 2-6: Each box plot represents a summary of estimates from 1,000 simulations using the parameters estimated from data, and is constructed as in Fig 2-5. Box plots on the left show final sizes of the simulated trajectories used as input epidemic curves to estimate $\mathcal{R}_0$ values shown in Figure 2-5. Resulting estimates of the final sizes are shown with box plots in the right column.

Table 2.2: Precision of the pseudo-maximum likelihood method. For each range below, simulations were made for 10,000 equally spaced values of $\mathcal{R}_0$ and for $s_0 = 1000$, $i_0 = 1$, $m = 0.6$. Trajectories were then used to estimate $\hat{\mathcal{R}}_0$. The entries in the rows of the table fractions of simulations in each range that resulted with a particular $\mathcal{R}_0$ estimate.

	$\mathcal{R}_0$							
$\hat{\mathcal{R}}_0$	1 - 1.5	1.5 -2	2 - 2.5	2.5 - 3	3 - 3.5	3.5 - 4	4 - 4.5	4.5 - 5
<1	1	0	0	0	0	0	0	0
1 - 1.5	0.78	0.22	0	0	0	0	0	0
1.5 - 2	0.01	0.79	0.20	0	0	0	0	0
2 - 2.5	0	0.02	0.74	0.25	0	0	0	0
2.5 - 3	0	0	0.03	0.65	0.30	0.01	0	0
3 - 3.5	0	0	0	0.05	0.57	0.34	0.04	0
> 3.5	0	0	0	0	0.02	0.17	0.26	0.55

comes from the same range, and in the other 22% cases it comes the range of larger values, $1.5 < \mathcal{R}_0 \leq 2$ (Table 2.2). The negative bias is larger for $3 < \hat{\mathcal{R}}_0 \leq 2.5$, when in only 57% of the cases the true $\mathcal{R}_0$ lies in the same range, 34% of the cases $3.5 < \mathcal{R}_0 \leq 4$, and for 4% of the cases $4 < \mathcal{R}_0 \leq 4.5$. However, the method does extremely well for large population sizes (> 100,000), for all values of $\mathcal{R}_0$ (Figure 2-5.

One source of bias is in the round-off error in the reconstruction of the incidence series, equation (2.30). Rounding off $\hat{x}$ to the nearest integer towards minus infinity inevitably underestimates the final size of the epidemic, thereby underestimating $\mathcal{R}_0$. This bias is strongest for small populations as the contribution of round-off error is relatively larger. Figure 2-6 compares the final sizes of the epidemic trajectories used to estimate $\mathcal{R}_0$ in Figure 2-5, and the resulting estimated final sizes.

The population sizes of almost all haul-out regions in the data set that I am using to estimate $\mathcal{R}_0$ of PDV outbreaks fall in the range 1,000 – 10,000 (see Table 2.3 for details). For these population sizes, we can expect our method to give reliable, but negatively biased, estimates of $\mathcal{R}_0$.

2.6 $\mathcal{R}_0$ estimates from 1988 and 2002 outbreaks

I estimated $\mathcal{R}_0$ values for 1988 and 2002 outbreaks for the following regions: North Skagerrak, South Skagerrak, Swedish Kattegat, Danish Kattegat, Limfjord, Baltic, Dutch Wadden Sea (abbreviated as WS NL), Nieder-Sachsen Wadden Sea (WS NS), Schleswig-Holstein and Danish Wadden Sea (WS SH&DK), The Wash, Tay, and

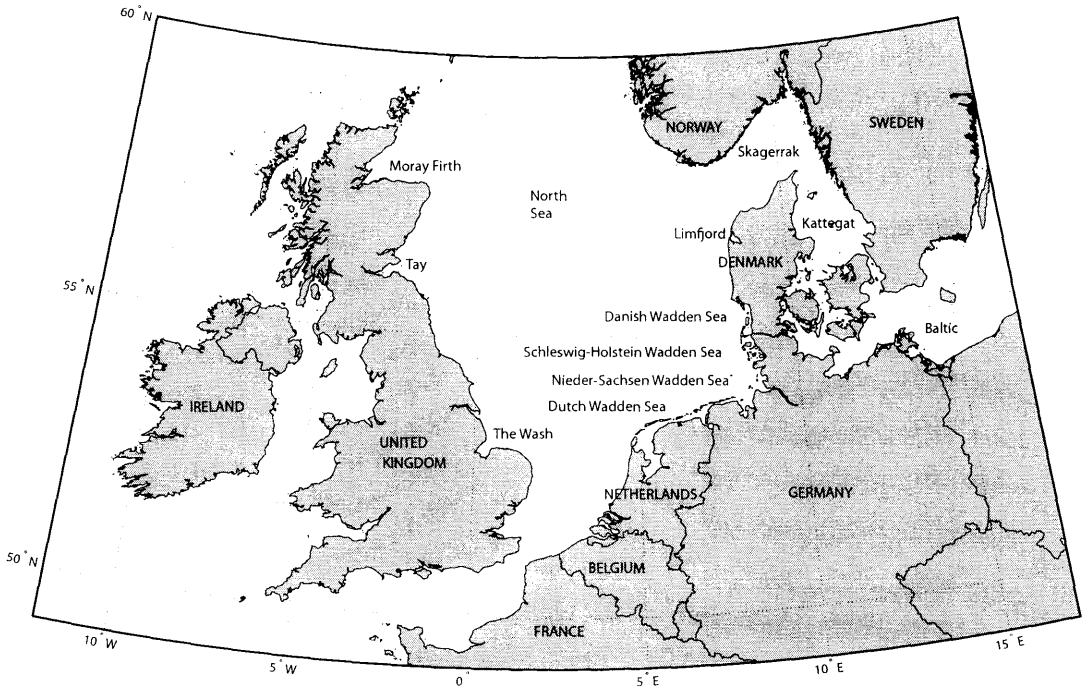

Figure 2-7: Map of North Europe with locations of PDV outbreaks mentioned in the text.

Table 2.3: Population sizes of harbor seal populations before 1988 and 2002 PDV outbreaks for the regions whose epidemic curves were used in estimating $\mathcal{R}_0$. $D(\infty)$ designates the total number of seals that have died in each location during the outbreaks (Harding *et al.*, in preparation). Degree of spatial sub-structure is given by the number of haul-out units that each region consists of.

	1988 outbreak		**2002 outbreak**		
Region	N	$D(\infty)$	N	$D(\infty)$	haul-out units
N Skagerrak	2,623	1,183	7,466	4,932	4
S Skagerrak	n/a	n/a	2,702	1,485	4
SW Kattegat	2,884	1,823	4,518	2,086	3
DK Kattegat	5,654	3,266	6,131	1,484	3
Limfjord	1,474	614	1,740	333	2
Baltic	439	218	802	127	4
WS NL	1,800	914	7,002	2,851	6
WS NS	4,602	2,634	10,042	4,690	5
WS SH & DK	9,937	5,774	18,220	8,747	8
The Wash	6,646	3,535	6,958	1,439	2
Tay	700	31	1,171	363	4
Moray Firth	1,598	200	1,198	86	5

Moray Firth (see map in Figure 2-7 for reference).

The population of seals was unexposed to PDV before the 1988 outbreak, as indicated by serological studies (Osterhaus *et al.*, 1988, 1989b; Thompson *et al.*, 1992). I therefore assume that the entire population was susceptible at the beginning of the 1988 outbreak (*i. e.*, $s_0 = N, i_0 = 1, r_0 = 0$). Exposed individuals acquire life-long immunity to PDV, so a certain fraction of the 2002 population consists of survivors of the 1988 epizootic. To calculate the fraction of the 2002 population immune to PDV, I assume that all of the individuals were exposed to the virus in 1988 (final size = 1), so all of the survivors from the 1988 epizootic are immune. This assumption is close to the truth for Kattegat locations, such as Anholt, where over 95 % of the females were infected, as estimated from the abortion rates and pup survival during the epizootic year (Heide-Jørgensen & Härkönen, 1992). The population grows at the rate λ and all of the newborn individuals are susceptible (*i. e.*, there is no inherited immunity). Assuming the 95% survival rate (based on data on survival of adult seals from Härkönen & Heide-Jørgensen (1990); Heide-Jørgensen *et al.* (1992)) during the 14 years between two outbreaks, yields the fraction of the population immune in 2002 equal to $0.95^{14}/\lambda^{14}$. Average population growth rates (λ) for different regions and estimates of fraction of the population immune to PDV are given in Table 2.4.

In order to reconstruct the incidence series in step (2.30), we need to know the probability that an infected individual dies from the disease (m). This probability is equal to the ratio of the number of individuals that have died in the outbreak, $D(\infty)$ (see Table 2.3 for actual numbers), and the total number of individuals that were infected. In the absence of serological data, I calculated the estimates of epidemiological parameters for a range of final sizes of the epidemic: 0.5, 0.6, 0.7, 0.8, 0.9 and 1, and show the results in Figures 2-8 - 2-10.

Final sizes below 0.5 are not possible for most locations for the observed values of $D(\infty)$. For some localities, even some final sizes larger than 0.5 cannot be observed for the number of seals that have died in those locations. In that case, graphs for these locations are left blank for those particular values of final size. For example, given the number of seals that have died in the 1988 outbreak in SW Kattegat, the final size of the epizootic for that locality must have been at least 0.7, so there are no box-plots for final sizes 0.5 and 0.6 in the graph for SW Kattegat in Figure 2-8.

To determine the precision of the estimates, I simulated 1,000 epidemic curves using the estimated values of parameters for each location. I discarded the non-

Table 2.4: The fraction of the 2002 population immune to PDV was calculated using population growth rates λ and assuming 95% survival rate, and the final size of the 1988 outbreak equal to 1. Assuming that 50% of susceptible seals were exposed to PDV in 1988 (final size = 0.5) halves the fraction immune in 2002.

Region	λ	**fraction immune in 2002**
N. Skagerrak	1.14	0.08
S. Skagerrak	1.13	0.09
SW Katt	1.13	0.09
DKKatt	1.06	0.22
Limfjord	1.07	0.19
Baltic	1.05	0.25
WS NL	1.17	0.05
WS NS	1.11	0.11
WS SHDK	1.13	0.09
The Wash	1.06	0.22
Tay	1.04	0.28
Moray Firth	0.99	0.56

outbreak trajectories (ones that did not reach 20% of the approximated final size $1 - \exp(-\mathcal{R}_0)$), and estimated the values of $\mathcal{R}_0$ from the remaining trajectories. Figures 2-8 and 2-10 show the range of estimates in box-plots. Estimates of $\mathcal{R}_0$ values fall in the range 1.4–3.15 for the 1988 outbreak, and 0.9 – 3.76 for the 2002 outbreak (over all final sizes).

2.6.1 Variance of $\mathcal{R}_0$ among locations

Figures 2-8 - 2-10 illustrate the variability of estimates within a location. Estimates also vary among locations. In this section I address the question of whether the difference in $\mathcal{R}_0$ values among locations is due to estimation error or biological significance.

For the 1988 outbreak, the variance of $\mathcal{R}_0$ estimates assuming the final size equal to one is $\sigma_1^2 = 0.103$. The variance is smaller for $f = 0.7$, $\sigma_{0.7}^2 = 0.014$. Can this variance in estimates be observed by chance alone (the null hypothesis H_0), or are the differences in $\hat{\mathcal{R}}_0$ among locations statistically significant? To find out, I did a randomization test by permuting observations among locations (*e. g.* Caswell, 2001). For the 1988 outbreak, the data consists of 11 epidemic curves, and I treat each recovered seal with its respective relative day of recovery (day since the first seal was found dead in that location) as a data point. Under H_0, the combination of time-series of dead seals that consist the observed epidemic curves for different locations

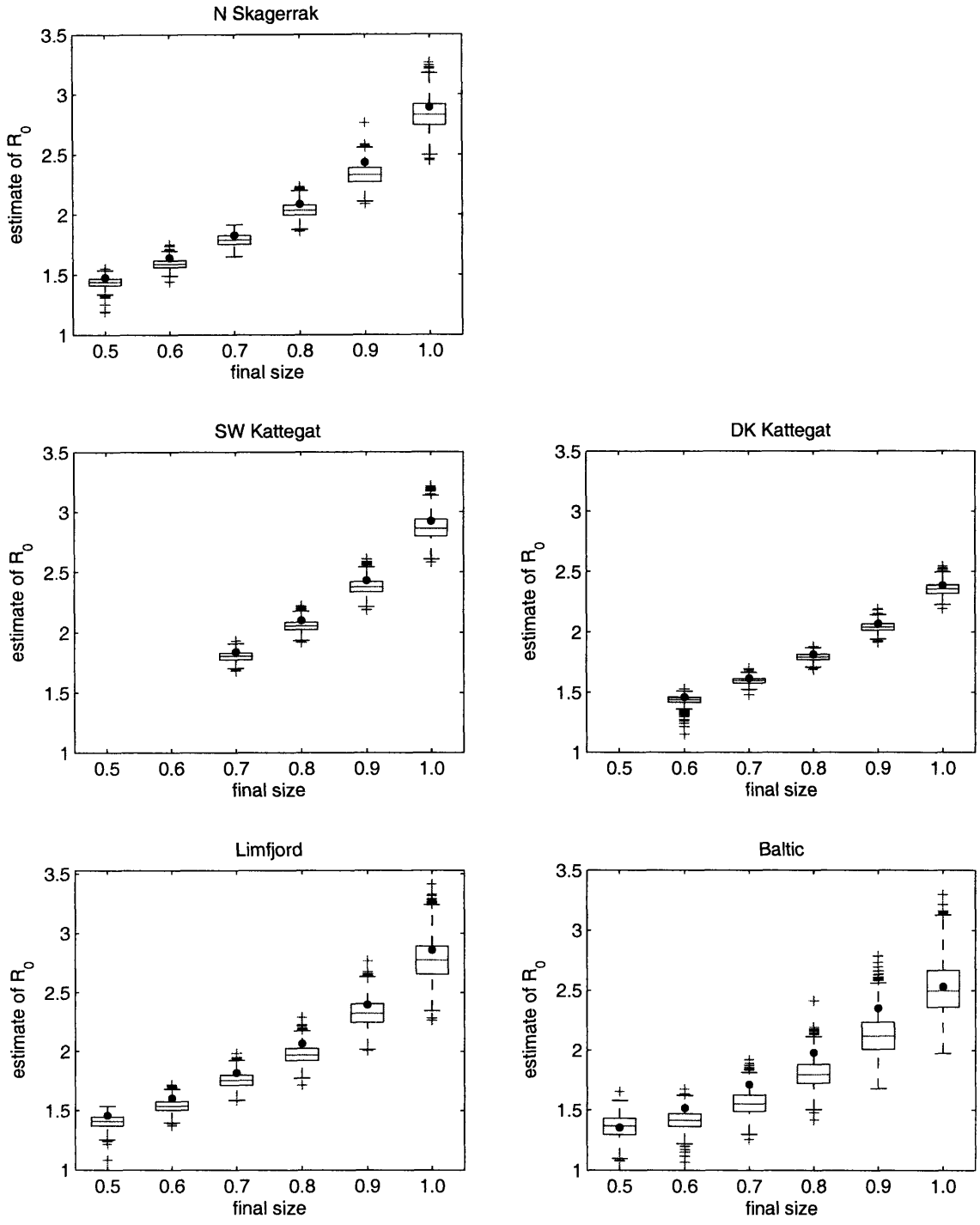
N Skagerrak
SW Kattegat
DK Kattegat
Limfjord
Baltic
estimate of R_0
final size
3.5
3
2.5
2
1.5
1
0.5
0.6
0.7
0.8
0.9
1.0

(a)

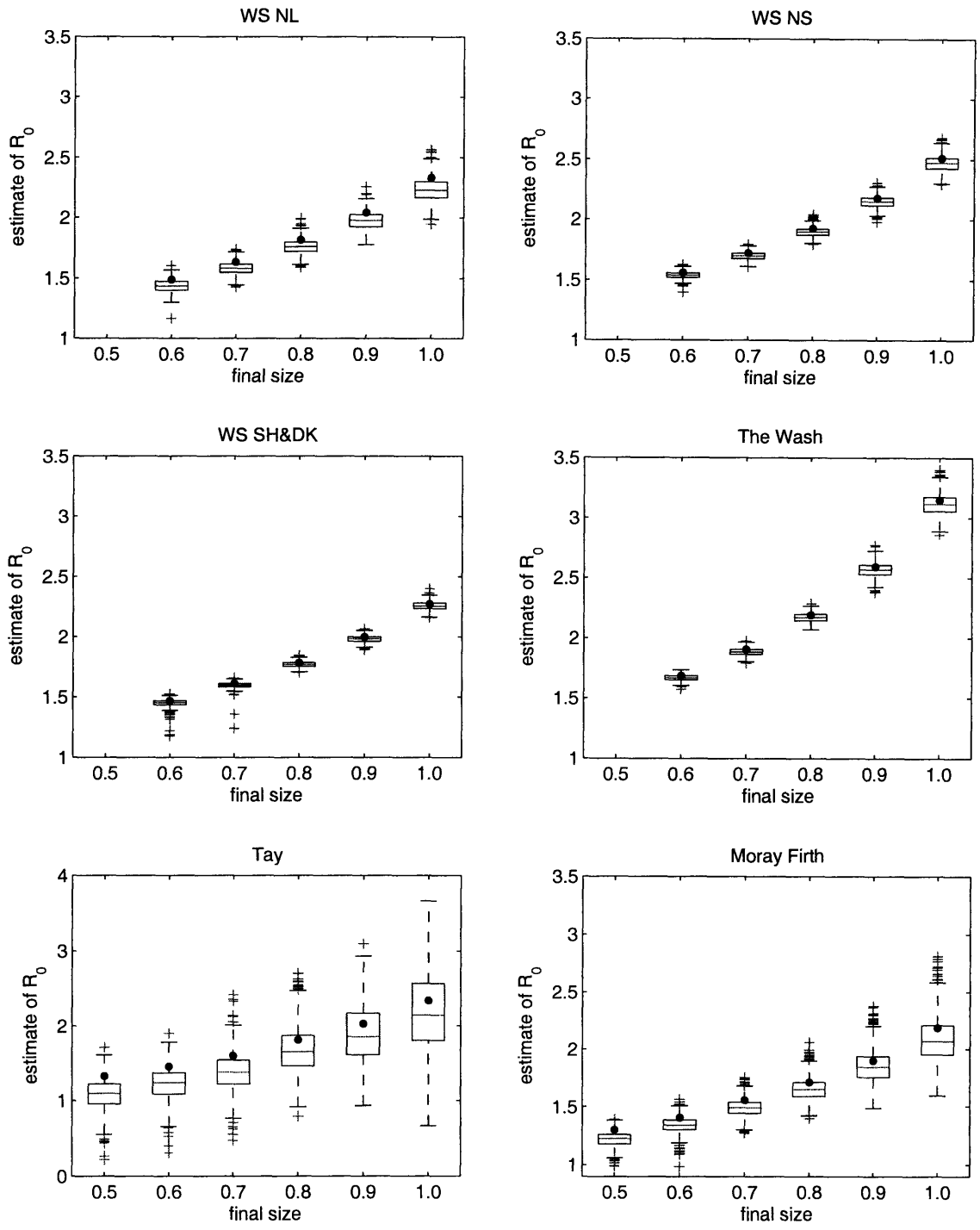

(b)

Figure 2-8: Estimates of $\mathcal{R}_0$ from data (black dots) assuming different final sizes of the epidemic for various locations in Europe for 1988 outbreak. Each box plot represents a summary of estimates from 1,000 simulations using the parameters estimated from data, and is constructed as in Fig 2-5.

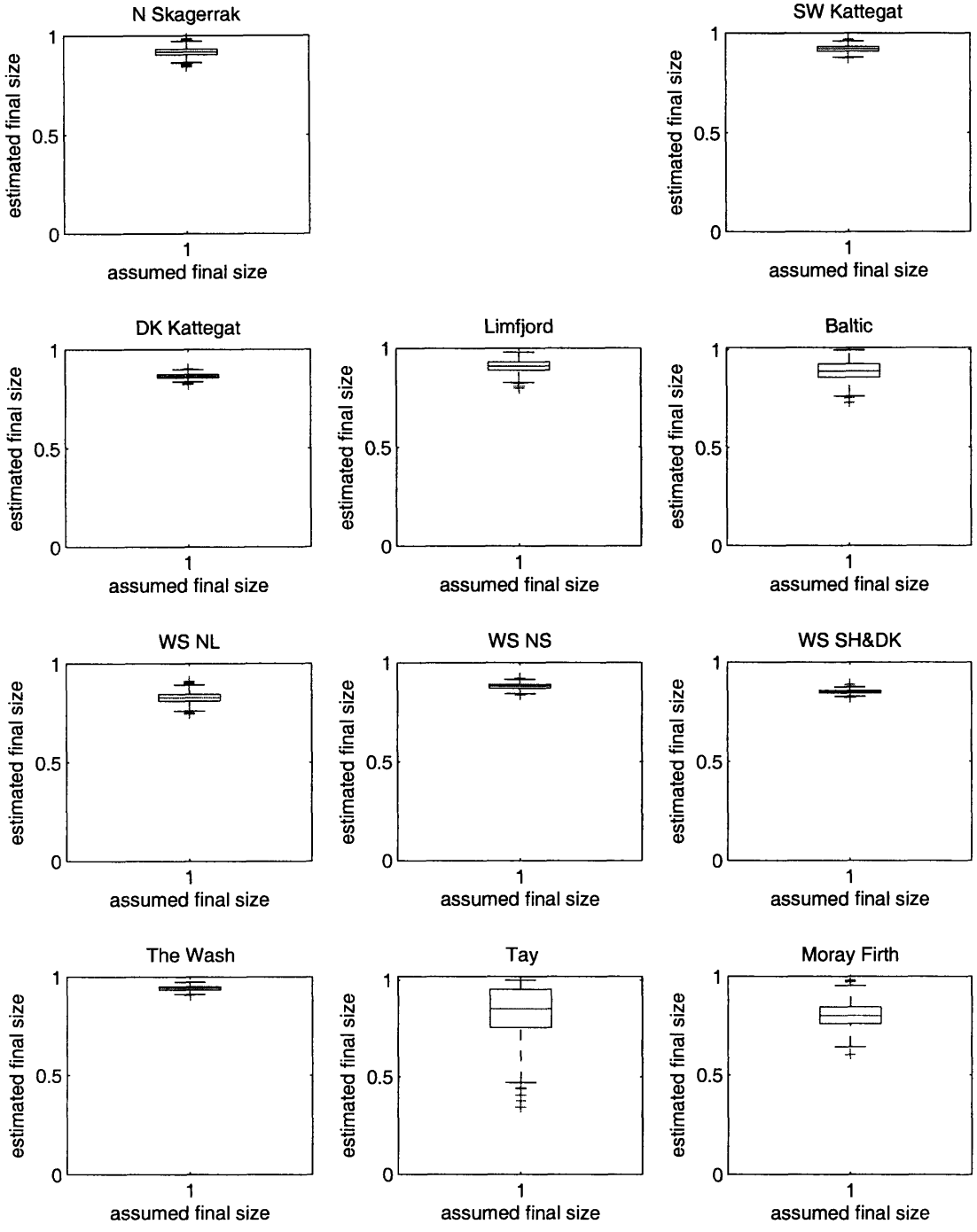

Figure 2-9: Box plots summarize estimates of the final size of the 1,000 trajectories simulated with the parameters corresponding to Figure 2-8 and final size 1.

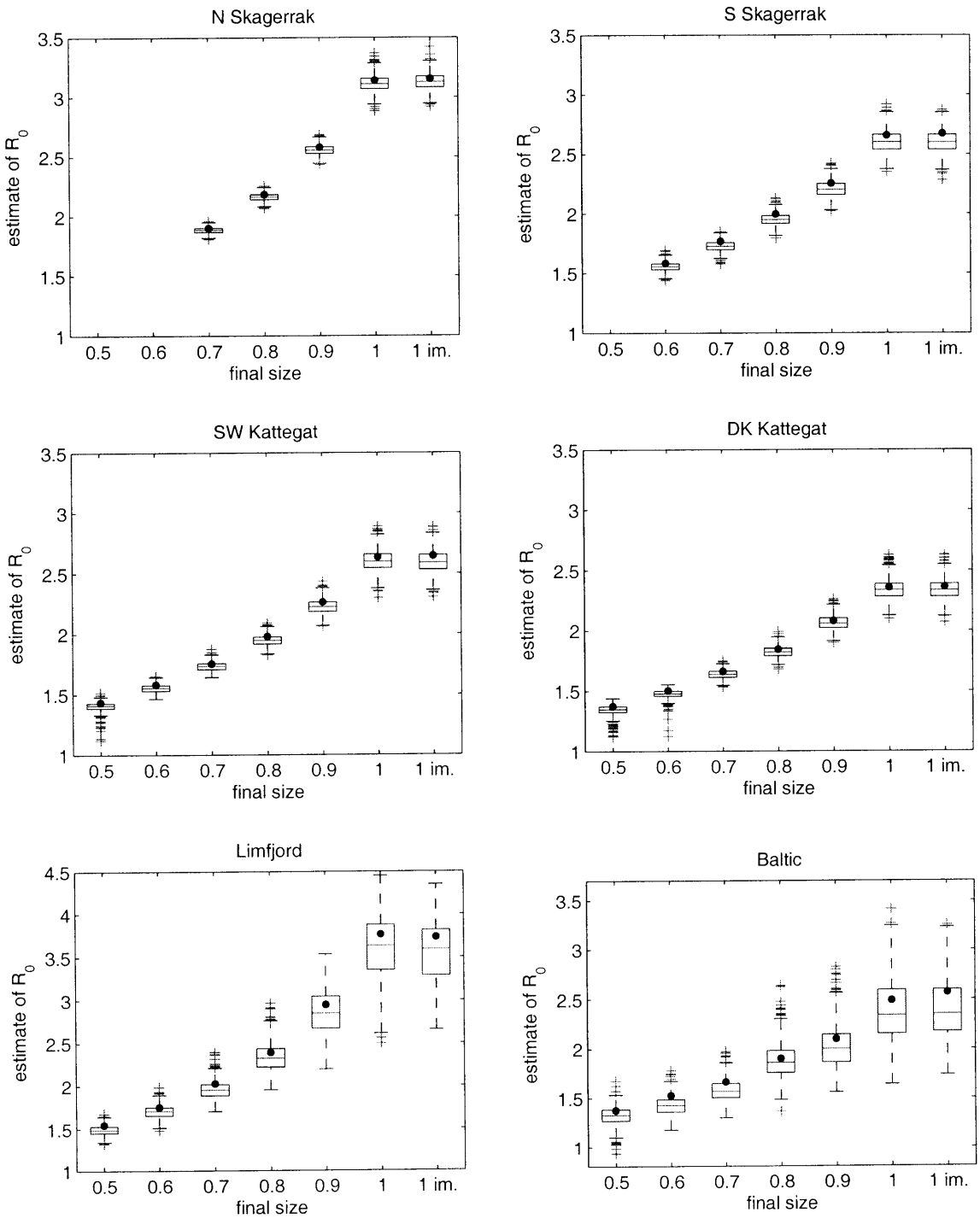
N Skagerrak
S Skagerrak
SW Kattegat
DK Kattegat
Limfjord
Baltic
estimate of R_0
final size
0.5
0.6
0.7
0.8
0.9
1
1 im.

(a)

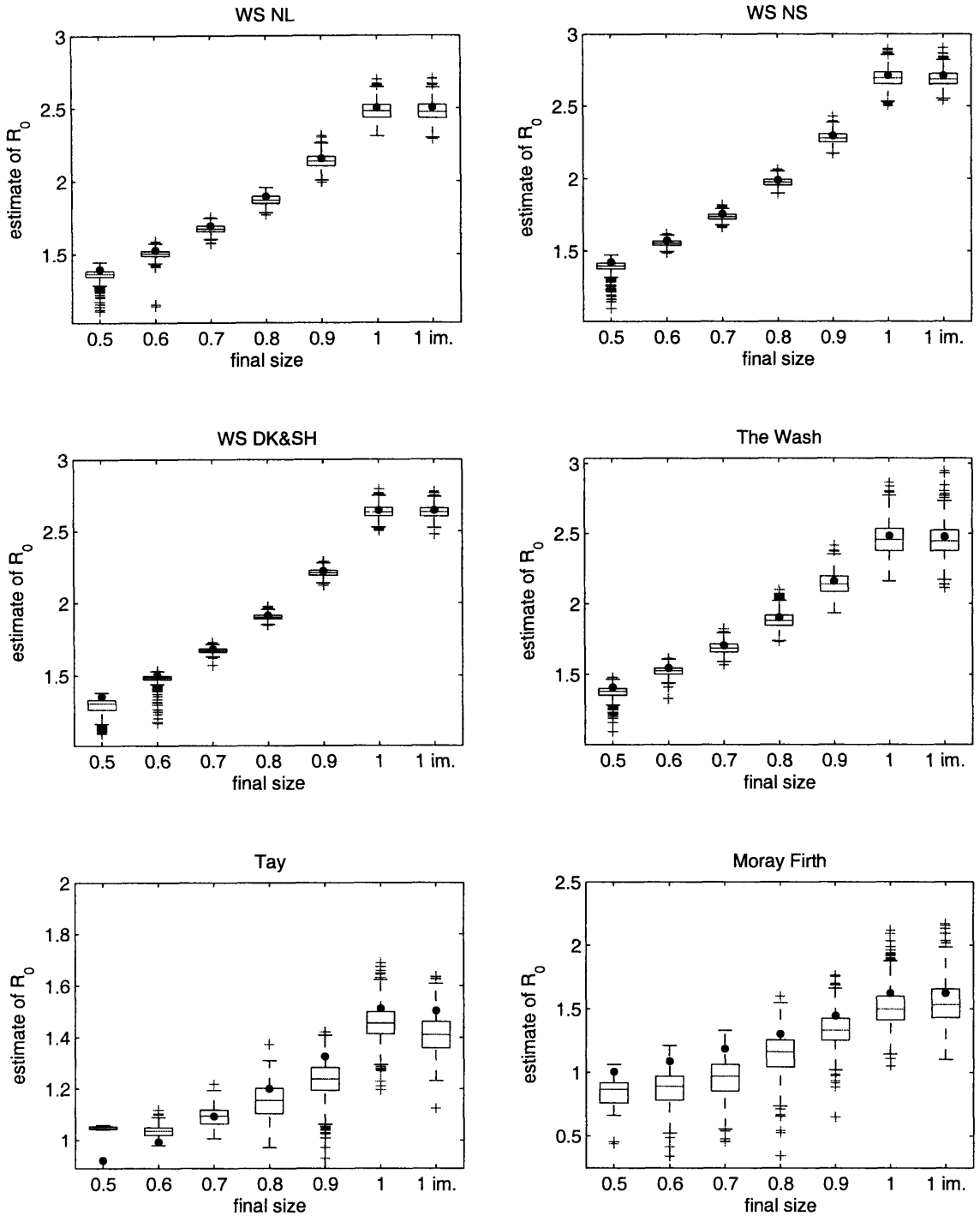

(b)

Figure 2-10: Estimates of $\mathcal{R}_0$ from data (black dots) assuming different final sizes of the epidemic for various locations in Europe for 2002 epizootic. A fraction of the population that is assumed immune in final size "1 im." is shown in Table 2.4. Each box plot represents a summary of estimates from 1,000 simulations using the parameters estimated from data, and is constructed as in Fig 2-5.

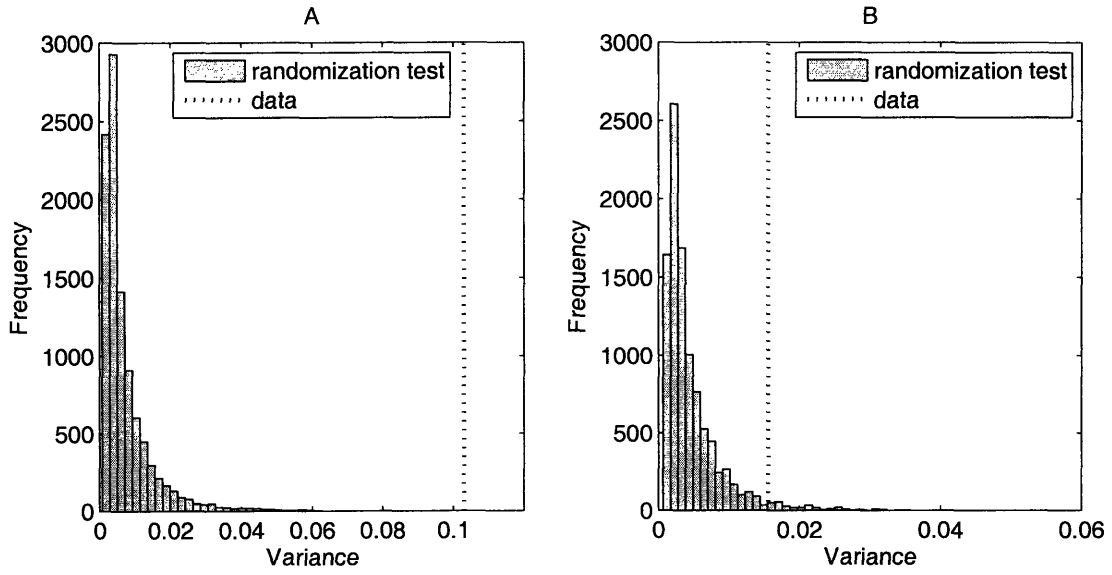

Figure 2-11: Randomization test for the 1988 outbreak assuming two different values of final size, f: A) $f = 1$; B) $f = 0.7$. Dotted lines represent the variance in $\hat{\mathcal{R}}_0$ from original data, $\sigma_1^2 = 0.103$ and $\sigma_{0.7}^2 = 0.014$.

is just as likely as any other series, and can be observed by chance alone. To obtain the distribution of the variance of $\hat{\mathcal{R}}_0$ under H_0, I permuted the seals to create new epidemic curves for each location, by randomly drawing $D_i(\infty)$ individual dead seals from the original data set without replacement. ($D_i(\infty)$ is the total number of seals that have died in location i given in Table 2.3.) This is repeated 10,000 times and for each of the 10,000 permutations, I estimate $\mathcal{R}_0$ for all locations, calculate the variance of the estimates, and obtain a distribution of variance shown in Figure 2-11. For $f = 1$, the probability of observing the variance in $\hat{\mathcal{R}}_0$ that is larger than one observed in the original data by chance alone is about 1 in 10,000. For $f = 0.7$, the probability of observing larger variance than in the original data is less than 0.04.

The randomization test for the 2002 outbreak, shows that the variance in $\hat{\mathcal{R}}_0$ values falls outside of the distribution of variance under H_0. The variance in $\mathcal{R}_0$ estimates assuming final sizes $f = 1$ and $f = 0.7$ are $\sigma_1^2 = 0.35$ and $\sigma_{0.7}^2 = 0.07$, respectively. Figure 2-12 shows that the probability of observing the variance greater than or equal to one observed in data by chance alone is less than 1 in 10,000. Therefore, we can conclude that the observed difference in $\mathcal{R}_0$ estimates among locations is statistically significant.

Since the variance in $\mathcal{R}_0$ is significant, the observed difference is a result of a biological or epidemiological process, or habitat differences. To identify the patterns

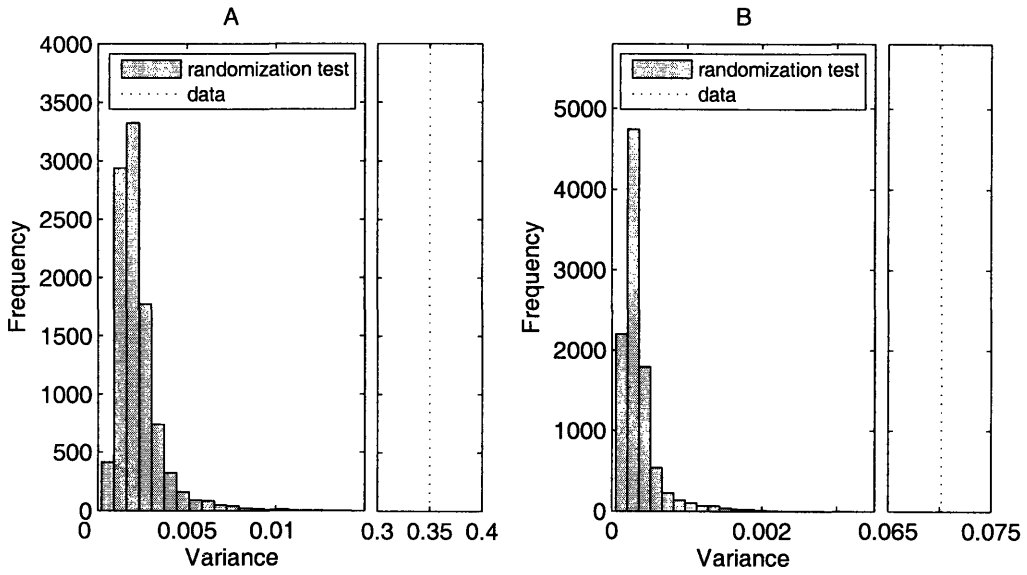

Figure 2-12: Randomization test for the 2002 outbreak assuming two different values of final size, f: A) $f = 1$; B) $f = 0.7$. Dotted lines represent the variance in $\hat{\mathcal{R}}_0$ from original data, $\sigma_1^2 = 0.35$ and $\sigma_{0.7}^2 = 0.07$.

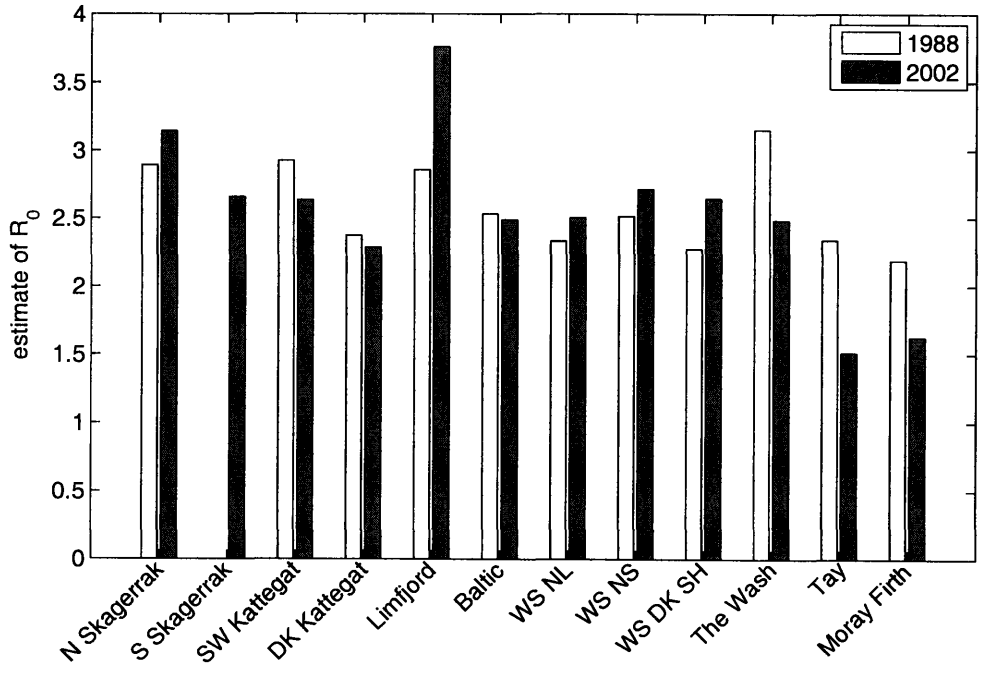

Figure 2-13: Comparison of regional $\mathcal{R}_0$ estimates between two outbreaks.

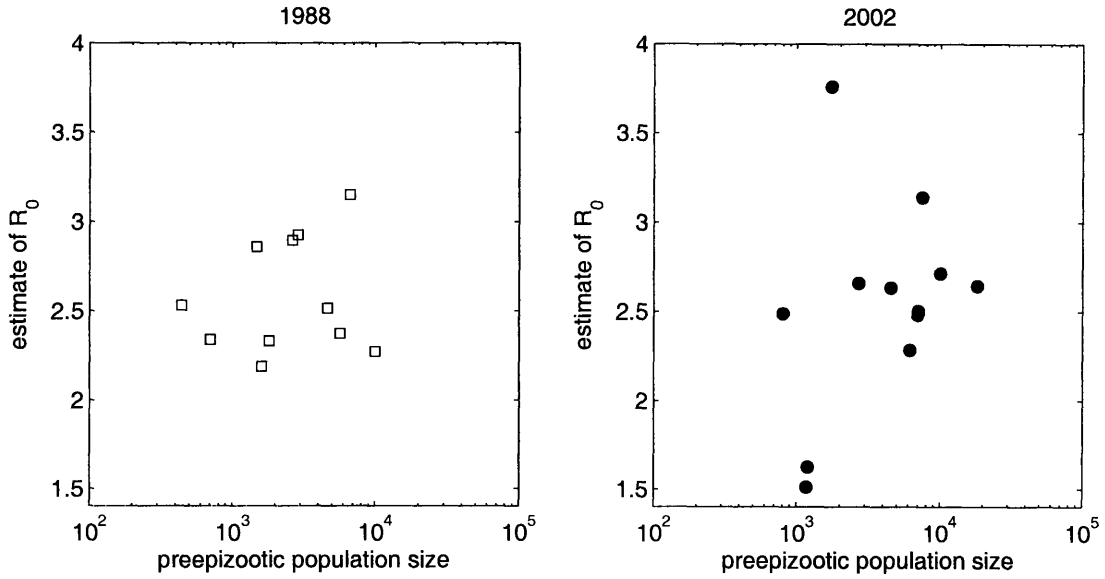

Figure 2-14: Relationship of $\mathcal{R}_0$ and the pre-epizootic population size.

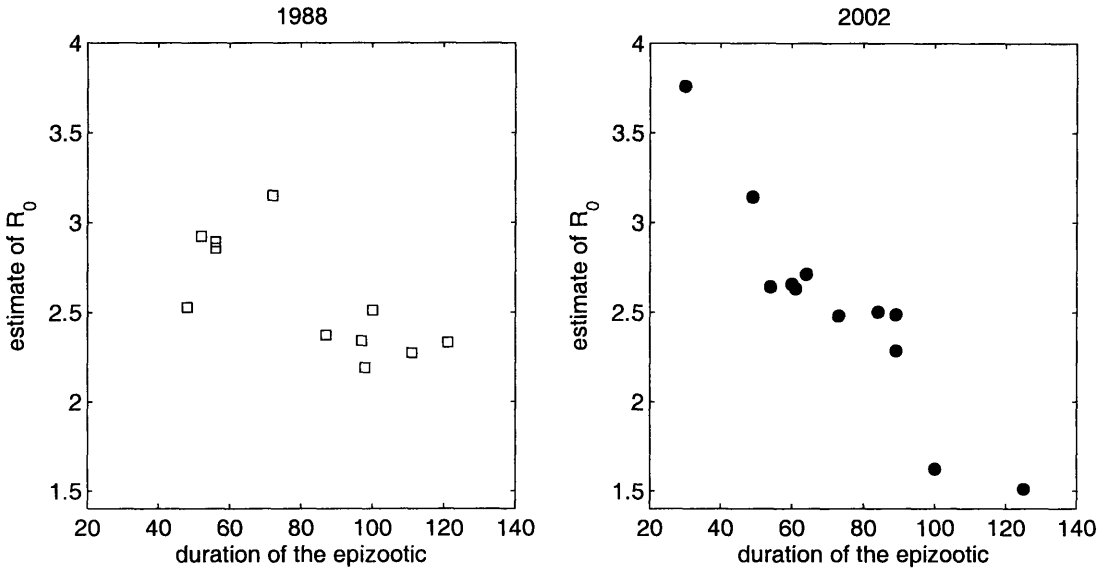

Figure 2-15: Relationship of $\mathcal{R}_0$ and duration of the epizootic (in days).

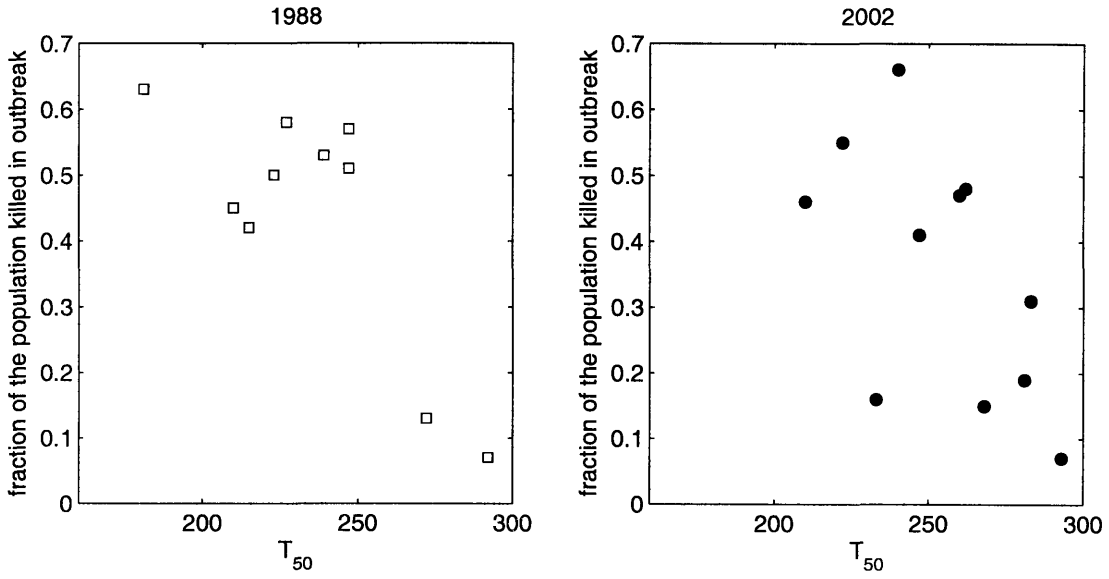

Figure 2-16: The proportion of the population killed during the outbreak decreases with the peak mortality dateT_{50}, the day of the year when 50% of the final disease mortality was reached.

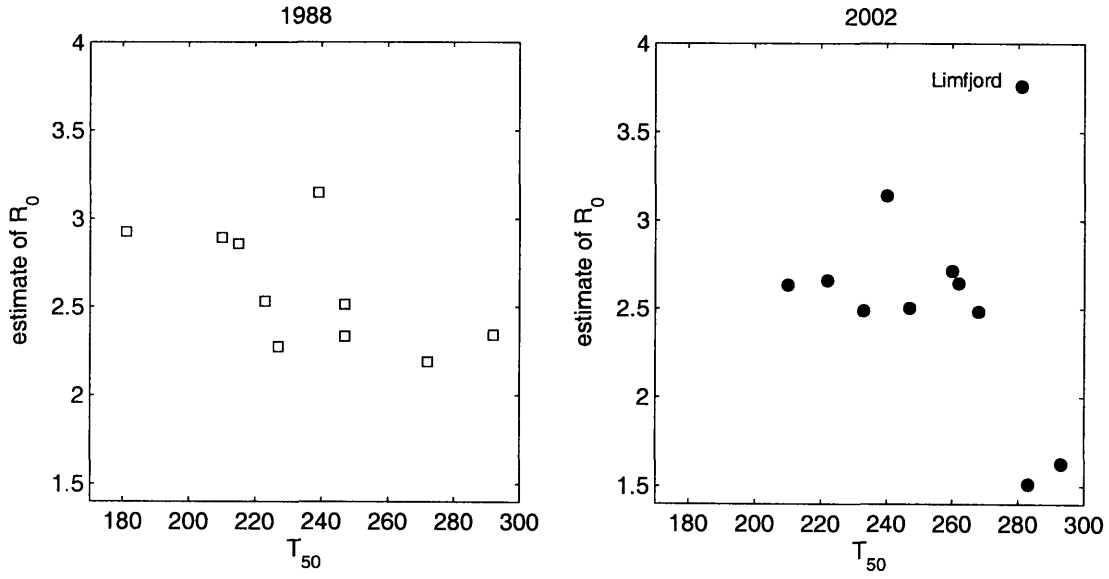

Figure 2-17: Relationship of $\mathcal{R}_0$ and T_{50}.

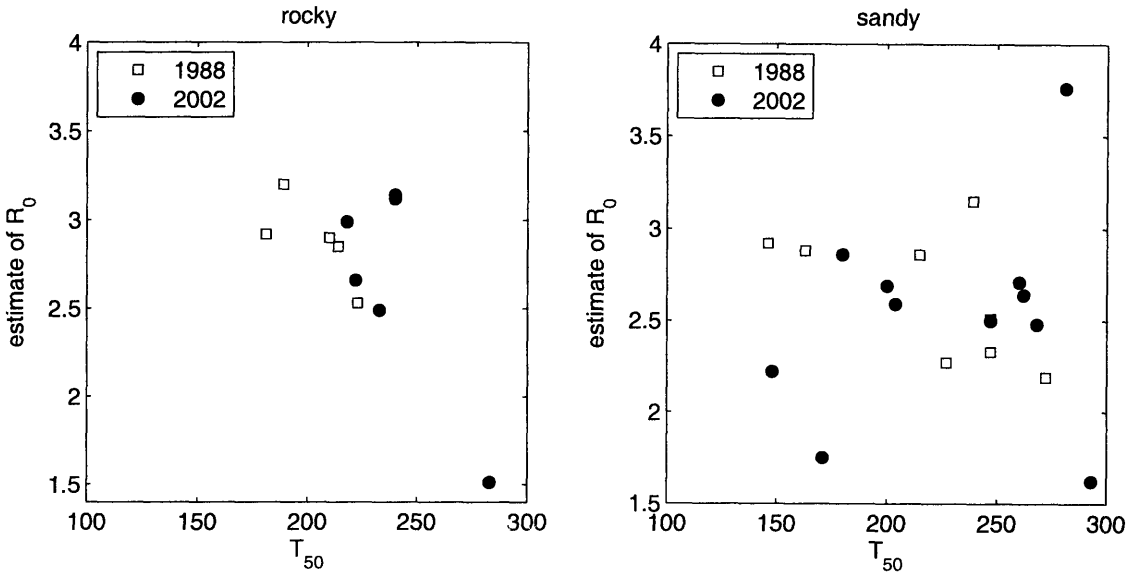

Figure 2-18: The influence of topography on $\mathcal{R}_0$ estimates.

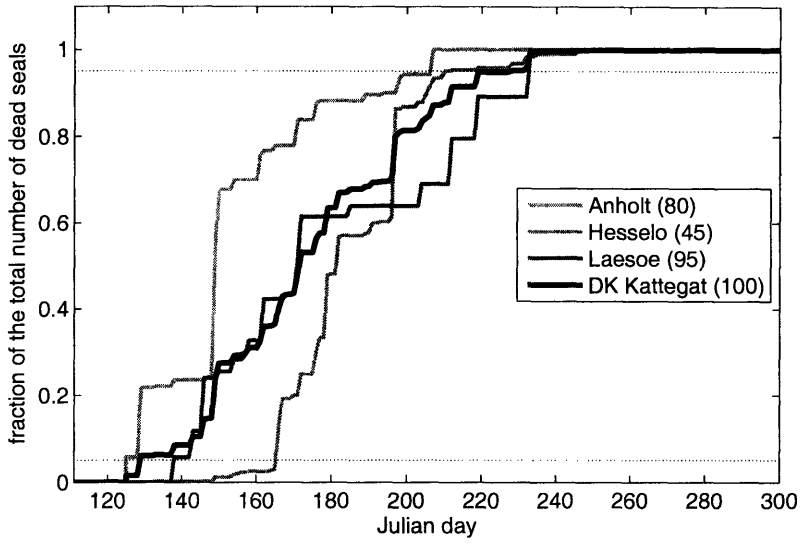

Figure 2-19: Epidemic curves for 2002 outbreak for 3 haul-out locations in Danish Kattegat, and pooled data for Danish Kattegat. Dotted lines represent first 5% and last 5% of the reported cases. The numbers in the parentheses give the duration of each outbreak in days, defined as the period between the first 5% and the last 5% of the reported cases (indicated by dotted lines).

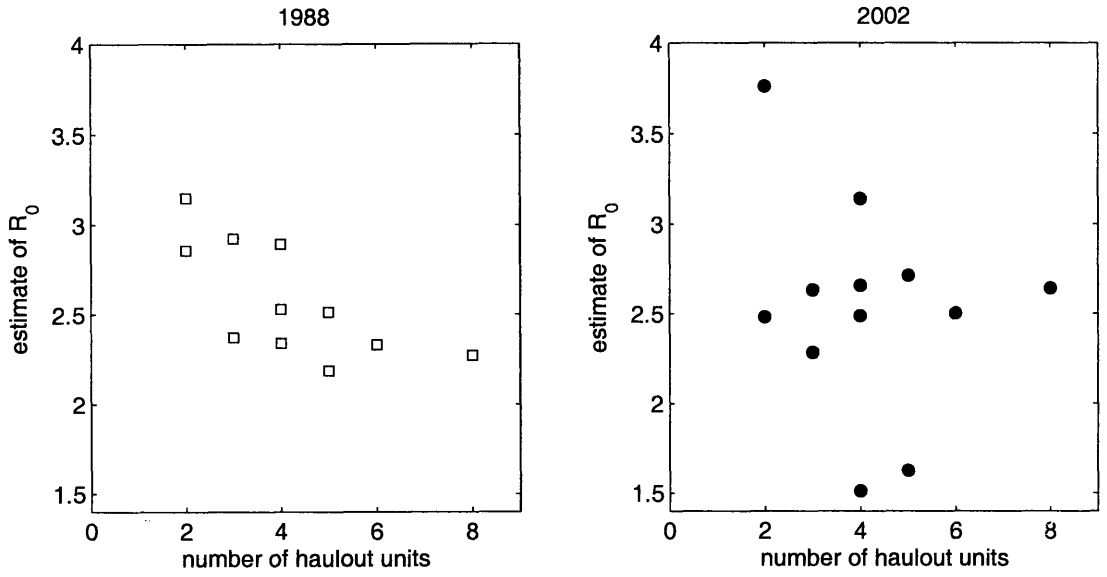

Figure 2-20: Relationship of $\mathcal{R}_0$ and the number of haul-out units within each region for 1988 and 2002 outbreaks.

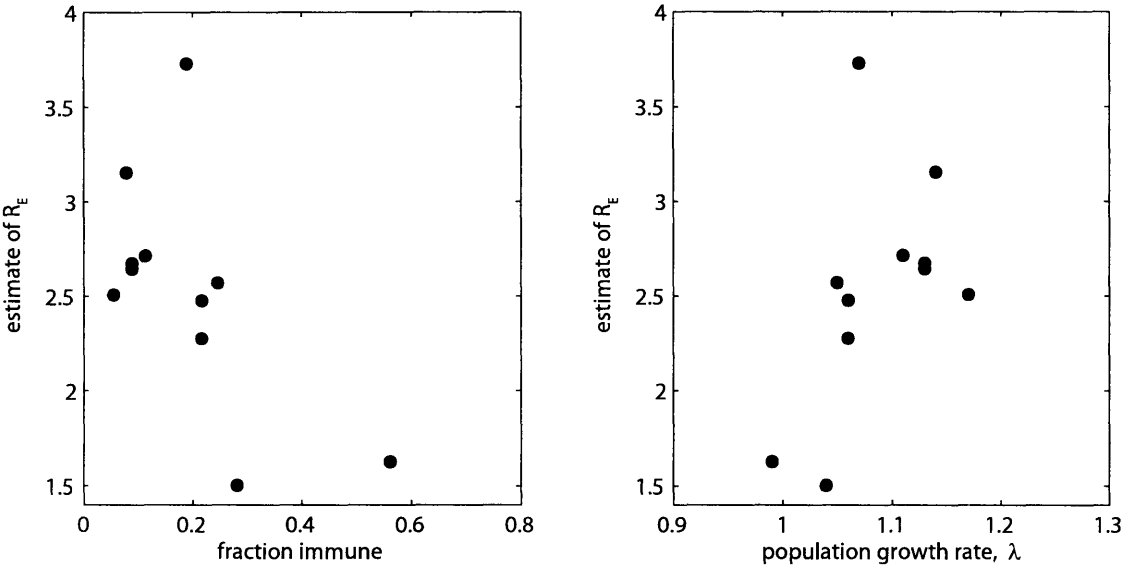

Figure 2-21: Relationship of effective reproductive number, $\mathcal{R}_E$, and population growth rate, and fraction immune for 2002 outbreak.

in $\hat{\mathcal{R}}_0$ differences and what influences them, I examine the relationship of $\hat{\mathcal{R}}_0$ to initial susceptible population size, duration of the epizootic, peak mortality date, degree of spatial structure, and the level of immunity.

For density-dependent transmission, we expect $\mathcal{R}_0$ to be proportional to population size, all other parameters being equal. Since the population level on the continent in 2002 was about double that of 1988, we would expect to observe higher $\mathcal{R}_0$ values on the continent in 2002 than in 1988, assuming that all else were equal. However, $\mathcal{R}_0$ estimates shown in Figure 2-13 show no consistent differences between two outbreaks, and $\mathcal{R}_0$ does not depend on the population size (Figure 2-14).

The relationship of $\mathcal{R}_0$ to the duration of the epizootic is shown in Figure 2-15. Differences in sampling and reporting effort are highest at the beginning and the end of the epizootic, so I represent the duration of the epizootic (ΔT) with the period between the first 5% and last 5% of the dead seals reported for each location (Härkönen *et al.*, 2006). The higher $\mathcal{R}_0$ the faster disease will spread and the shorter its duration.

Phocine distemper peaked in different times of the year in different regions. I describe this different timing by T_{50}, or the Julian day of the year when half of the final mortality in a particular region was reached. This parameter is more reliable than the date of the first finding (the day when the first dead seal was reported in each region) as there is high uncertainty in the reporting at the beginning of the outbreak. In general, the fraction killed by PDV decreases with T_{50} and is smallest for locations where the outbreak started at the latest (Figure 2-16). For the 1988 outbreak, the value of $\mathcal{R}_0$ drops in the regions where the outbreak peaked late in the year (Figure 2-17), suggesting that there might be a seasonal mechanism that affects the transmission of the virus. For 2002 outbreak, this relationship is obscured by the Limfjord locality. The Limfjord population suffered an additional source of mortality in 2002, linked to malnutrition (Karin Harding, personal communication), that can increase the observed $\mathcal{R}_0$. It has been difficult to discriminate disease-related mortality from other causes of death, so the contribution of the non-disease-related mortality to the value of the Limfjord $\mathcal{R}_0$ remains unknown.

Timing of infection, together with the topography of the location, can influence the dynamics of an outbreak. Figure 2-18 groups the locations according to their sea-bottom substrate, into rocky or sandy regions. In the rocky regions, $\hat{\mathcal{R}}_0$ drops with the peak mortality date, whereas in the sandy regions this relationship is absent.

Spatial structuring of the epidemic data can also influence the estimate of $\mathcal{R}_0$. PDV sets up a sequence of local outbreaks, that, once initiated, proceed independently. Pooling data from several localities from a larger region into a single epidemic curve, prolongs the duration of the epizootic in that region and decreases the slope of the epidemic curve, thereby decreasing $\mathcal{R}_0$. I illustrate this with Danish Kattegat data from the 2002 outbreak in Figure 2-19, for which the individual epidemic curves from different haul-out units are available (Härkönen *et al.*, 2006). The larger the number of the haul-out units with different starting dates of the outbreak included in the epidemic curve, the smaller $\mathcal{R}_0$. This expected relationship is also observed for the 1988 outbreak (Figure 2-20), and $\mathcal{R}_0$ drops as the spatial structuring, *i. e.*, the number of haul-out units, in a particular region increases. The pattern disappears in 2002, suggesting that another process, such as immunity, absent in 1988, is influencing $\mathcal{R}_0$ in 2002.

A certain fraction of the 2002 population are the survivors from the 1988 epizootic. It is therefore natural to assume that immunity could play an important role in the 2002 outbreak, and change the patterns observed in the 1988 outbreak. To account for immunity, I have estimated the fraction of each population that can be immune to PDV in 2002 (Table 2.4), and have estimated new $\mathcal{R}_0$ values by decreasing initial susceptible population accordingly. Correcting for immunity did not change the estimates of $\mathcal{R}_0$ significantly (Figure 2-10), because in general the fraction of the population that was likely to be immune in 2002 is small.

2.7 Discussion

Estimating epidemiological parameters from data is a challenging task. Information on infectious diseases is frequently lacking in detail, since it is hard to observe the exact times when individuals become infected and by whom. Data on infectious diseases in wildlife are even more incomplete than human epidemiological data or data on diseases in domestic animals. In the case of phocine distemper the only available data is the number of seals that have died from the disease.

I present a novel method for estimating $\mathcal{R}_0$ that can be useful for epidemics where the number of dead is the only information we observe. Model (2.24) assumes a closed epidemic, so the method is not applicable for diseases with long infectious periods, such as HIV/AIDS, where the susceptible population is being replenished

by birth during the outbreak. Even though the method is *ad hoc* I tried to base it on the maximum-likelihood framework. Simulation results show that the estimates are reliable for population sizes in the range covered by the data. The method is negatively biased, but for the observed population sizes this bias is small. One source of bias is numerical, due to the round-off error in the reconstruction of the time-series for incidence. Additional sources of bias can come from assumptions about infectious period and from observational errors. We assume a 3-day latent period followed by a 12-day infectious period. In reality, infectious period can vary between 5 and 16 days (Harder *et al.*, 1990), which can affect overall transmission during the period of infection and thereby influence the estimated number of secondary cases. Another source of error is "built into" our series of dead seals, which we use to reconstruct the time series of incidence and infectious case counts. Data on seals that have died from PDV is collected by counting carcasses that stranded ashore, which depends on the weather conditions and sampling and reporting effort, so there is inevitably an error associated with the observation process.

Averaging data over large-scale spatial structure can lead to further underestimation of $\mathcal{R}_0$. Phocine distemper epizootic sets up a sequence of local outbreaks that, once initiated, proceed independently. The spatial unit at which an outbreak occurs is a single haul-out location. Treating several haul-out units as one, or pooling data from several haul-out units into one, will result in a smaller estimate of $\mathcal{R}_0$ than for a single haul-out. Looking at the outbreak at a larger spatial scale than it occurs, artificially prolongs the duration of the epizootic thereby reducing $\mathcal{R}_0$ (see Figure 2-15).

One potential way to improve the method and reduce the bias would be to use EM algorithm to find the maximum-likelihood estimates. The EM algorithm, first named by Dempster *et al.* (1977) is a computation that iterates between an "Expectation-step" and a "Maximization-step." It is a broadly applicable algorithm for estimating parameters from incomplete data sets by maximum likelihood methods. In epidemiology, the EM algorithm is not only used for the estimation of parameters, but also for reconstruction of the entire time series of unobservable classes. For example, the most reliable data on HIV/AIDS epidemic are often incidences of cases diagnosed with AIDS. It is much harder to observe the times of infection with HIV. Becker (1997) used the EM algorithm to back-project HIV infection curve from the AIDS incidence data. Andersson & Britton (2000) show how the algorithm can be used

to estimate the probability of infection in chain-binomial models. In the case of the distemper outbreak in seals, the only time-series data at hand is actually the series of *estimates* of the number of seals that have died each day, so EM approach is not applicable.

Estimates of $\mathcal{R}_0$ values for phocine distemper outbreaks fall in the range 1.4–3.15 for the 1988 outbreak, and 0.9–3.76 for the 2002 outbreak, over all final sizes. Since the method described in Section 2.3 is negatively biased, the true value of $\mathcal{R}_0$ for phocine distemper outbreaks is likely to be higher. Estimates for 1988 outbreak reported in this chapter agree with $\mathcal{R}_0$ for the 1988 epizootic from the literature — $\mathcal{R}_0$ was estimated to be 2.8 by Swinton *et al.* (1998) and between 2.1 and 3 by de Koeijer *et al.* (1998). There are no published estimates of $\mathcal{R}_0$ for the 2002 outbreak.

Phocine distemper virus has a small $\mathcal{R}_0$ compared to some of its relatives belonging to the genus Morbilliviridae. Measles, one of the most infectious childhood diseases and the most famous member of the Morbillivirus group, has $\mathcal{R}_0$ that ranges between 10 and 20, depending on location (Anderson, 1996; Keeling & Grenfell, 2000; Bjørnstad *et al.*, 2002). Highly transmissible infections include some other childhood diseases like chickenpox ($7 \leq \mathcal{R}_0 \leq 12$), mumps ($11 \leq \mathcal{R}_0 \leq 14$), and also sexually transmitted diseases such as HIV/AIDS epidemic with $\mathcal{R}_0$ around 10 in sub-Saharan Africa (Anderson, 1996). However, even diseases with small $\mathcal{R}_0$ and transmissibility compared to measles can cause pandemics and outbreaks of severe morbidity and mortality; estimates of $\mathcal{R}_0$ for 1918 pandemic influenza lie between 2 and 3 (Mills *et al.*, 2004), whereas seasonal influenza epidemics have $\mathcal{R}_0$ around 1.35 (Viboud *et al.*, 2006), and SARS outbreak of 2002 had $\mathcal{R}_0$ value around 3 (Lipsitch *et al.*, 2003). In naïve populations, diseases with relatively low transmissibility and $\mathcal{R}_0$ can cause severe morbidity and mortality, which appears also to have been the case with phocine distemper outbreaks in harbor seal populations.

Values of $\mathcal{R}_0$ estimated for PDV can also give us insight on the transmission process going on between seals. If transmission is density-dependent, as has been assumed in the model (2.24), $\mathcal{R}_0$ should increase with initial population size, S_0, all else being equal. In the case with phocine distemper, there is no clear relationships between S_0 and $\mathcal{R}_0$ (Figure 2-14). Since Figure 2-14 compares different locations, the 'all else being equal' assumption does not hold, so it's hard to determine how much other habitat differences contribute to relationship of S_0 and $\mathcal{R}_0$. Nevertheless, estimates of $\mathcal{R}_0$ are not very different (they are all the same order of magnitude)

even though populations sizes varied between 400 and 20,000. On the other hand, for frequency-dependent transmission $\mathcal{R}_0$ in equation (2.6) is constant irrespective of S_0. This suggests that in reality the mixing of seals is somewhere in the continuum between those to extremes.

Processes that affect the mixing of seals are likely to affect the value of $\mathcal{R}_0$ as well. Figure 2-17 suggest that $\mathcal{R}_0$ is smaller for the locations where the disease appeared late in the year, especially in the 1988 outbreak. Seasonal processes that result in lower mixing rates late in the year can help explain this pattern. One of those seasonal processes is the haul-out behavior of seals. Seals give birth, rear their offspring and molt on land, leading to their haul-out behavior to peak in the summer, when up to 57% of the colony can be found on land (Heide-Jørgensen & Härkönen, 1992). Since PDV is an airborne virus, it is believed its spreads by inhalation while seals are hauled-out on land. Seasonal haul-out behavior can influence the mixing and the contact processes in seals leading to reduced transmission of infection in the fall and winter, and to small $\mathcal{R}_0$ values.

The haul-out behavior differs from region to region, and in Kattegat and Skagerrak it depends on the sea-bottom substrate of the locations. This also influences the dynamics of the outbreak, so in the rocky regions $\mathcal{R}_0$ decreases with the peak mortality date, whereas in the sandy regions this is not so. In the rocky regions, food is abundant and seals don't have to travel far in search for food, so they spend more time on land. In the sandy regions, the food is scarce so seals spend less time on land, and more time in search for food. Throughout the year the fraction of the population hauled-out on land is lower in the sandy regions than in the rocky regions, so it will be more influenced by the stochasticities of the epidemic processes leading to more variable $\mathcal{R}_0$ estimates. The effects of the seasonal haul-out behavior and the timing of the outbreak on the dynamics of the phocine distemper epizootics are studied in further detail in Chapter 3.

References

Abbey, Helen. 1952. An examination of the Reed-Frost theory of epidemics. *Human Biology*, **24**, 201–233.

Anderson, R. M. 1996. *AIDS in the World II: Global Dimensions, Social Roots, and Responses. The Global AIDS Policy Coalition.* Oxford University Press. Chap. The spread of HIV and sexual mixing patterns, pages 71–86.

Anderson, Roy M., Jackson, Helen C., May, Robert M., & Smith, Anthony M. 1981. Population dynamics of fox rabies in Europe. *Nature*, **289**, 765–771.

Andersson, H., & Britton, T. 2000. *Stochastic Epidemic Moidels and Their Statistical Analysis.* Lecture Notes in Statistics, vol. 151. Springer-Verlag New York, Inc.

Bailey, N. T. J. 1957. *The Mathematical Theory of Epidemics.* Charles Griffin, London.

Barlow, N. D. 1991. Control of Endemic Bovine Tb in New Zealand Possum Populations: Results From a Simple Model. *The Journal of Applied Ecology*, **28**(3), 794–809.

Bartlett, M. S. 1960. *Stochastic Population Models in Ecology and Epidemiology.* Methuen, London.

Becker, N. G. 1997. Uses of the EM algorithm in the analysis of data on HIV/AIDS and other infectious diseases. *Statist. Meth. Med. Res.*, **6**, 24–37.

Begon, M., Bennett, M., Bowers, R. G., French, N. P., Hazel, S. M., & Truner, J. 2002. A clarification of transmission terms in host-microparasite models: numbers, densities and areas. *Epidemiology and Infection*, **129**, 127–153.

Bjørnstad, O. N., Finkenstädt, B. F., & Grenfell, B. T. 2002. Dynamics of measles epidemics: estimating scaling of transmission rates using a time series SIR model. *Ecol. Monogr.*, **72**, 169–184.

Brauer, F., & Castillo-Chávez, C. 2001. *Mathematical Models in Population Biology and Epidemiolgy.* Text in Applied Mathematics, vol. 40. Springer-Verlag, New York, Inc.

Brauer, Fred. 2006. Some simple epidemic models. *Mathematical Biosciences and Engineering*, **3**(1), 1–15.

Caswell, H. 2001. *Matrix population models.* Second edn. Sinauer Associates, Inc.

Cosby, S. L., McQuaid, S., Duffy, N., Lyons, C., Rima, B.K., Allan, G.M., McCullough, S. J., & Kennedy, S. 1988. Characterization of a seal morbillivirus. *Nature*, **336**, 115–116.

Coyne, M. J., Smith, G., & McAllister, F. E. 1989. Mathematical model for the population biolofy of rabies in raccoons in the mid-Atlantic states. *American Journal of Veterinary Research*, **50**, 2148–2154.

Daley, D. J., & Gani, J. 1999. *Epidemic Modelling: An Introduction.* Cambridge Studies in Mathematical Biology, vol. 15. Cambridge University Press.

de Jong, M.C.M., Diekmann, O., & Heesterbeek, J.A.P. 1994. The computation of R_0 for discrete-time epidemic models with dynamics heterogeneity. *Math. Biosci.*, **119**, 97–114.

de Koeijer, A., Diekmann, O., & Reijnders, P. 1998. Modelling the spread of phocine distemper virus among harbour seals. *Bull. Math. Biol.*, **60**, 585–596.

Dempster, A. P., Laird, N. M., & Rubin, D. B. 1977. Maximum likelihood from incomplete data via the EM algorithm. *J. Roy. Statist. Soc. B*, **39**, 1–38.

Diekmann, O., & Heesterbeek, J. A. P. 2000. *Mathematical epidemiology of infectious diseases: model building, analysis and interpretation.* John Wiley & son, LTD.

Diekmann, O., Hesterbeek, J. A. P., & Metz, J. A. J. 1990. On the definition and the computation of the basic reproduction ratio R_0 in models for infectious diseases in heterogeneous populations. *J. Math. Biol.*, **28**, 365–382.

Dietz, K. 1975. *Epidemiology.* Philadelphia: SIAM. Chap. Transmission and control of arboviruses, pages 104–121.

Dietz, K. 1993. The estimation of the bassic reproduction number for infectious diseases. *Stat. Methods Med. Res.*, **2**(1), 23–41.

Dietz, R., Heide-Jørgensen, M.P., & Härkönen, T. 1989. Mass deaths of harbour seals (*Phoca vitulina*) in Europe. *Ambio*, **18**, 258–264.

Dublin, L.I., & Lotka, A.J. 1925. On the true rate of natural increase. *J. Am. Stat. Assoc.*, **150**, 305–339.

Grachev, M. A., Kumarev, V. P., Mamaev, L. V., Zorin, V. L., Baranova, L. V., Denikina, N. N., Belikov, S. I., Petrov, E. A., Kolesnik, V. S., Kolesnik, R. S., Dorofeev, V. M., Beim, A. M., Kudelin, V. N., Nagieva, F. G., & Sidorov, V. N. 1989. Distemper virus in Baikal seals. *Nature*, **338**, 209.

Grenfell, B. T., & Dobson, A. P. (eds). 1995. *Ecology of Infectious Diseases in Natural Populations.* Publications of the Newton Insitute. Cambridge, UK: Cambridge University Press.

Harder, T., Willhaus, T., Frey, H.R., & Liess, B. 1990. Morbillivirus infections of seals during the 1988 epidemic in the Bay of Helgoland III. Transmission studies of cell culture-propagated phocine distremper virus in harbor seals serological results. *Journal of Veterinary Medicine*, **37**, 641–650.

Harding, K. C., Härkönen, T., & Caswell, H. 2002. The 2002 European seal plague: epidemiology and population consequences. *Ecol. Letters*, **5**(6), 727–727.

Harding, Karin C., Harkonen, Tero, Klepac, Petra, Reijnders, Peter, Dietz, Rune, Hall, Ailsa, Brasseur, Sophie, Duck, Callan, Jepson, Paul D., Siebert, Ursula, Teilmann, Jonas, Thompson, Dave, Thompson, Paul, & Neubert, Michael G. in preparation. Regional variation in the rate of spread of the Phocine Distemper Virus.

Härkönen, T., & Heide-Jørgensen, M. P. 1990. Comparative life histories of East Atlantic and other harbour seal populations. *Ophelia*, **32**, 211–235.

Härkönen, T., Harding, K. C., & Heide-Jørgensen, M. P. 2002. Rates of increase in age-structured populations: a lesson from the European harbour seals. *Can. J. Zool.*, **80**, 1498–1510.

Härkönen, T., Dietz, R., Reijnders, P., Teilmann, J., Harding, K., Hall, A., Brasseur, S., Siebert, U., Goodman, S.J., Jepson, P.D., Rasmussen, T.D., & Thompson, P. 2006. A review of the 1988 and 2002 phocine distemper virus epidemics in European harbour seals. *Dis. Aquat. Org.*, **68**, 115–130.

Heesterbeek, J. A. P., & Roberts, M. G. 1995. *Ecology of Infectious Diseases in Natural Populations.* Cambridge University Press. Chap. Mathematical Models for Microparasites of Wildlife, pages 90–122.

Heesterbeek, J.A.P. 2002. A brief history of R_0 and a recipe for its calculation. *Acta Bioheor.*, **50**(3), 189–204.

Heide-Jørgensen, M. P., & Härkönen, T. 1992. Epizootiology of the seal disease in the eastern North Sea. *Journal of Applied Ecology*, **29**, 99–107.

Heide-Jørgensen, M. P., Härkönen, T., & Åberg, P. 1992. Long-term effects of epizootic in harbor seals in the Kattegat-Skagerrak and adjacent areas. *Ambio*, **21**, 511–516.

Keeling, M. J., & Grenfell, B.T. 2000. Individual-based perspectives on R_0. *J. theor. Biol.*, **203**, 51–61.

Kermack, W. O., & McKendrick, A. G. 1927. Contributions to the mathematical theory of epidemics - I. *Proc. Roy. Soc. Edinb. A*, **115**, 700–721. (reprinted in Bull. Math. Biol. 1991. 53, 33–55).

Lipsitch, Marc, Cohen, Ted, Cooper, Ben, Robins, James M., Ma, Stefan, James, Lyn, Gopalakrishna, Gowri, Chew, Suok Kai, Tan, Chorh Chuan, Samore, Matthew H., Fisman, David, & Murray, Megan. 2003. Transmission Dynamics and Control of Severe Acute Respiratory Syndrome. *Science*, **300**(5627), 1966–1970.

Mahy, B. W. J., Barret, T., Evans, S., Anderson, E. C., & Bostock, C. J. 1988. Characterization of a seal morbillivirus. *Nature*, **336**, 115.

Mills, Christina E., Robins, James M., & Lipsitch, Marc. 2004. Transmissibility of 1918 pandemic influenza. *Nature*, **432**, 904–906.

Osterhaus, A. D. M. E., Groen, J., De Vries, P., & UytdeHaag, F. G. C. M. 1988. Canine distemper virus in seals. *Nature*, **335**, 403–404.

Osterhaus, A. D. M. E., UytdeHaag, F. G. C. M., Visser, I. K. G., Vedder, E. J., Reijnders, P. J. H., Kuiper, J., & Brugge, H. N. 1989a. Seal vaccination success. *Nature*, **337**, 21.

Osterhaus, A.D., Groen, J., UytdeHaag, F.H., Visser, I.K., Vedder, E.J., Crowther, J., & Bostock, C.J. 1989b. Morbillivirus infections in European seals before 1988. *Vet. Rec.*, **125**(12), 326.

Osterhaus, A.D.M.E., UytdeHaag, F.G.C.M., Visser, I.K.G., Bildt, M.W.G.v.d., Bergman, A., & Klingeborn, B. 1989c. Distemper virus in Baikal seals. *Nature*, **338**, 209–210.

Pomeroy, P.P., Hammond, J. A., Hall, A.J., Lonergan, M., Duck, C.D., Smith, V.J., & Thompson, H. 2005. Morbillivirus neutralising antibodies in Scottish greay seals *Halichoerus grypus*: assessing the effects of the 1988 and 2002 PDV epizootics. *Mar. Ecol. Prog. Ser.*, **287**, 241–250.

Rima, B. K., Curran, M. D., & Kennedy, S. 1992. Phocine distemper virus, the agent responsible for the 1988 mass mortality of seals. *Sci. Tot. Environ.*, **115**, 45–55.

Ross, R. 1911. *The Prevention of Malaria.* London: John Murray.

Sharpe, F.R., & Lotka, A.J. 1911. A problem in age distribution. *Philosophical Magazine*, **21**, 435–438.

Swinton, J., Harwood, J., Grenfell, B. T., & Gilligan, C. A. 1998. Persistence thresholds for phocine distemper virus infection in harbour seal *Phoca vitulina* metapopulations. *J. Anim. Ecology*, **67**(1), 54–54.

Thompson, P. M., Cornwell, H. J. C., Ross, H. M., & Miller, D. 1992. Serologic study of phocine distemper in a population of harbor seals in Scotland. *J. Wild. Dis.*, **28**, 21–27.

Thompson, P. M., Thompson, H., & Hall, A.J. 2002. Prevalence of morbillivirus antibodies in Scottish harbour seals. *Vet. Rec.*, **151**(20), 609–610.

Thrall, P. H., & Antonovics, J. 1997. Polymorphism in sexual versus non-sexual disease tranmission. *Proc. R. Soc. Lond. B*, **264**, 581–587.

van den Driessche, P., & Watmough, J. 2002. Reproduction numbers and subthreshold endemic equilibria for compartmental models of disease transmission. *Math. Biosci.*, **180**, 32–34.

Viboud, C., Bjørnstad, O.N., Smith, D. L., Simonsen, L., Miller, M. A., & Grenfell, B. T. 2006. Synchrony, waves and spatial hierarchy in the spread of influenza. *Science*, **312**, 447–451.

Chapter 3

Seasonal haul-out behavior and the dynamics of the phocine distemper virus

3.1 Introduction

Phocine distemper virus was first described in 1988 after it killed over 23,000 harbor seals (*Phoca vitulina*) in Northern Europe (Osterhaus, 1988; Osterhaus & Vedder, 1988; Osterhaus *et al.*, 1989a; Dietz *et al.*, 1989; Heide-Jørgensen *et al.*, 1992). The disease appeared at the Danish island of Anholt in April, and in the following months spread throughout Europe, reaching Scotland in the fall. Over the next 14 years the harbor seals populations recovered to double the 1988 pre-epizootic population size on the Continent, and reaching levels comparable to 1988 in the UK.

An interesting feature of PDV outbreaks is that the proportion of seals that died during the outbreak varied among regions (Figure 3-1). The Danish, Swedish and Norwegian populations experienced much higher mortalities ($50 - 60\%$) than the populations in England, Scotland and Ireland ($10-20\%$) (Dietz *et al.*, 1989; de Koeijer *et al.*, 1998; Harding *et al.*, 2002; Härkönen *et al.*, 2006). The mortality was lowest in the regions where PDV appeared last. Estimates of $\mathcal{R}_0$ also differ significantly among locations (Chapter 2). $\mathcal{R}_0$ was estimated to be lower in locations where the disease appeared late in the year, suggesting a seasonal mechanism might be influencing the transmission of the virus. One potential mechanism is the roughly annual cycle in the haul-out behavior of harbor seals.

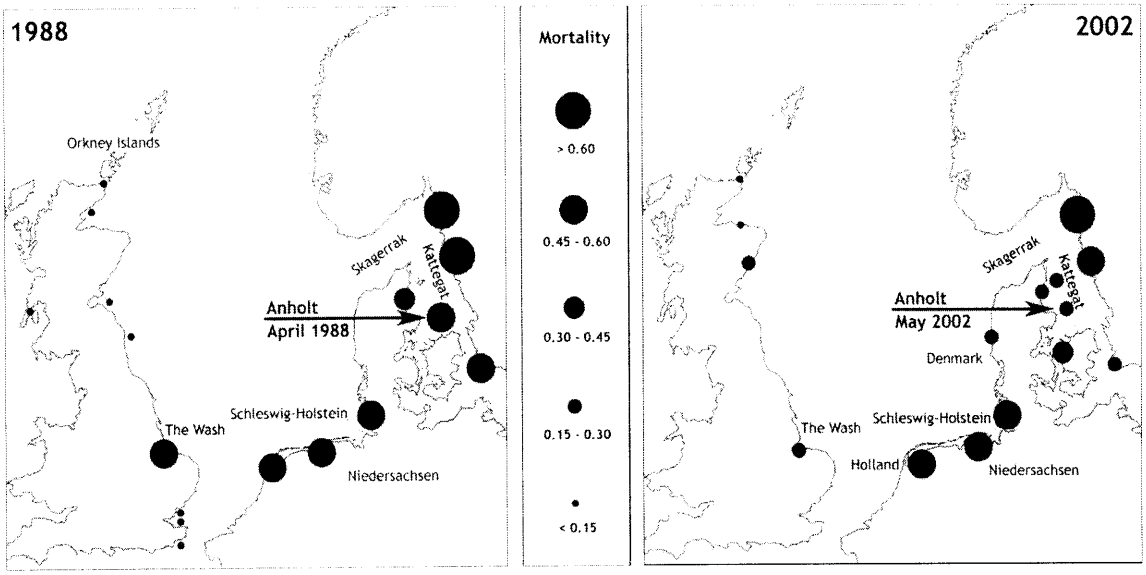

Figure 3-1: Map of mortalities of 1988 and 2002 PDV outbreaks.

Seals give birth, rear their offspring and molt on land. As a result, the fraction of a population "hauled-out" on land at any time peaks during the pupping and molting seasons in late spring and summer. At that time, approximately 60% of a colony are on land (Thompson *et al.*, 1997; Ries *et al.*, 1998; Härkönen *et al.*, 1999). The percentage of animals on land also varies with age and sex (Thompson, 1989; Härkönen *et al.*, 1999, 2002).

In addition to demography, the haul-out pattern is influenced by the sea-bottom topography. In the regions of the Kattegat and Skagerrak Seas with rocky sea-bottom substrate, food is abundant and seals do not have to travel far in search for food, so they spend more time on land. Where the substrate is sandy, food is scarce so seals spend less time on land, and more time in search for food. As a result, throughout the year the fraction of the population hauled-out on land is lower in the sandy regions than in the rocky regions (Figure 3-2).

Phocine distemper virus is an airborne virus, that spreads by inhalation (Kennedy, 1990, 1998) and can only be transmitted between seals that are hauled-out on land. Haul-out behavior determines the contact process between the seals, so it will influence the transmission of the virus and make it seasonal whenever haul-out behavior is seasonal. In this chapter, I account for the haul-out behavior by including it in the model of transmission. The result is a non-autonomous model for the epidemic. I modify the pseudo-maximum-likelihood estimation procedure from Chapter 2 to estimate the probability of infection, and derive an expression for $\mathcal{R}_0$.

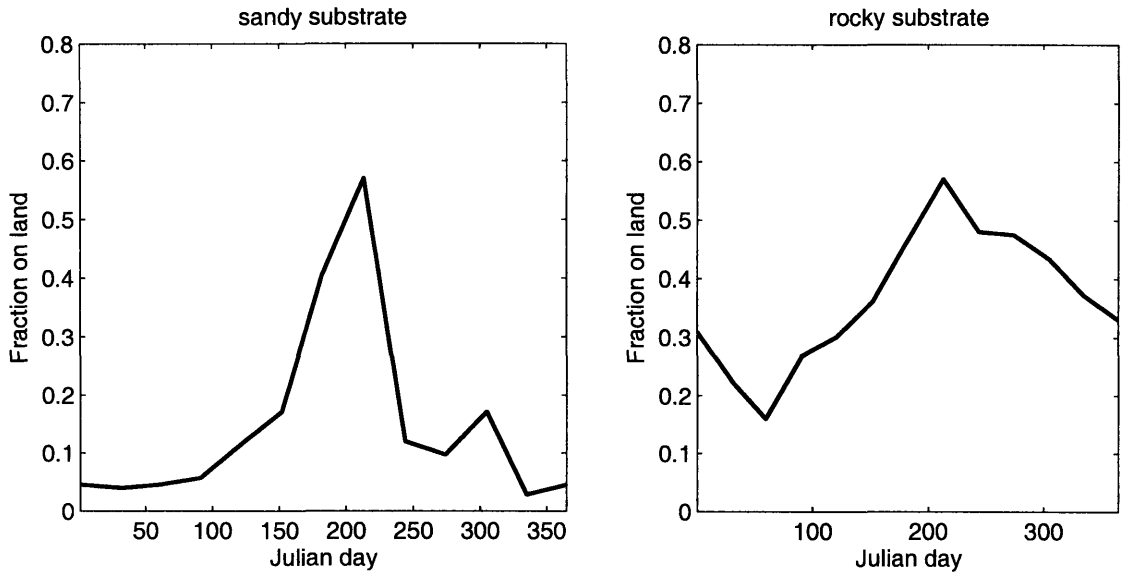

Figure 3-2: Haul-out patterns in Kattegat (left) and Skagerrak Seas (right) depend on sea bottom topography.

When the model includes the haul-out behavior, the importance of the timing of the virus introduction becomes apparent. I use simulations to illustrate how seasonal behavior and the timing of the beginning of infection influence the dynamics of the outbreak. My results show that the mortality and the final size of the outbreak will be low if the virus is introduced to the population in the winter, when the population numbers on land are lowest.

3.2 Model

The duration of phocine distemper outbreaks is short compared to the lifespan of harbor seals, so I assume that the seal population did not grow significantly during any of the two epizootics and model PDV outbreaks in any haul-out location as a closed epidemic. The seal population on day t consists of susceptible seals (S_t), infectious seals (I_t), and a removed class (R_t), which accounts for both immune and dead seals. The incidence, or the number of seals that are infected on day t, is given by the random variable X_t. The random variables are denoted by upper-case letters here, and their realizations by lower case. After getting infected, a seal goes through a latent period of 3 days, after which it becomes and remains infectious for 12 days, when it finally becomes immune or dies. In Chapter 2, I modeled the dynamics of

this epidemic process as

$$\begin{aligned} S_{t+1} &= s_t - X_t, && \text{(3.1a)} \\ I_{t+1} &= i_t + x_{t-3} - x_{t-15}, && \text{(3.1b)} \\ R_{t+1} &= r_t + x_{t-15}, && \text{(3.1c)} \\ X_t &\sim \text{Bin}[s_t, 1-(1-p)^{i_t}], && \text{(3.1d)} \end{aligned}$$

where x_t is zero for t negative (Heide-Jørgensen & Härkönen, 1992).

System (3.1) does not account for haul-out behavior, so a contact between any pair of infectious and susceptible seals can result in a new infection, with the probability p. The probability that a susceptible does not get infected after contacting a given infective is $1-p$, and $(1-p)^{i_t}$ is the probability of avoiding getting infected by any of the i_t infectives at time t. The total probability that a susceptible gets infected on day t is then $1-(1-p)^{i_t}$.

Since PDV is an airborne virus, I assume that it can only be transmitted between seals that are hauled-out. On any given day t, every seal has the same probability h_t of being hauled-out. Let $\underline{S}_t$ and $\underline{I}_t$ be binomially distributed random variables that describe the number of susceptible and infectious seals hauled-out on day t, respectively.

$$\begin{aligned} \underline{S}_t &\sim \text{Bin}[s_t, h_t], && \text{(3.2a)} \\ \underline{I}_t &\sim \text{Bin}[i_t, h_t] && \text{(3.2b)} \end{aligned}$$

The probability that an infective seal on land meets and infects a susceptible seal on land during one day is p. The incidence, X_t, is now a function of hauled-out susceptibles and hauled-out infectious seals

$$X_t \sim \text{Bin}[\underline{s}_t, 1-(1-p)^{\underline{i}_t}]. \tag{3.3}$$

After the infectious period, seals either recover or die. If the the probability of death is m, the number of seals that die on day t (Y_t) is binomially distributed

$$Y_t \sim \text{Bin}[x_{t-15}, m]. \tag{3.4}$$

System (3.1)–(3.3) is non-autonomous; the probability of being hauled-out on land is

a function of time.

3.2.1 $\mathcal{R}_0$ for constant haul-out

Seasonal behavior of seals affects the dynamics of the model. We are particularly interested in how the haul-out changes the threshold behavior of the model and its $\mathcal{R}_0$. In nature, the seasonal behavior of seals varies in time, but for mathematical simplicity I will first derive an expression for $\mathcal{R}_0$ for the case where haul-out is constant in time.

When the fraction of seals on land is constant in time, $h_t = h$, seals have a fixed probability of being hauled out on land throughout the year. For a given p, the number of seals that become infected during the outbreak depends on the value of h – the smaller value of h, the smaller the size of the outbreak (Figure 3-3). When $h = 1$, the model reduces to the model without haul-out behavior from Chapter 2, given in equations (2.24) and (2.25).

The basic reproductive number $\mathcal{R}_0$ now depends on the haul-out behavior in addition to transmission probability. One infectious individual in a population of s_0 susceptibles, will on average cause $(phs_0)h$ new infections during one day, as it has the probability of being on land equal to h, and once it is on land it will come into contact with hs_0 susceptibles. An individual remains infectious for 12 days, so the expected number of new infections it will produce during its infectious lifetime is equal to

$$\mathcal{R}_0 = 12h^2ps_0. \tag{3.5}$$

For $\mathcal{R}_0 < 1$ only small outbreaks outbreaks occur, and the distribution of final sizes is unimodal. When $\mathcal{R}_0 > 1$ both minor and major outbreaks are possible, and the final sizes have a bimodal distribution (Figures 3-3 and 3-4).

3.2.2 $\mathcal{R}_0$ for time-varying haul-out behavior

When haul-out behavior is constant (or absent), the probability of an outbreak is the same regardless of what day the virus is introduced to the population. Equal percentage of the population is on land every day, so for every day of the virus introduction, the expected number of new infections is the same. $\mathcal{R}_0$ does not change with the timing of the virus introduction. When different percentages of the population are hauled-out at different times of the year, the expected number of seals that

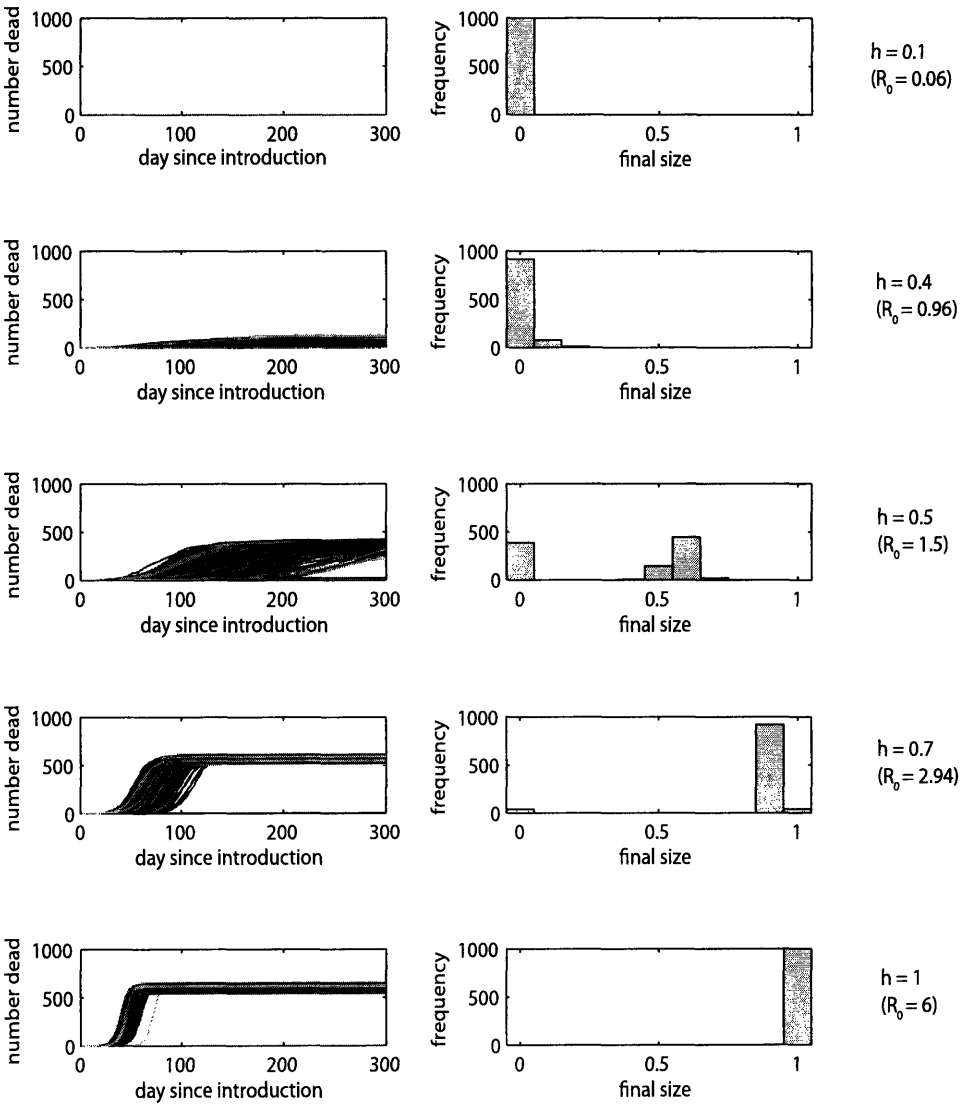

Figure 3-3: The final size of an outbreak depends on the fraction of seals hauled out on land, h. Parameter values: $s_0 = 1000, p = 0.0005, m = 0.6$. The $\mathcal{R}_0$ values corresponding to these parameter values are indicated on the graph.

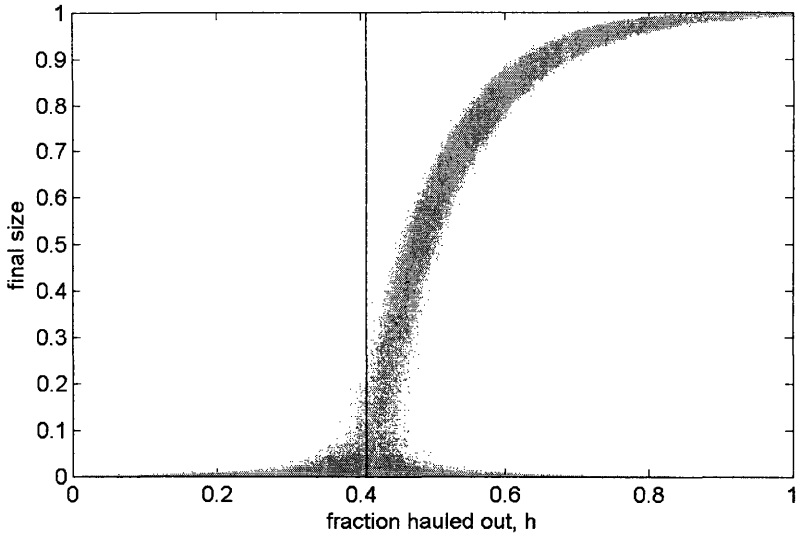

Figure 3-4: The distribution of final sizes as the function of the haul-out fraction. For each of the values of h, this graph shows final sizes of 1000 epidemic trajectories with equal parameter values ($p = 0.0005, s_0 = 1000$). The vertical line designates the value of haul-out fraction for which $\mathcal{R}_0 = 1$. When $\mathcal{R}_0 > 1$ major outbreaks are possible, and the distribution of final sizes is bimodal.

become infected depends on the day the virus is introduced to the population. When the number of seals on land is low, the potential for a successful contact is small and there is no outbreak. As the number of seals on land increases, so does the probability and final size of outbreak.

Figure 3-5 shows 1,000 epidemic trajectories for three different days of the introduction of infection. In Fig 3-5A, one infectious individual is introduced to an otherwise susceptible population on Julian day 110, when only about 10% of the population is hauled-out on land. In this case, a major outbreak occurs in only 4 of the 1,000 trajectories. If we introduce one infectious seal to the population on Julian day 160, almost every simulation results in an outbreak, but the total number of seals infected during the outbreak (*i. e.*, the final size) varies. If the disease appears later in the year, Julian day 200, when the numbers on land are declining, the final size of the outbreak decreases, as does the final mortality.

Figure 3-5 shows only 3 of the possible 365 days on which the infection may begin. To illustrate how the mortality and the final size of the epidemic would change with different starting days of the infection, I introduce one infectious seals to an otherwise susceptible population on each day of the year. For h_t, I use two different types of haul-out curves shown in Figure 3-2, for sandy and rocky sea-floor topography. For

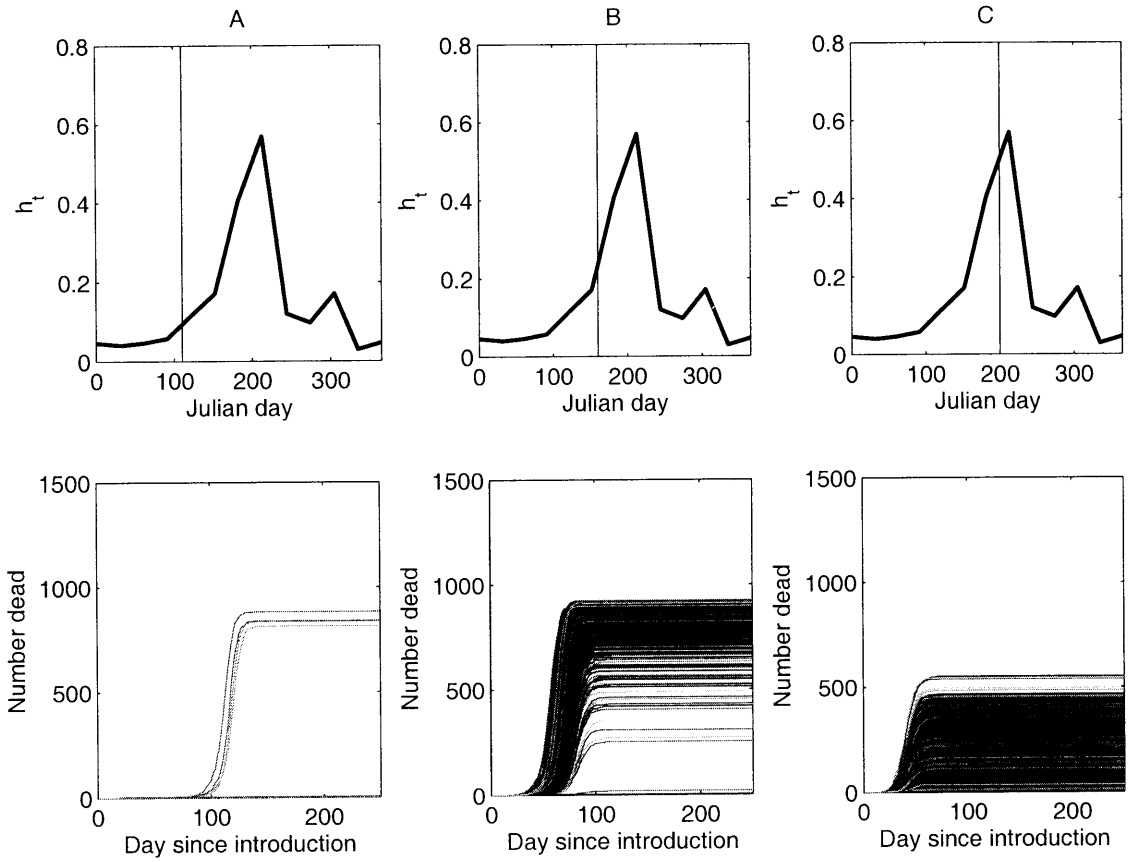

Figure 3-5: Influence of the day of the introduction of the virus on the dynamics of the outbreak. Graphs on the top show the haul-out pattern for the sandy regions that was used in simulations. The vertical lines in the top graphs indicate the day that the first infectious seal appeared (t_0). Each graph on the bottom shows 1,000 epidemic trajectories for t_0 given above. All other parameters are equal in the graphs: $S_0 = 1500$, $p = 0.001$, $m = 0.6$. (A) $t_0 = 110$, (B) $t_0 = 160$, (C) $t_0 = 200$.

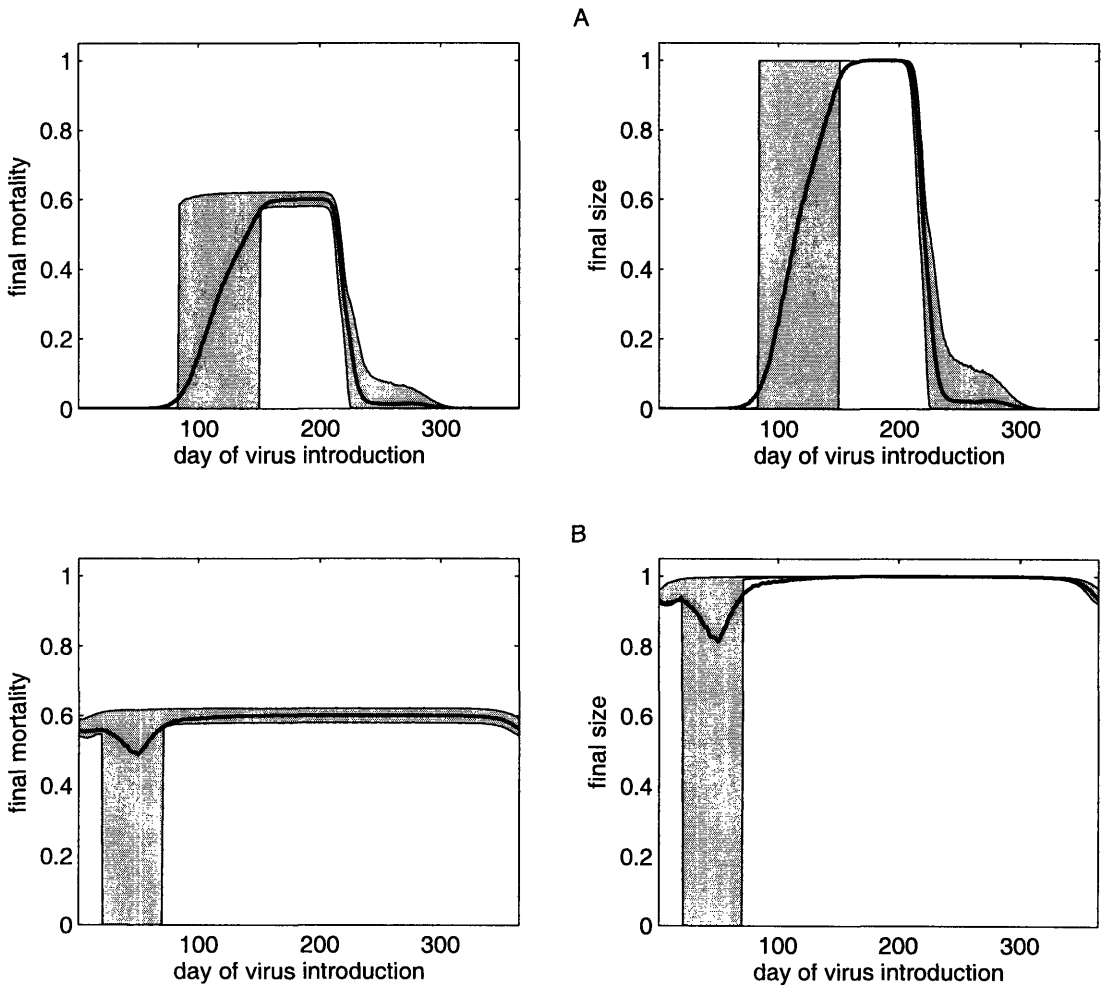

Figure 3-6: Seasonal haul-out behavior and the timing of the virus introduction both influence the mortality observed at the end of the outbreak. For each day of the year I simulated 10,000 epidemic trajectories using that day as the day of virus introduction. I summarize the final mortality and final size (total number infected during an outbreak) observed in those 10,000 simulation with the mean (solid line) and with the 5th and 95th percentile (gray envelope). $S_0 = 1500$, $p_h = 0.005$, $m = 0.6$. A) sandy regions, B) rocky regions.

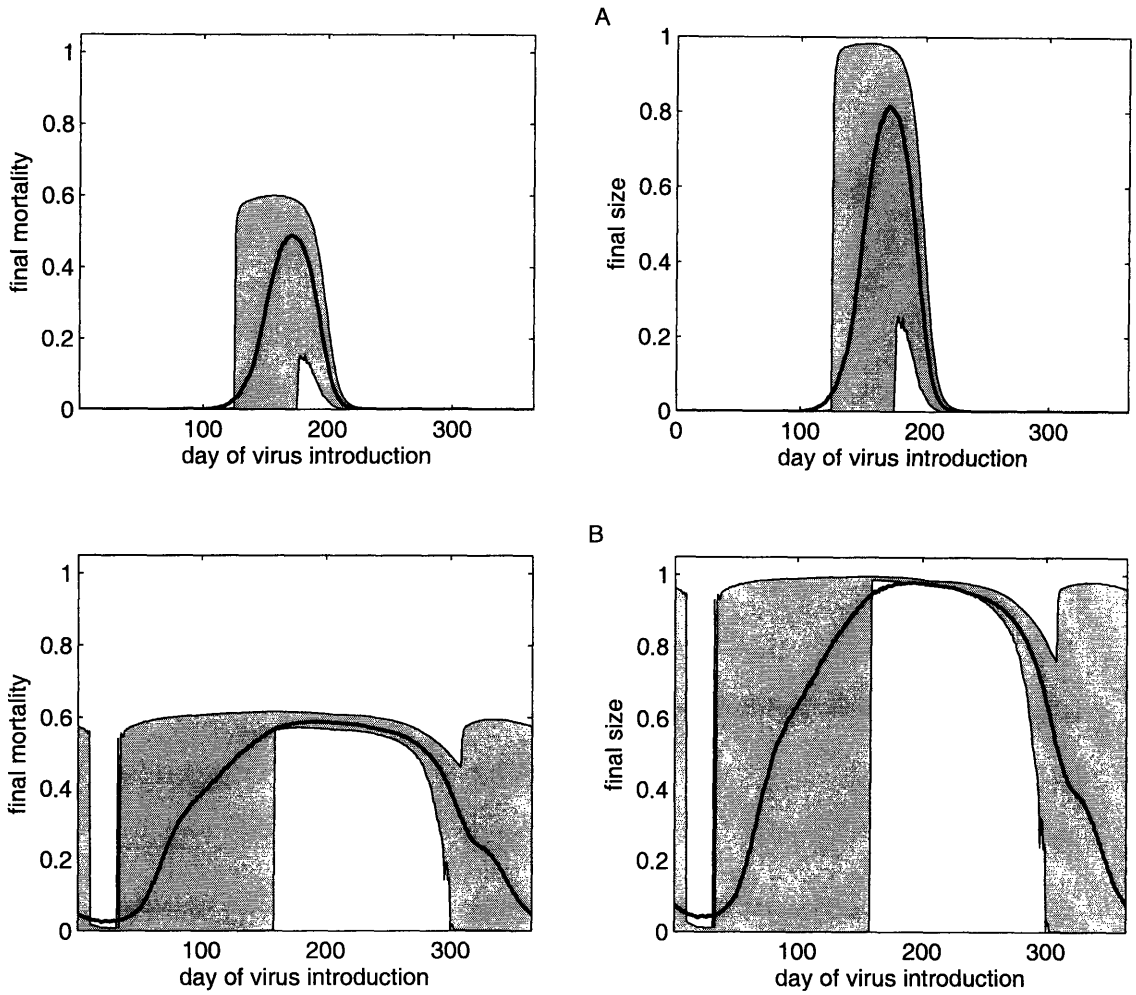

Figure 3-7: Seasonal haul-out behavior and timing of the virus introduction influence the mortality observed at the end of the outbreak. For each day of the year I simulated 10,000 epidemic trajectories using that day as the day of virus introduction. I summarize the final mortality and final size observed in those 10,000 simulation with the mean (solid line) and with the 5th and 95th percentile (gray envelope). $S_0 = 1500$, $p_h = 0.001$, $m = 0.6$. A) sandy regions, B) rocky regions.

each day of the virus introduction, I simulate 10,000 epidemic trajectories 300 days long. The last point of each trajectory provides the final mortality. For each starting day of the outbreak, I get 10,000 values of the final mortality. I summarize those values of final mortality for different values of p in Figures 3-6 and 3-7 with the mean value (solid line), and the envelope defined by the 5th and 95th percentile.

In the winter (the beginning and the end of the year; approximate Julian days 0-100, 350-365), there is virtually no possibility of an outbreak as only a small number of seals are hauled-out on land. In the spring, the number of seals on land increases, and we can observe outbreaks of various final sizes. In the summer, the majority of the population is hauled out, the final size is determined by the law of large numbers and we can observe major outbreaks. The mean final size of outbreaks gradually decreases in the fall. In short, for sandy haul-out pattern, and parameters used in simulations, there can be no outbreaks in the winter, whereas at other times of the year there can be outbreaks of various final sizes. In the rocky regions, seals are hauled-out in large numbers throughout the year, so the possibility of a large outbreak exists year-round.

Qualitatively similar dynamics are observed for different probability of transmission p — the final size of infection is smaller in the winter than in the summer, and for the same initial infection date the size of the outbreak is larger in the rocky than in sandy regions. For smaller value of p (Figure 3-7) the final size of the outbreaks in the rocky regions drops in the winter, and the envelope defined by the 5th and 95th percentile becomes wider.

It is intuitive that when haul-out behavior varies with season, the expression for $\mathcal{R}_0$ must incorporate the timing of the outbreak. Let t_0 be the day when the first infectious seal is introduced to an otherwise susceptible population of size s_0. The probability that this infectious seals is on land on day t_0 is equal to h_{t_0}, and the average number of new infections during day t_0 is $p\, s_0\, (h_{t_0})^2$. The probability that this infective is on land on its second day of infection is h_{t_0+1}. The average number of new infections on the second day of the infection is $p\, s_0\, (h_{t_0+1})^2$. Taking the sum of all the new infections caused by one infectious individual throughout its entire infectious period that lasts 12 days, gives

$$\mathcal{R}_0(t_0) = p\, s_0 \sum_{t=t_0}^{t_0+11} h_t^2 \tag{3.6}$$

that is different for different days of the year.

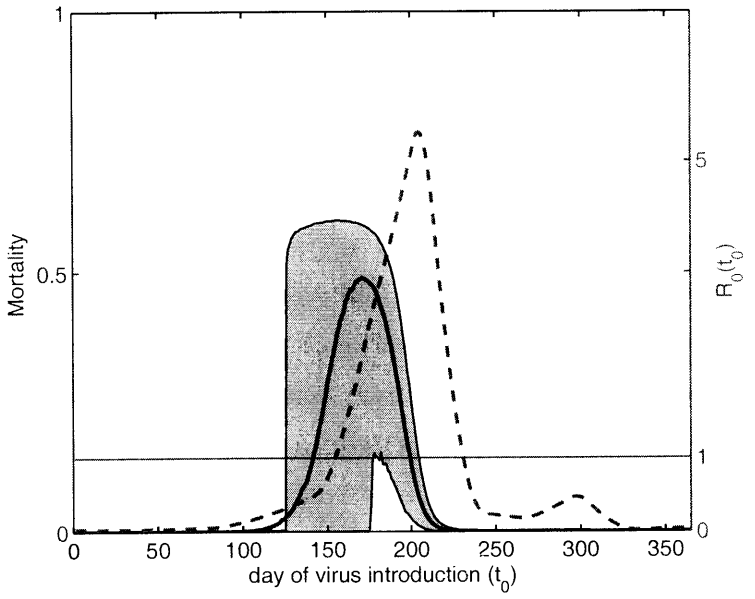

Figure 3-8: $\mathcal{R}_0(t_0)$ and the timing of virus introduction (dashed line). $S_0 = 1500$, $p_h = 0.001$, $m = 0.6$. Figure also shows the mortality (solid line) for sandy regions from Figure 3-7 and the threshold level $\mathcal{R}_0 = 1$ (horizontal line) for reference.

Figure 3-8 shows $\mathcal{R}_0$ against t_0 corresponding to the parameters of the sandy areas shown in Figure 3-7. We would expect that the region of elevated mortality corresponds with the region of graph where $\mathcal{R}_0(t_0) > 1$. However, it turns out that $\mathcal{R}_0$ predicts the final mortality poorly in this case, and increase in mortality occurs occurs before $\mathcal{R}_0$ reaches the levels beyond the threshold.

The graph 3-8 show the mortality at the end of a 300-day long outbreak. For example, take day 110 as the day the virus is introduced to the population. On day 110, I introduce one infected individual to an otherwise susceptible population and, for a given set of parameters, I simulate 10,000 epidemics each lasting 300 days. The mortality observed at the end of those 300 days is plotted in the graph with 110 on the x-axis.

The value of $\mathcal{R}_0(t_0)$ is calculated based on the haul-out levels during the infectious period; $\mathcal{R}_0(110)$ only accounts the haul-out levels during days 110-121. In the Figure 3-5, we can see that if the virus is introduced on day 110, some of the trajectories will result in an outbreak. However, the number of dead in these trajectories does not begin to increase until 100 days after the beginning of the outbreak (whereas the number of dead increases much sooner for days of introduction 160 and 200). This

late increase in number dead reflects the elevated fraction of the population hauled-out well after the introduction day. If the number of seals on land is low, the infection can linger in the population at a low level, and turn into an outbreak well after the initial infection day. Since the value of $\mathcal{R}_0(t_0)$ only incorporates the changes in h_t for the duration of one infectious period (12 days), it does not reflect the 'delay' in the increase in mortality.

3.3 Estimation of $\mathcal{R}_0$ from data

When the initial population size (s_0) the haul-out behavior and the date of the first infection are known, estimating $\mathcal{R}_0$ reduces to estimating the probability of infection p. The use of maximum likelihood methods for estimating p would require knowledge of the number of seals in each class for every day of the epizootic. Let t_0 be defined as above (day of virus introduction), and let t indicate the duration of the outbreak in days. The likelihood of an epidemic trajectory is

$$L(p) = \prod_{k=t_0}^{t_0+t} f\left(x_k|\underline{s}_k, 1-(1-p)^{i_k}\right), \tag{3.7}$$

where f is the binomial probability density function,

$$f(x \mid s,p) = \binom{s}{x} p^x (1-p)^{s-x}. \tag{3.8}$$

Had we observed the number of seals in each epidemic compartment throughout the outbreak, and the number of infectious and susceptible seals on land throughout the outbreak, we could calculate $L(p)$ and estimate the value of p, as the value $\hat{p}$ that maximizes this likelihood.

The only observation of the epidemic data in case of PDV is the information on the stranded carcasses. The number of seals that gets stranded and reported will depend on many factors such as the weather conditions and reporting effort, so it will include an observation error. The cumulative number of stranded seals provides the total number of seals that have died of distemper in a particular location. A more reliable way to obtain the total mortality is from the difference in census data before and after the outbreak. As in Chapter 2, I let the observation error be equal to the ratio of the total number recovered stranded seals to the difference in census

data. I assume the observation error is constant throughout the outbreak and scale the epidemic curve to match the total number of seals that died according to the population counts. The scaled daily counts of dead seals are then used to construct the estimates of $\hat{s}_t, \hat{x}_t$ and $\hat{i}_t$.

To reconstruct the series of incidence, I equated the observed mortality with its expectation under (2.26) and find

$$\hat{x}_t = \frac{y_{t+15}}{m}. \tag{3.9}$$

The incidence is integer-valued. Rounding $\hat{x}$ to the nearest integer introduces the possibility that the number of the total individuals infected is larger than the initial susceptible population size. Therefore, to keep $\hat{x}$ series in integer form, I round the right-hand side of the equation (2.30) to the nearest integer towards minus infinity using the MATLAB command `floor()`.

After obtaining $\hat{x}_t$, I use assumptions of the model (3.1) to reconstruct the series for susceptible seals

$$\hat{s}_{t+1} = \hat{s}_t - \hat{x}_t; \quad \hat{s}_1 = N. \tag{3.10}$$

and the series of infectious seals via

$$\hat{i}_t = \hat{i}_{t+1} - \frac{y_{t+12} - y_t}{m}; \quad \hat{i}_T = 0. \tag{3.11}$$

If the haul-out pattern h_t is known, we can use it together with $\hat{s}$ and $\hat{i}$ to estimate $\underline{\hat{s}}$ and $\underline{\hat{i}}$ by taking the expected value of (3.2),

$$\underline{\hat{s}}_t = \texttt{floor}(h_t\, \hat{s}_t), \tag{3.12a}$$

$$\underline{\hat{i}}_t = \texttt{floor}(h_t\, \hat{i}_t) \tag{3.12b}$$

We then treat estimates $\underline{\hat{s}}, \hat{x}, \underline{\hat{i}}$ as though they were actual observations and estimated $\hat{p}$ by maximizing the log-likelihood of the estimates

$$\ell(p) = \sum_{k=0}^{T} \ln \left[f\left(\hat{x}_k, \underline{\hat{s}}_k, 1 - (1-p)^{\underline{\hat{i}}_k} \right) \right]. \tag{3.13}$$

over p.

3.3.1 Accuracy and the precision of estimation

Figures 3-9–3-11 summarize the accuracy, precision, and the bias of the $\mathcal{R}_0$ estimates, for constant haul-out behavior and two different patterns of seasonal haul-out. In these figures, each box plot represents a summary of $\mathcal{R}_0$ estimates from 1,000 simulated epidemic trajectories with known parameters. The value of $\mathcal{R}_0$ used in simulated trajectories is indicated by a horizontal black line. When $\mathcal{R}_0 > 1$, the distribution of final sizes is bimodal, consisting of non-outbreaks and outbreaks. To unambiguously distinguish between an outbreak and a non-outbreak, I set a threshold of what constitutes an outbreak to be 20% of the expected deterministic final size $1 - \exp(-R_0)$, and discard any trajectories that did not reach this threshold.

As observed in the previous Chapter, the method is negatively biased. When haul-out behavior is present this bias is stronger, especially for small population size (100 individuals) and for small haul-out levels. For constant haul-out, estimates are more accurate, precise, and less biased for larger population sizes. When the haul-out behavior varies in time, the negative bias remains strong for the population sizes observed in the data set.

The main source of error is again a numerical one. In Chapter 2 main source of bias was in the round-off error in the reconstruction of the incidence data. In addition to underestimating incidence by rounding off the equation (3.9) to the nearest integer towards zero, there are two other round-off steps in equations (3.12) that further underestimate the transmission.

3.4 Application to phocine distemper data

After developing the model with the haul-out behavior, studying its dynamics, and deriving a method to estimate its epidemiological parameters, I want to apply this methodology to the available phocine distemper virus data. Here I focus on those seal populations for which both the haul-out data and the epidemic curves are available for both 1988 and 2002 outbreaks: Anholt, German Wadden Sea (WSNS), Dutch Wadden Sea (WSNL), and Moray Firth. The population sizes before the outbreaks for these locations, the total number of seals that have died, and initial infection dates are listed in Table 3.1.

The information on the probability of being on land, h_t, is obtained from the studies of the haul-out behavior of seals.

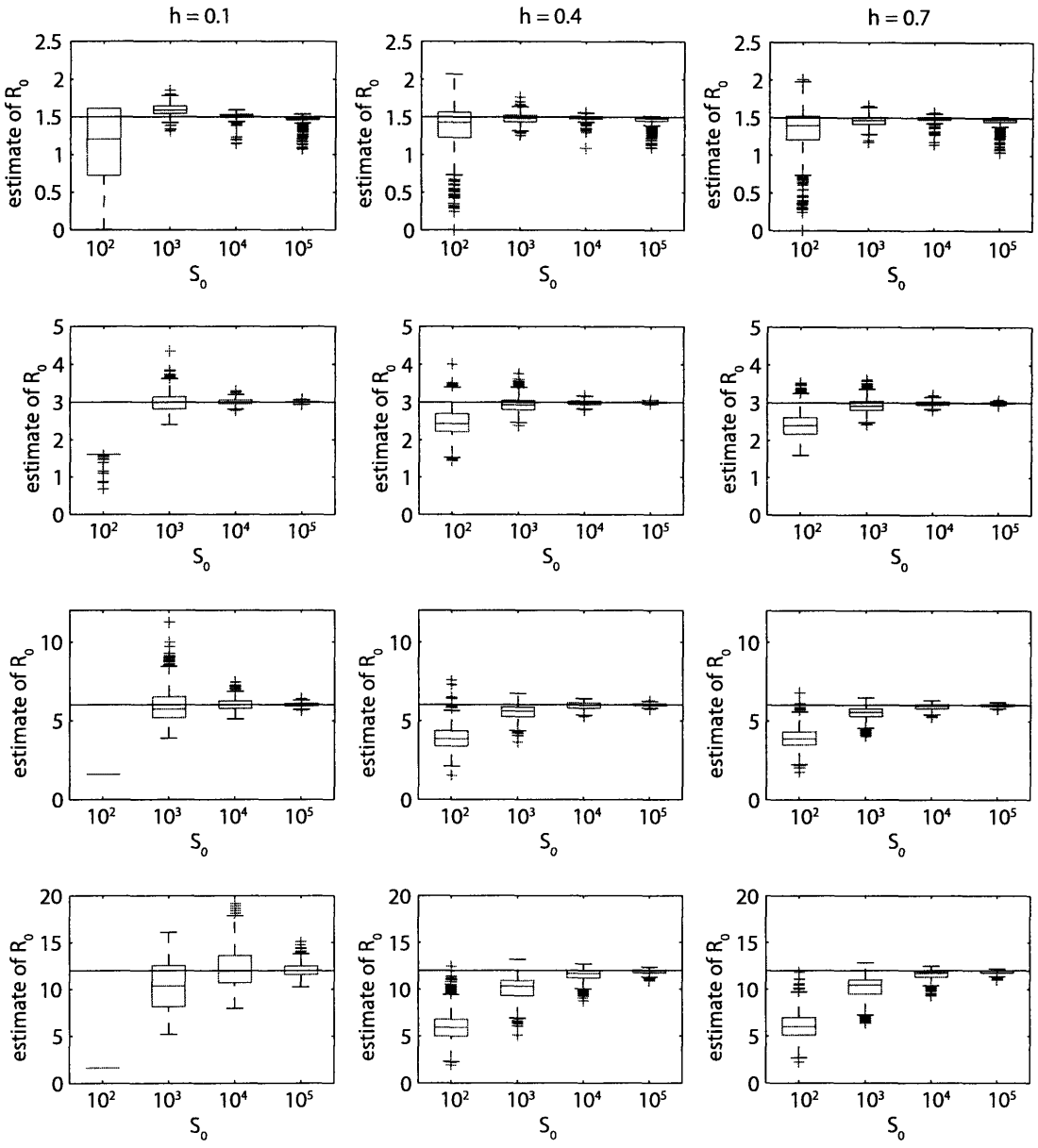

Figure 3-9: Estimation accuracy of the method for estimating $\mathcal{R}_0$ from epidemic curves of the model with constant haul-out, for various values of $\mathcal{R}_0$ and S_0. Each box plot represents a summary of estimates from 1,000 simulations using the $\mathcal{R}_0$ value indicated by the black horizontal line. The box represents the inter-quartile range of the estimates, and the red line is the median. The whiskers are lines extending from each end of the box to show the extent of the rest of the data; the maximum length of the whiskers is 1.5 times the inter-quartile range. Data that fall beyond the ends of whiskers are are shown with red plus signs.

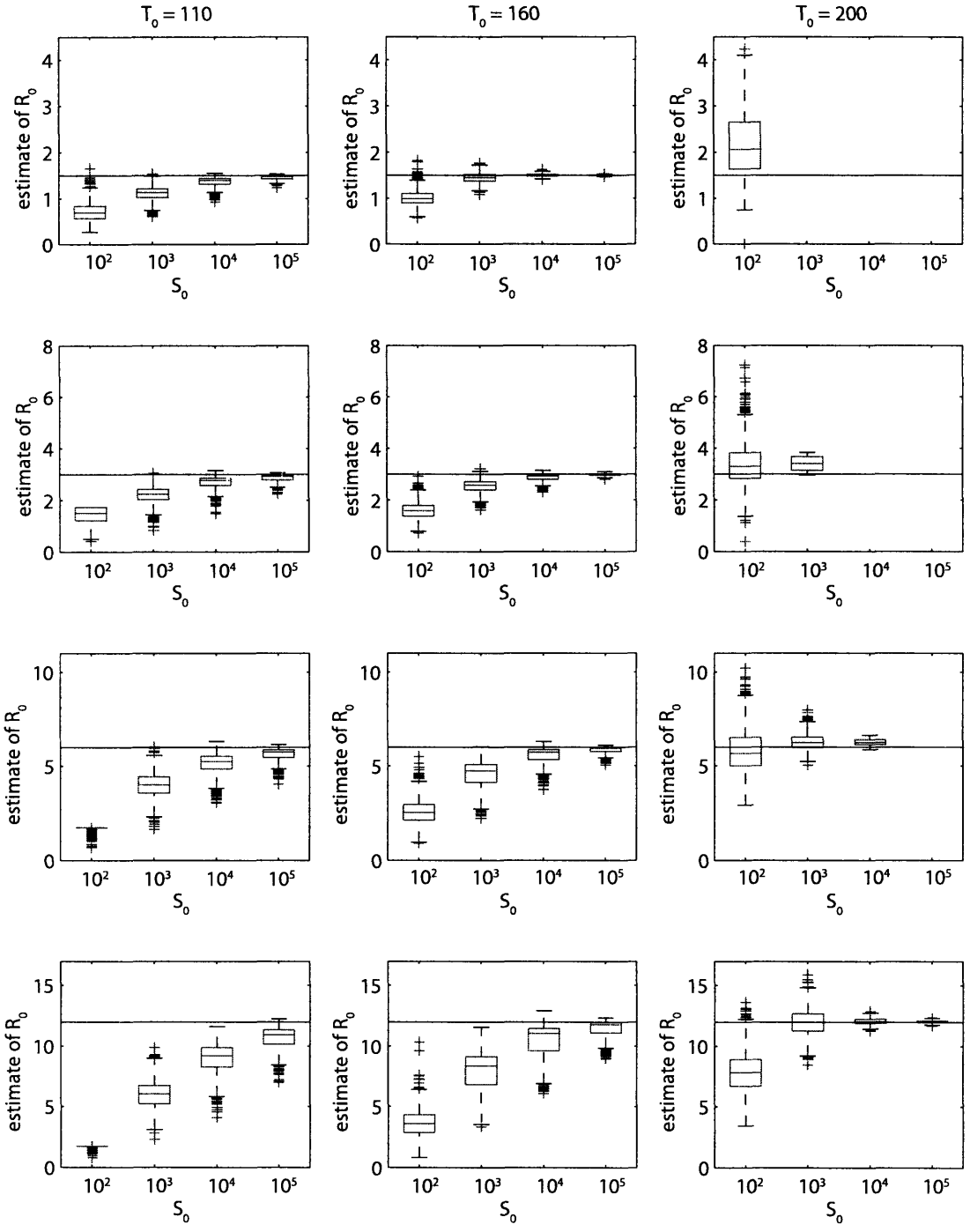

Figure 3-10: Estimation accuracy of the method for estimating $\mathcal{R}_0$ from epidemic curves of the model with haul-out pattern for sandy regions, for various values of $\mathcal{R}_0$ and S_0. Each box plot represents a summary of estimates from 1,000 simulations using the $\mathcal{R}_0$ value indicated by the black horizontal line. Box plots are constructed as described in Figure 3-9.

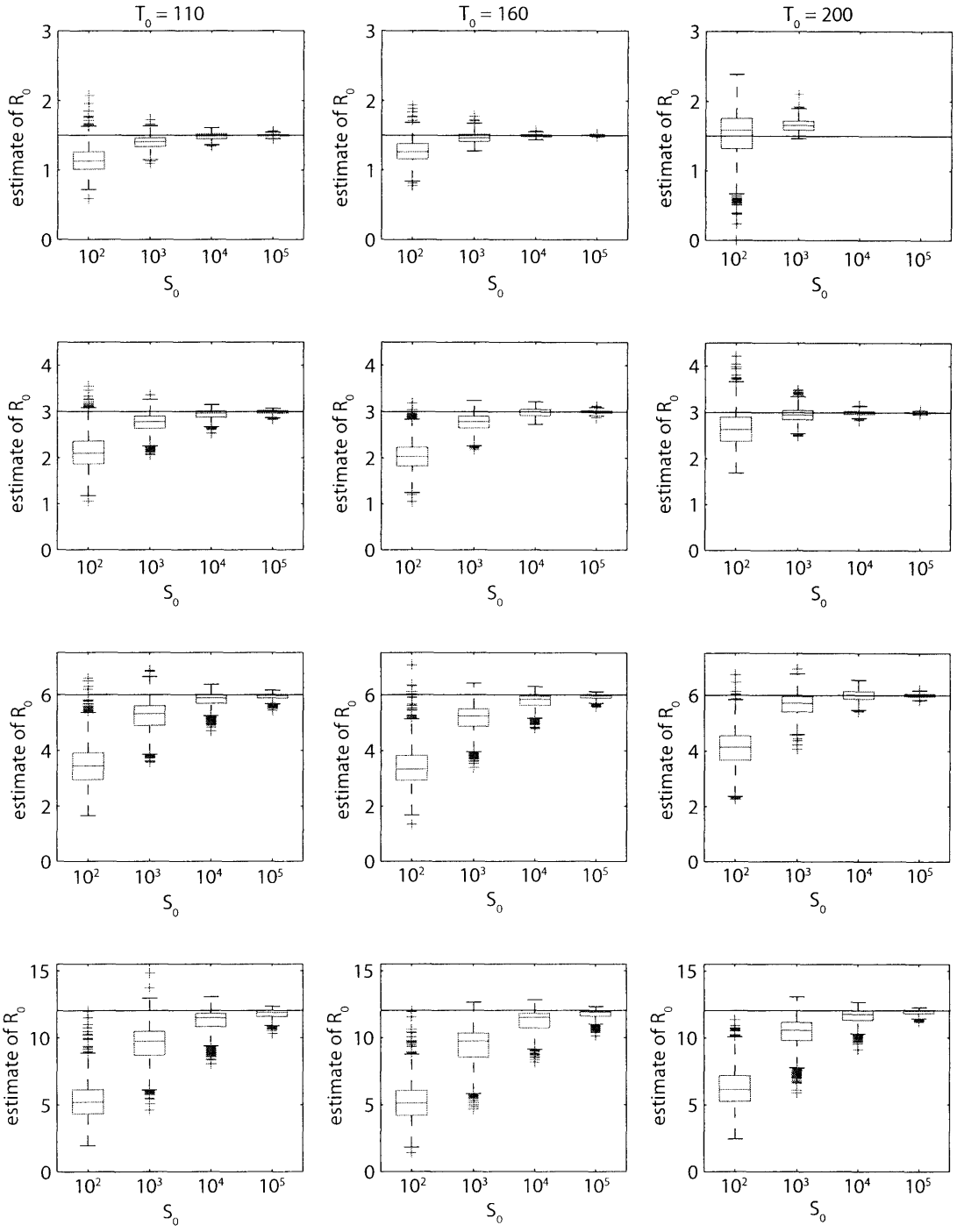

Figure 3-11: Estimation accuracy of the method for estimating $\mathcal{R}_0$ from epidemic curves of the model with haul-out pattern for rocky regions, for various values of $\mathcal{R}_0$ and S_0. Each box plot represents a summary of estimates from 1,000 simulations using the $\mathcal{R}_0$ value indicated by the black horizontal line. Box plots are constructed as described in Figure 3-9.

Table 3.1: Sizes of harbor seal populations before 1988 and 2002 PDV outbreaks for the regions whose epidemic and haul-out curves were used in estimating $\mathcal{R}_0$. $D(\infty)$ is the total number of seals that have died in each location, and t_0 designates the Julian day of 15 days before the day when the first dead seal was recovered in each location. Data provided by Karin Harding and Tero Härkönen.

	1988			2002		
	N	$D(\infty)$	t_0	N	$D(\infty)$	t_0
Anholt	863	477	88	1467	200	109
WSNS	4602	2633	147	10042	4689	183
WSNL	1800	914	149	7002	3251	152
Moray Firth	1598	93	178	1198	86	238

3.4.1 Haul-out behavior

Harbor seals have been studied at their haul-out sites for decades. During 1979-1986 aerial surveys were conducted simultaneously for Swedish and Danish haul-out locations, which were photographed in the peak haul-out season. Seals were later counted from the photographs (Heide-Jørgensen *et al.*, 1992; Härkönen *et al.*, 1999, 2002). The observations were reintroduced after the 1988 PDV outbreak.

Systematic observations and counts of seals have been carried out on Anholt since 1978 (Heide-Jørgensen & Härkönen, 1988). Sand dunes at the beaches where the seals haul out were used as platforms for observations. Seals were counted twice on every occasion, and the average number was reported. When several observations were reported for the same day, I consider only the maximum value for that day. Each year, the number of seals hauled-out peaks; Figure 3-12 shows the hauled-out data as a proportion of that maximum.

From telemetry studies of seals equipped with VHF transmitters, we can infer that the proportion of the total population hauled-out at maximum is between 65-71% excluding pups (Thompson *et al.*, 1997; Ries *et al.*, 1998; Härkönen *et al.*, 1999) or between 57-59% including pups and assuming that pups of the year haul out 10% of their time during surveys (Karin Harding, personal communication).

The four locations I am considering here, differ in the number of observations of haul-out behavior. For Anholt, there are 12 years worth of observations, for Dutch Wadden Sea there is only one year, whereas for Scotland and German Wadden Sea the data is in the form of monthly averages. In order to have the data for all locations in the same form, I calculate the monthly averages for Anholt and Dutch Wadden

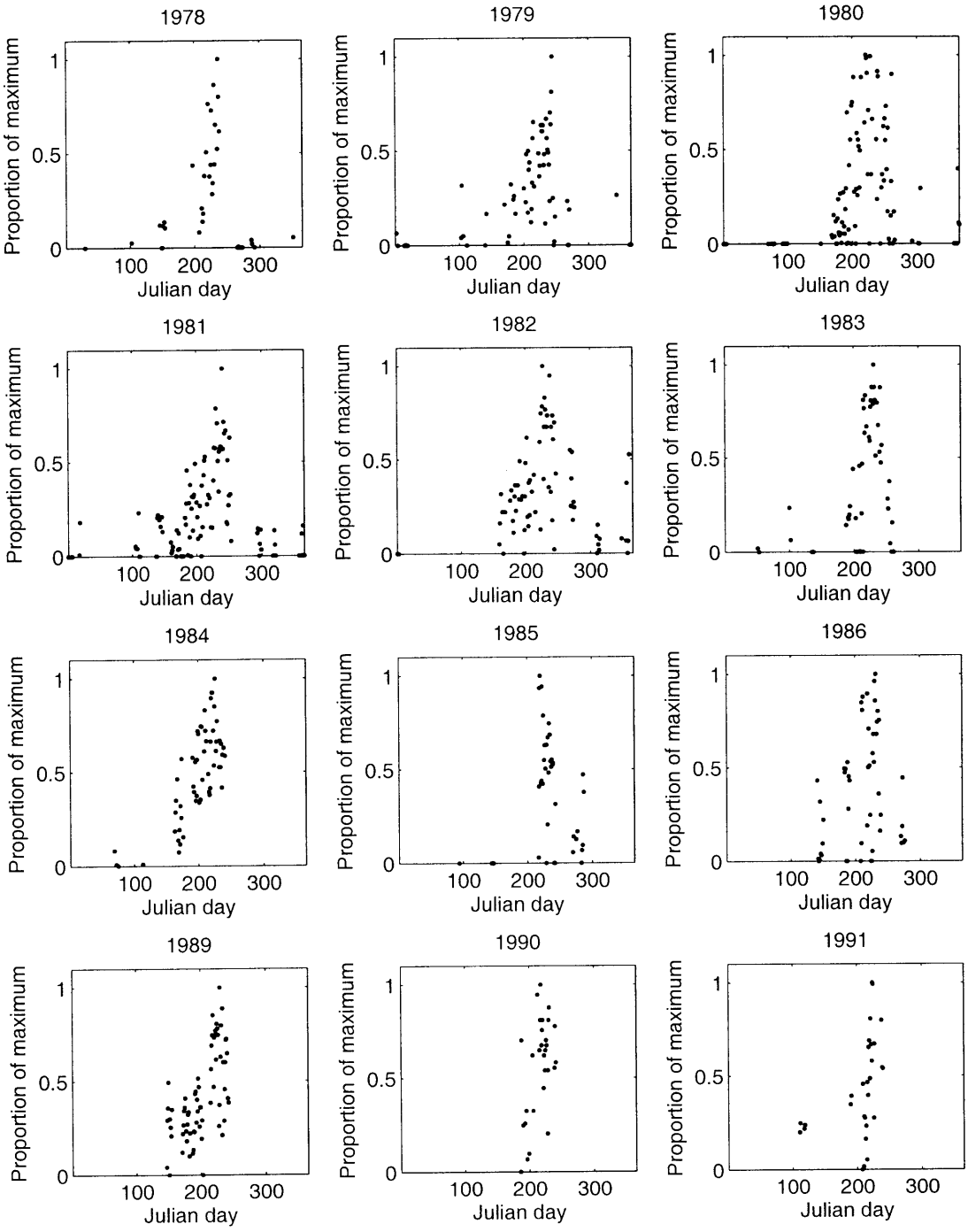

Figure 3-12: Observation data for haul-out behavior of seals on Anholt for the years 1978-1986 and 1989-1991.

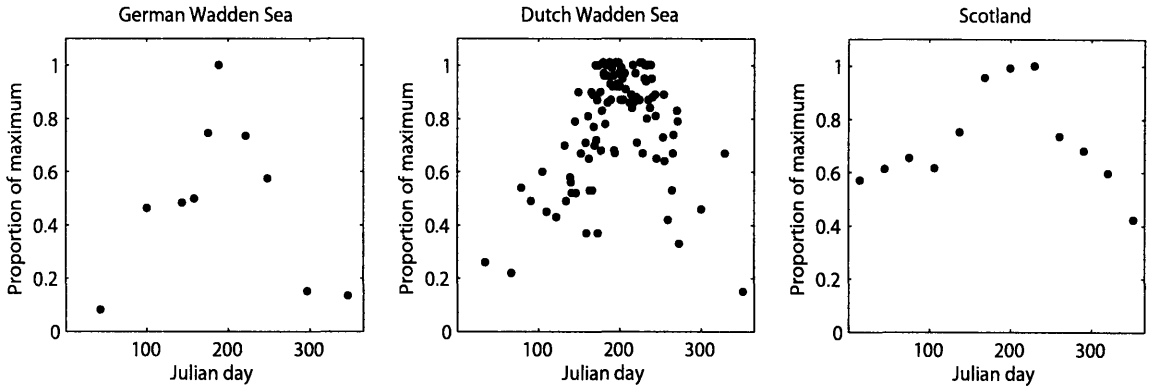

Figure 3-13: Haul-out data for German and Dutch Wadden Sea and Scotland

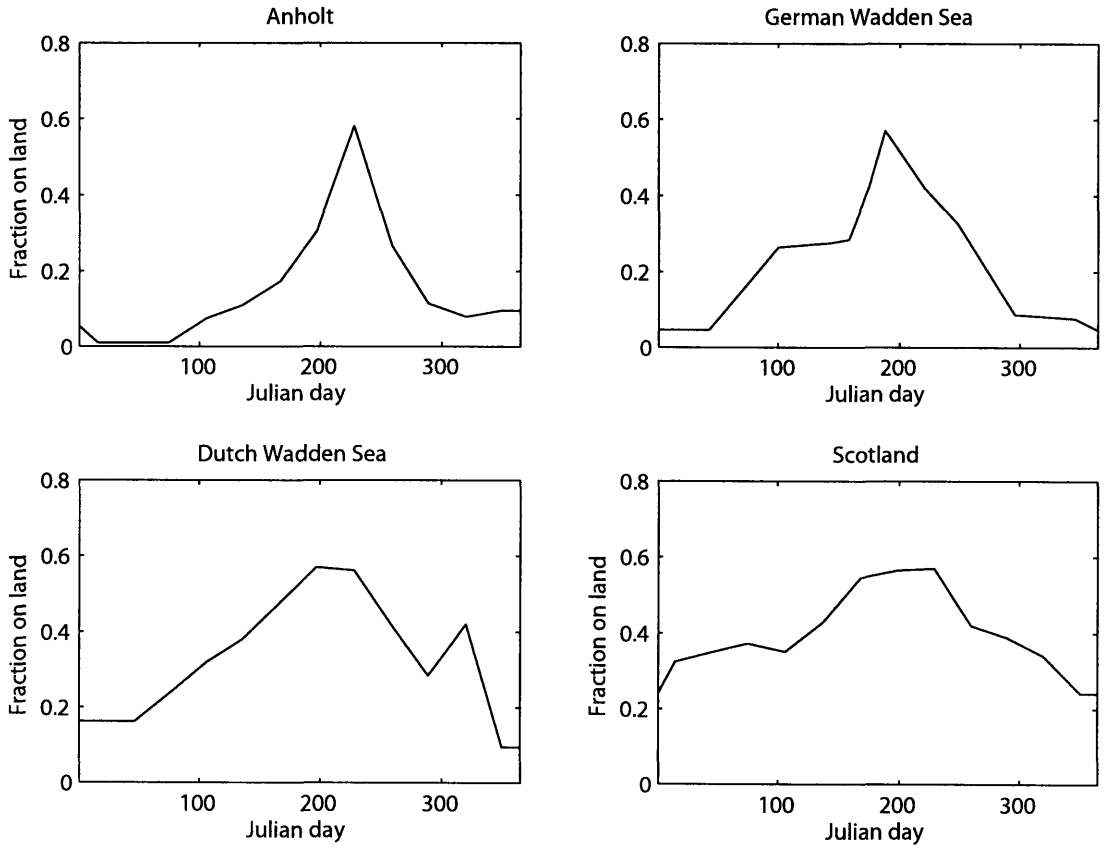

Figure 3-14: Monthly averages of haul-out data for Anholt, German Wadden Sea, Dutch Wadden Sea and Scotland.

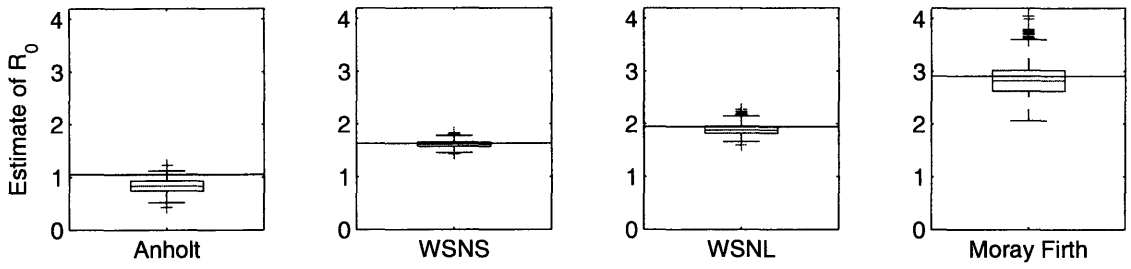

(a) 1988 outbreak

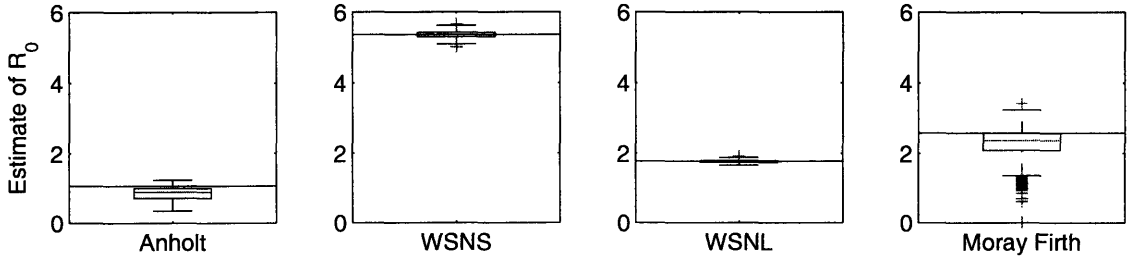

(b) 2002 outbreak

Figure 3-15: Estimation of $\mathcal{R}_0$ from epidemic curves and haul-out data for Anholt, Nieder-Sachsen Wadden Sea (WSNS), Dutch Wadden Sea (WSNL), and Moray Firth. Solid lines represent $\mathcal{R}_0$ values estimated from data, and box-plots illustrate accuracy and precision of the method, based on 1000 epidemic trajectories simulated for each location. Final size assumed to be equal to 1 in all plots.

Sea. In order to estimate the transmission probability for the model with haul-out behavior, we need to know h_t for every day of the year ($t = 1, \ldots, 365$). Therefore, I use linear interpolation to missing data points, and scale them so that the obtained haul-out curves in Figure 3-14 peak according to the telemetry levels.

3.4.2 $\mathcal{R}_0$ estimates for 1988 and 2002 PDV outbreaks

Using epidemic curves from Härkönen *et al.* (2006), population levels and t_0 values listed in Table 3.1, and the haul-out curves in Figure 3-14, I estimated $\mathcal{R}_0$ values for 1988 and 2002 PDV outbreaks for Anholt, German (Nieder-Sachsen region) and Dutch Wadden Sea, and Moray Firth. The probability of death m was calculated assuming that all seals become infected over the course of the outbreak (final size = 1). Table 3.2 summarizes $\mathcal{R}_0$ estimates with and without accounting for the haul-out behavior.

I evaluated the accuracy, precision and bias of each $\mathcal{R}_0$ estimate by simulating 1,000 epidemic trajectories using the values of parameters estimated for each location. Since the resulting trajectories consist of both non-outbreaks and outbreaks, I discard

Table 3.2: Comparison of the $\mathcal{R}_0$ estimates with and without accounting for haul-out behavior.

	1988			2002		
	m	no haul-out	haul-out	m	no haul-out	haul-out
Anholt	0.55	2.92	1.05	0.14	2.22	1.06
WSNS	0.57	2.51	1.17	0.47	2.71	5.36
WSNL	0.52	2.33	1.94	0.41	2.5	1.77
Moray Firth	0.06	2.19	2.91	0.07	1.62	2.66

any trajectories that did not reach the 20% of the expected deterministic final size $1 - \exp(-R_0)$. Estimates of $\mathcal{R}_0$ from the remaining simulated trajectories are shown with box plots in Figure 3-15 for both outbreaks.

The simulations suggest that bias is negative in Anholt and in Moray Firth for both 1988 and 2002. Further, the simulations suggest that $\mathcal{R}_0$ estimates are both more accurate and more precise for the Wadden Sea populations. This may be because the population size in the Wadden Sea is larger than in Anholt or Moray Firth, especially in 2002 when the German Wadden Sea population alone numbers over 10,000. Figures 3-9–3-11 all indicate the estimates are more accurate and more precise for large S_0.

The fractions of the population that died in the epidemic (I refer to this fraction as the final morality) vary among locations in both PDV outbreaks. Since each year PDV appeared only once in each location, we do not know whether the mortality within the location would also vary, had there been multiple outbreaks throughout the same year. To study how mortality would vary within a location for different days of virus introduction, I simulated multiple epidemic trajectories using the parameters for Anholt, WSNS, WSNL and Moray Firth corresponding to 1988 (Figure 3-16) and 2002 outbreak (Figure 3-17). For both outbreaks, the observations of mortality provide the probability of death m, so the data falls on the upper bound of the simulated trajectories.

In all locations, except for Moray Firth, in both the 1988 and the 2002 PDV-outbreak scenario the final mortality is zero at the beginning of the year, starts to increase between days 50 and 100, peaks around day 200, and drops back to zero at the end of the year. The peak in mortality occurs before the peak in the haul-out behavior. The mortality in the Moray Firth, although small, is constant throughout the year. The final sizes of the simulated outbreaks start also at zero at the beginning of the year, begin to increase after day 50, peak before 200, and then drop down to

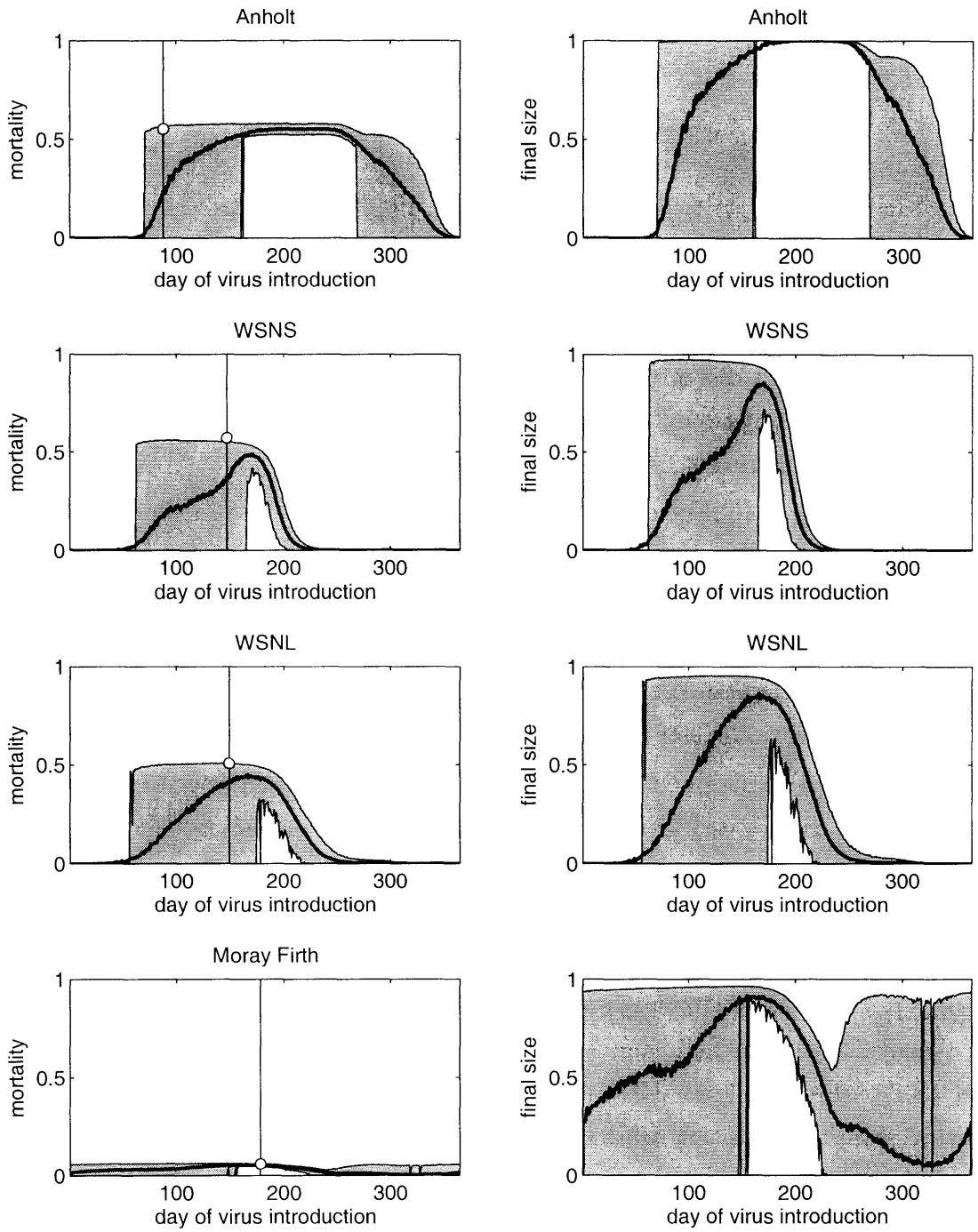

Figure 3-16: Simulations of PDV outbreaks for Anholt, WSNS, WSNL, and Moray Firth using the parameters corresponding to the 1988 outbreak (Tables 3.1 and 3.2). For each day of the year I simulated 1,000 epidemic trajectories using that day as the day of virus introduction, and summarized the final mortalities and final sizes with the mean (solid line) and with the 5th and 95th percentile (gray envelope). Vertical line and the circle represent 15 days before the first dead seal was found and observed final mortality in each location.

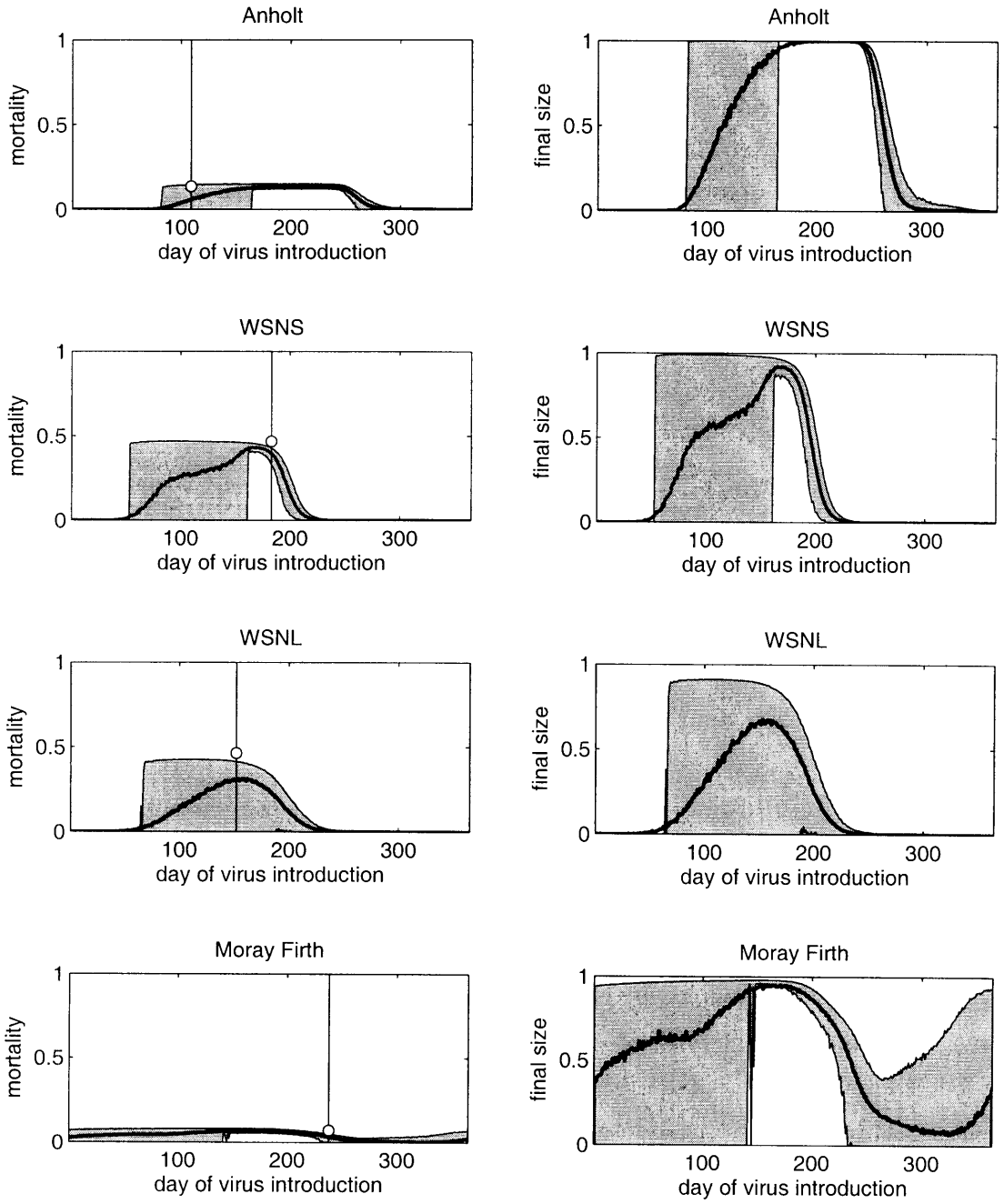

Figure 3-17: Simulations of PDV outbreaks for Anholt, WSNS, WSNL, and Moray Firth using the parameters corresponding to the 2002 outbreak (Tables 3.1 and 3.2). For each day of the year I simulated 1,000 epidemic trajectories using that day as the day of virus introduction, and summarized the final mortalities and final sizes with the mean (solid line) and with the 5th and 95th percentile (gray envelope). Vertical line and the circle represent 15 days before the first dead seal was found and observed final mortality in each location.

zero. But, in the Moray Firth, almost all values of final sizes are possible throughout the year, which is why mortality is positive throughout the year in that location. Since the haul-out levels are well beyond zero throughout the year in the Moray Firth, there is enough interaction between the seals to promote the transmission of the virus year round. The level of mortality in Moray Firth is low because of the low probability of death, m, estimated for that location. It is only 6% whereas m is over 50% in other three locations for the 1988 outbreak.

In addition to variation in the final mortality throughout the year, Figures 3-16 and 3-17 point out there can be significant variation in mortality even for the same day of virus introduction. During the first half of the year, when the fraction of the population that is hauled-out increases, the envelope determined by the 5th and 95th percentiles is very wide and includes outbreaks of all possible final sizes. When the numbers on land are decreasing, this envelope is narrow and final sizes are distributed around some deterministic value. Even though the haul-out curve has a roughly symmetric shape, the envelopes are not symmetric. This is because the total number of infections does not depend only on the fraction of seals hauled-out on the initial infection day, but also on the fraction of seals hauled-out throughout the outbreak.

3.5 Discussion

The combination of the seasonal behavior of seals and the timing of the virus introduction alone can explain the large differences in mortality among regions. If the virus is introduced to the population in the winter when the population levels on land are low, there will be a small outbreak and the population will suffer low mortality. A large outbreak is most probable in the summer, before the number of the seals on land peaks.

The importance if the timing of the virus introduction and its influence on the mortality cannot be detected unless the seasonal behavior is present in the model. The importance of seasonality has been well documented for other diseases. For childhood diseases like measles and chicken pox, seasonality comes from the aggregation and dispersal of schoolchildren during and after the school year (*e. g.*, Anderson, 1996; Bjørnstad *et al.*, 2002). For vector-borne diseases such as malaria, the seasonality comes from the fluctuations in the mosquito, *i. e.*, vector, abundance (Anderson,

1996). In all of these examples, the seasonality influences the transmission of the disease and ignoring it can lead to wrong conclusions about the dynamics of the epidemic in the population.

Haul-out behavior and the timing of the virus introduction not only explain the variation in mortalities among regions, but can also explain the differences in the mortality between two outbreaks at the same location. Seasonality is not the only explanation for the difference in mortality among locations. Two other interpretations are: (i) Differences in mortalities are linked to pollution, because mortality rates are higher in regions with higher concentration of PCBs, pollutants known to suppress the immune system of many animals (Bergman *et al.*, 1992; Mortensen *et al.*, 1992; De Swart, 1995; de Koeijer *et al.*, 1998). (ii) Harbor seal populations are genetically differentiated, and different gene frequencies could lead to different susceptibility of different sub-populations and influence the mortality of local populations (Stanley *et al.*, 1996; Goodman, 1998).

Even though the combination of the seasonality of transmission and the timing of the virus introduction clearly play a substantial role in determining the final size and the final mortality of an outbreak, other factors cannot be entirely ruled out. Differences in pollution levels exist, and many pollutants have proven immunotoxic effects. Immunosuppressants, such as PCBs, and different inherent susceptibility to disease can elevate, or, in the case of decreased susceptibility, lower the levels of mortality predicted by the model. However, I think mortality levels "correcting" for immunosuppression and genetic differentiation would fall within or close to the bounds described by the model with seasonal behavior alone.

Contamination with organochlorines may, however, play an important role in determining the time a certain population takes to recover from such a serious mortality event, since organochlorine pollution can lower the reproductive success of seals (Reijnders, 1986, 2003). Growth rate of harbor seals is already constrained by a single birth per female per year (Härkönen & Heide-Jørgensen, 1990), so any further decrease in growth rate due to lowered reproduction success can lead to much slower recovery of the population which can be hazardous in the case of recurrent virus outbreaks.

References

Anderson, R. M. 1996. *AIDS in the World II: Global Dimensions, Social Roots, and Responses. The Global AIDS Policy Coalition.* Oxford University Press. Chap. The spread of HIV and sexual mixing patterns, pages 71–86.

Bergman, A., Järplid, B., & Svensson, B.M. 1990. Pathological findings indicative of distemper in European seals. *Vet. Microbiol.*, **23**, 331–341.

Bergman, A., Olsson, M., & Reiland, S. 1992. Skull-bone lesions in the Baltic grey seal (*Halichoerus grypus*). *Ambio*, **21**, 517–519.

Bjørnstad, O. N., Finkenstädt, B. F., & Grenfell, B. T. 2002. Dynamics of measles epidemics: estimating scaling of transmission rates using a time series SIR model. *Ecol. Monogr.*, **72**, 169–184.

de Koeijer, A., Diekmann, O., & Reijnders, P. 1998. Modelling the spread of phocine distemper virus among harbour seals. *Bull. Math. Biol.*, **60**, 585–596.

De Swart, R. L. 1995. *Impaired immunity in seals exposed to bioaccumulated environmental contaminants.* Ph.D. thesis, Erasmus University, Rotterdam.

Dietz, R., Heide-Jørgensen, M.P., & Härkönen, T. 1989. Mass deaths of harbour seals (*Phoca vitulina*) in Europe. *Ambio*, **18**, 258–264.

Goodman, S. J. 1998. Patterns of extensive genetic differentiation and variation among European harbour seals (*Phoca vitulina vitulina*) revealed using microsatellite DNA polymorphisms. *Mol. Biol. Evol.*, **15**, 104–118.

Hall, A., Law, R. J., Wells, D. E., Harwood, J., Ross, H. M., Kenedy, S., Allchin, C. R., Campbell, L. A., & Pomeroy, P. P. 1992. Organochlorine levels in common seals (Phoca vitulina) that were victims and survivors of the 1988 phocine distemper epizootic. *Science of the Total Environment*, **115**, 145–162.

Harding, K. C., Härkönen, T., & Caswell, H. 2002. The 2002 European seal plague: epidemiology and population consequences. *Ecol. Letters*, **5**(6), 727–727.

Härkönen, T., & Heide-Jørgensen, M. P. 1990. Comparative life histories of East Atlantic and other harbour seal populations. *Ophelia*, **32**, 211–235.

Härkönen, T., Harding, K. C., & Heide-Jørgensen, M. P. 2002. Rates of increase in age-structured populations: a lesson from the European harbour seals. *Can. J. Zool.*, **80**, 1498–1510.

Härkönen, T., Dietz, R., Reijnders, P., Teilmann, J., Harding, K., Hall, A., Brasseur, S., Siebert, U., Goodman, S.J., Jepson, P.D., Rasmussen, T.D., & Thompson, P. 2006. A review of the 1988 and 2002 phocine distemper virus epidemics in European harbour seals. *Dis. Aquat. Org.*, **68**, 115–130.

Härkönen, Tero, Harding, Karin C., & Lunneryd, Sven Gunnar. 1999. Age- and sex-specific behaviour in harbour seals *Phoca vitulina* leads to biased estimates of vital population parameters. *J. Appl. Ecology*, **36**(5), 825–825.

Heide-Jørgensen, M. P., & Härkönen, T. 1988. Rebuilding seal stocks in the Kattegat-Skagerrak. *Mar. Mamm. Sci.*, **4**, 231–246.

Heide-Jørgensen, M. P., & Härkönen, T. 1992. Epizootiology of the seal disease in the eastern North Sea. *Journal of Applied Ecology*, **29**, 99–107.

Heide-Jørgensen, M. P., Härkönen, T., Dietz, R., & Thompson, P. M. 1992. Retrospective of the 1988 European seal epizootic. *Diseases of Aquatic Animals*, **13**, 37–62.

Kennedy, S. 1990. A review of the 1988 European seal morbillivirus epizootic. *Vet. Rec.*, **127**, 563–567.

Kennedy, S. 1998. Morbillivirus infections in aquatic mammals. *J. Comp. Path.*, **119**, 210–205.

Kennedy, S. 1999. Morbilliviral infections in marine mammals. *Journal of Cetacean Research and Management*, **1**, 267–273.

Mortensen, P., Bergman, A., Hansen, H. J. H., Härkönen, T., & Olsson, M. 1992. Prevalence of skull lesions in harbour seals *Phoca vitulina* in Swedish and Danish museum collections during the period 1835-1988. *Ambio*, **21**, 520–524.

Osterhaus, A. D. M. E. 1988. Seal death. *Nature*, **334**, 301–302.

Osterhaus, A. D. M. E., UytdeHaag, F. G. C. M., Visser, I. K. G., Vedder, E. J., Reijnders, P. J. H., Kuiper, J., & Brugge, H. N. 1989a. Seal vaccination success. *Nature*, **337**, 21.

Osterhaus, A.D.M.E., & Vedder, E.J. 1988. Identification of virus causing recent seal deaths. *Nature*, **335**, 20.

Osterhaus, A.D.M.E., UytdeHaag, F.G.C.M., Visser, I.K.G., Bildt, M.W.G.v.d., Bergman, A., & Klingeborn, B. 1989b. Distemper virus in Baikal seals. *Nature*, **338**, 209–210.

Reijnders, P. J. H. 1986. Reproductive failure in common seals feeding on fish from polluted coastal waters. *Nature*, **324**, 456–457.

Reijnders, P. J. H. 2003. *Toxicology of Marine Mammals. New Perspectives: Toxicology and Environment.* Taylor & Francis. Chap. Reproductive and developmental effects of environmental organochlorines on marine mammals, pages 55–66.

Ries, Edith H., Hiby, Lex R., & Reijnders, Peter J. H. 1998. Maximum Likelihood Population Size Estimation of Harbour Seals in the Dutch Wadden Sea Based on a Mark-Recapture Experiment. *The Journal of Applied Ecology*, **35**(2), 332–339.

Stanley, H. F., Casey, S., Carnahan, J. M., Goodman, S., Harwood, J., & Wayne, R. K. 1996. Worldwide patterns of mitochondrial DNA differentiation in the harbour seal. *Mol. Biol. Evol.*, **13**, 368–382.

Thompson, P. M. 1989. Seasonal changes in distribution and composition of common seal (*Phoca vitulina*) haul-out groups. *J. of Zoology*, **217**, 281–294.

Thompson, Paul M., Tollit, Dominic J., Wood, David, Corpe, Heather M., Hammond, Philip S., & Mackay, Ann. 1997. Estimating Harbour Seal Abundance and Status in an Estuarine Habitat in North-East Scotland. *The Journal of Applied Ecology*, **34**(1), 43–52.

Chapter 4

Mathematical epidemiology of HIV/AIDS in Cuba during the period 1986-2000

Brandy Rapatski,[1] Petra Klepac,[1] Stephen Dueck, Maoxing Liu, Leda Ivic Weiss

Rapatski, B., Klepac, P., Dueck, S., Liu, M. and L. I. Weiss. 2006. Mathematical epidemiology of HIV/AIDS in Cuba during the period 1986-2000. *Mathematical Biosciences and Engineering* **3**(3):545–556.

[1]authors contributed equally

Abstract

The dynamics of HIV/AIDS epidemics in a certain region is determined not only by virology and virus transmission mechanisms, but also by region's socioeconomic aspects. In this paper we study the HIV transmission dynamics for Cuba. We modify the model of Arazoza & Lounes (2002) according to the background about the virology, as well as the socioeconomic factors that impact the epidemiology of the Cuban HIV outbreak. The two main methods for detection of HIV/AIDS cases in Cuba are 'random' testing and contact tracing. As the detection equipment is costly and depends on biotechnological advances, the testing rate can be changed by many external factors. Therefore, our model includes time-dependent testing rates. By comparing our model to the 1986-2000 Cuban HIV/AIDS data and de Arazoza and Lounes model, we show that socioeconomic aspects are an important factor in determining the dynamics of the epidemic.

4.1 Introduction

Human Immunodeficiency Virus (HIV) is a global problem with an estimated 40 million infected worldwide (UNAIDS, 2004). Population infectivity estimates range as high as 8.5% for Sub-Saharan Africa, and as low as less than 0.1% for East Asia and Australia/New Zealand. Cuba, in this respect, is remarkable as its infectivity is estimated as less than 0.1% despite its status as a relatively resource-poor nation (Kirkpatrick, 1997; AAW, 2005). The understanding of Cuban HIV/AIDS infectivity dynamics may assist the design of preventive and reactive measures to HIV in countries with high HIV prevalence. This hypothesis is supported by Cuba's well-developed health care system despite its resource limitations (Kirkpatrick, 1997; AAW, 2005).

The purpose of this paper is to develop a new model that explains the dynamics of HIV/AIDS epidemic in Cuba, focusing on the period of 1986-2000. We built our model upon the work of Arazoza & Lounes (2002) and we confront both models with the available data (Arazoza & Lounes, 2002). We begin with a review of the virology of HIV/AIDS within the socioeconomic framework of Cuba 1986-2000 in Section 4.2. The formulation and brief analysis of the mathematical model follows in Section 4.3, as well as the comparison of the model with data. We finish with a discussion in Section 4.4.

Table 4.1: New cases of HIV, AIDS, AIDS-related deaths in Cuba 1986-2000 (Arazoza & Lounes, 2002).

Year	HIV-cases	AIDS-cases	Death due to AIDS
1986	99	5	2
1987	75	11	4
1988	93	14	6
1989	121	13	5
1990	140	28	23
1991	183	37	17
1992	175	71	32
1993	102	82	59
1994	122	102	62
1995	124	116	80
1996	234	99	92
1997	363	129	99
1998	362	150	98
1999	493	176	122
2000	545	251	142

4.2 Background

With a total population of 11 million, and less than 1000 infected, Cuba's HIV/AIDS epidemic is a small one. As part of the HIV/AIDS prevention program, Cuba has an active search of seropositives through the sexual contacts of known HIV-infected persons; this system is called contact tracing. Infected persons are also found through a 'blind' search of blood donors, pregnant women, persons with other sexually transmitted diseases, etc. (Arazoza & Lounes, 2002). Both methods are very successful in locating HIV-positive persons (Arazoza & Lounes, 2002). The numbers of newly diagnosed HIV cases, AIDS cases, and AIDS-related deaths per year in Cuba are detailed in Table 4.2 and plotted in Fig. 4-1 below Arazoza & Lounes (2002). However, fluctuations in these numbers are due to both the character of the HIV virus and the manner in which the Cuban population has been monitored for its presence. A model which does not distinguish between virology, the socioeconomic framework which this virology exists (i.e., the epidemiology), and how this framework has been observed, may generalize very poorly.

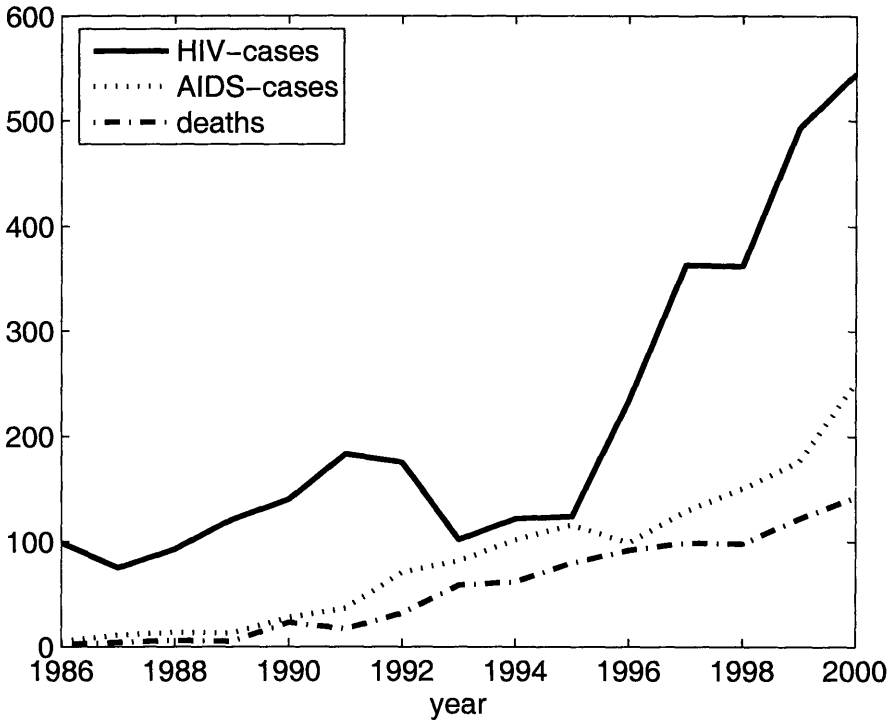

Figure 4-1: New cases of HIV, AIDS, AIDS-related deaths in Cuba 1986-2000 (Arazoza & Lounes, 2002).

4.2.1 Virology

An average HIV-infected individual progresses through distinct stages of the disease. The infectiousness (*i. e.*, the probability of transmission) varies greatly depending upon the stage of the disease. First comes a period of primary infection (lasting part of a year Ahlgren *et al.*, 1990). During the primary stage, infectiousness first rises and then drops. Seroconversion usually occurs before the end of the first year. HIV is an asymptomatic period (Ahlgren *et al.*, 1990, averaging 7 years without treatment) in which infectiousness is low. This is followed by a symptomatic stage (averaging three years until death without treatment Ahlgren *et al.*, 1990) where infectiousness rises again. Although toward the end of the symptomatic stage individuals are experiencing severe AIDS and activity is decreased, the symptomatic stage begins while individuals are relatively healthy and still very active. The average stage infectivity rates for semen has a of a small peak shortly after initial infection followed by a larger peak during the symptomatic phase (Rapatski *et al.*, 2005). This correlates with the changes in viral load observed as a person progresses through the disease (Pantaleo *et al.*, 1993; Clark *et al.*, 1991; Darr *et al.*, 1991; Anderson, 1996). This pattern is due to the physiology of the disease, the way the infected persons' bodies interact with the virus (Gray *et al.*, 2001; Saracco *et al.*, 1993; Piatak *et al.*, 1993; Vincenzi, 1994), and is largely independent of the sexual practices. In Cuba, most of the transmissions occur through sexual intercourse (about a 1:1 ratio of heterosexual to homosexual transmission, Holtz, n.d.; Hsieh *et al.*, 2001).

4.2.2 HIV in Cuba

Cuba treated the introduction of HIV into the country in 1986 as a public health emergency, introducing control measures to contain the spread of the disease. As a result, Cuba has one of the lowest prevalence rates of HIV infection in the world. Cuba's HIV prevalence of 0.03% is nearly 11 times lower than that of the United States (Perez-Stable, 1991; Burr, 1997). In 1986, Cuba introduced a national screening program. Cuba had a well-developed health care system that assigned a primary care physician to all citizens and conducted routine surveillance for infectious disease (Waitzkin *et al.*, 1997; Feinsilver, 1989). To reduce the risk of transmission Cuba instituted numerous measures, including contact tracing, isolation (quarantine) of HIV-infected individuals and a total ban on the import of blood and blood byprod-

ucts (Holtz, n.d.; Hsieh *et al.*, 2004). Initially, quarantine individuals lived in isolation in sanitariums. By 1993, patients could choose between living within a sanitarium or living at home. In the sanitariums, people are provided with good meals, a partial salary, free medications and care from physicians (Santana *et al.*, 1991). Most individuals could not provide the care necessary for them and therefore most choose to live in the sanitariums (Holtz, n.d.). Once a person is quarantined, they are no longer a factor in the transmission of the disease. Contact tracing in Cuba involves the search of HIV-positive persons through the sexual contacts of known HIV-infected individuals. This practice has proven to be quite effective in Cuba (Hsieh *et al.*, 2004). Since a significant fraction of those found to be HIV positive occur through contact tracing, a model of HIV in Cuba must allow for contact tracing.

HIV Data

To model the Cuban HIV epidemic, one has to acknowledge contact tracing and quarantines as well as any inconsistencies with the available data (Table 4.2, Figure 4-1). The first column in Table 4.2 represents those individuals that tested positive for HIV during that year; they may have acquired the disease some time before. The number of total HIV cases in column one includes both newly tested HIV-positives and the people in the AIDS stage. Because of this combination along with the aggressive testing of Cuba, we believe the AIDS data (column 3) to be more reliable than the HIV data. From Table 4.2, it appears as though from 1990-1992 there was an increase in the number of newly HIV infected persons. This increase was due to the discovery and contact tracing, from approximately 1990 to 1992, of a highly sexually active group (de Arazoza *et al.*, 2003). Because of a United States embargo in 1992, new HIV testing equipment was no longer available to Cuba (Holtz, n.d.), leading to a decrease in the number of newly HIV infected individuals being discovered that year. These two events are highlighted in Fig. 4-2 A model of the HIV epidemic in Cuba must account for these two significant events.

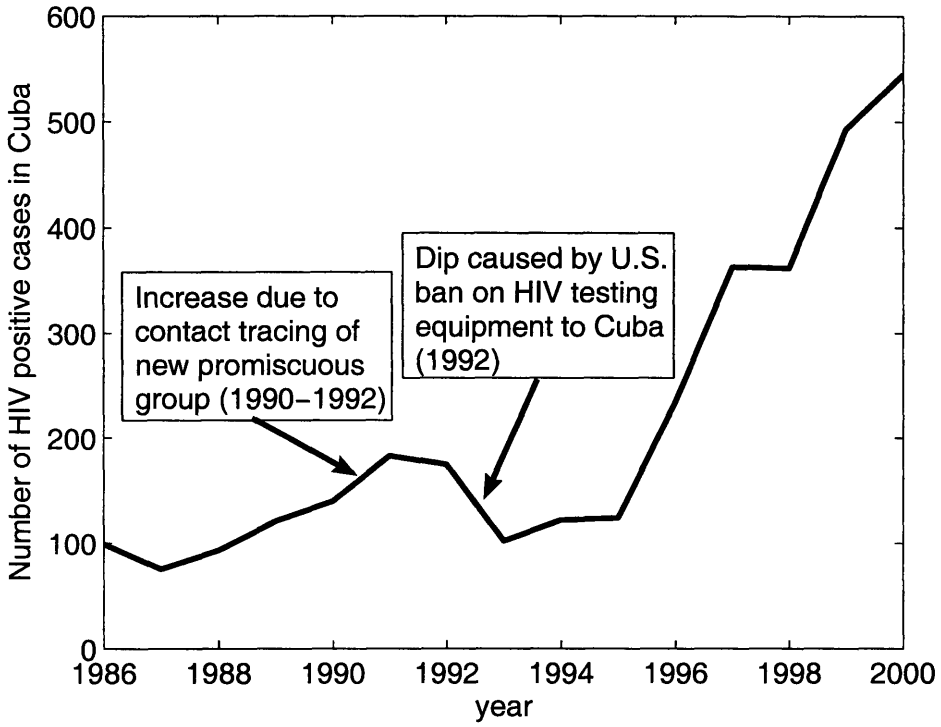

Figure 4-2: Socioeconomic factors that influenced diagnosis of HIV positive persons.

4.3 Mathematical models and analysis

4.3.1 Previous Model

De Arazoza and Lounes have modeled Cuba's HIV/AIDS epidemic. They consider three divisions of the population, undiagnosed HIV positive (U), diagnosed HIV positive (D), and AIDS (A) with the following constant coefficients (values listed in Table 2):

1. N, total size of the sexually-active population,
2. α, the rate of recruitment of new HIV-infected persons, infected by U,
3. α', the rate of recruitment of new HIV-infected persons, infected by D,
4. k_1, the rate at which the unknown HIV-infected persons are detected by the system ("random" search),
5. k_2, the rate at which the unknown HIV-infected persons are detected through contact tracing,

6. β, the rate at which the HIV positives develop AIDS,

7. μ, the mortality rate of the sexually active population,

8. μ', the mortality rate of the population with AIDS.

In this model there are two ways individuals can go from unknown HIV infected (U) to diagnosed HIV-infected (D), through contact tracing ($k_2 UD$)and detection through all other random searching for seropositives ($k_1 U$). Authors assume that the known HIV infected persons are infectious, but at a much lower rate than those that do not know they are infected.

Their model equations are:

$$U' = \alpha NU + \alpha' ND - (k_1 + \mu + \beta)U - k_2 UD, \tag{4.1a}$$

$$D' = k_1 U + k_2 UD - (\mu + \beta)D, \tag{4.1b}$$

$$A' = \beta(U + D) - \mu' A, \tag{4.1c}$$

4.3.2 Model Design

To improve upon the previous model by de Arazoza and Lounes, we have made three major changes:

1. We consider four divisions of the population, susceptible (S), undiagnosed HIV positive (U), diagnosed HIV positive (D), and AIDS (A). We considered this to be a closed population and all births equal deaths.

2. We incorporate the variation in infectivity as a person progresses through the disease, by considering the rate for a susceptible to be infected by an individual with AIDS, ω. With the aggressive "random" testing in Cuba, by the time individuals progress to the AIDS stage they have been diagnosed. Although individuals with AIDS are much more infectious than individuals with HIV (Rapatski *et al.*, 2005), an AIDS individual would have fewer contacts with susceptible persons compared to the contacts made by undiagnosed individuals with susceptibles thus, ω is lower than the rate for a susceptible to be infected by an undiagnosed HIV person, denoted α'. When comparing persons in the the AIDS stage and diagnosed HIV persons, since AIDS stage is more infectious, we assume the rate for a susceptible to be infected by an individual with AIDS, ω, to be higher than the rate of a diagnosed HIV positive individual, α'.

3. Undiagnosed individuals are diagnosed by their doctors at a rate k_1, and through contact tracing at a rate k_2. We consider three phases for contact tracing, 1986-1989, 1990-1991 and 1992-2000, and two phases for "random" testing, 1986-1991 and 1992-2000. In each period, k_1 and k_2 are constant. We estimate that during 1990 and 1991 contact tracing increased 25% because of the detection of a highly sexually active group, and that after 1992 diagnosis by doctors was reduced to 75% of its former value due to the United States embargo. We obtain values of k_1 and k_2 by fitting the Cuban HIV/AIDS data.

The dynamics of the Cuban HIV/AIDS epidemic are described by the following model:

$$\begin{aligned} S' &= -(\omega A + \alpha U + \alpha' D)S + \mu' A + \mu(U + D), && \text{(4.2a)} \\ U' &= (\omega A + \alpha U + \alpha' D)S - (k_1(t) + \mu + \beta)U - k_2(t)UD, && \text{(4.2b)} \\ D' &= k_1(t)U + k_2(t)UD - (\mu + \beta)D, && \text{(4.2c)} \\ A' &= \beta(U + D) - \mu' A, && \text{(4.2d)} \end{aligned}$$

This model holds within each of the periods. The initial conditions for each period are taken to keep the overall solution continuous (i.e., initial conditions are the final conditions for the previous period). Solutions to (4.2) with positive initial conditions remain positive for all periods. System (4.2) has a unique solution with initial conditions $(S(0), U(0), D(0), A(0)) = (5.5 \text{ million}, 230, 94, 3)$.

4.3.3 Numerical Results

Estimates of $k_1(t)$ and $k_2(t)$ are obtained by minimizing the following error function. For each of the fifteen years we compute the square of the difference between our model epidemic and the Cuban HIV data given in Table 4.2. Let RMS denote the square root of the average of those fifteen numbers,

$$RMS\,Error = \left[\frac{1}{15}\sum_{1986-2000}[D_{model}(t) - D_{HIV\,Data}(t)]^2\right]^{1/2}. \qquad (4.3)$$

We select the values of $k_1(t)$ and $k_2(t)$ that minimize RMS, by taking the gradient of the $(RMS\,Error)^2$ and using Newton's method to find a zero of the vector field. The parameter values are given in Table 4.2. The initial values for U, D and A

Table 4.2: Values of parameters used in simulations.

Parameter	Description	de Arazoza	Ours(Source)	
$S(0)$	Initial condition for Susceptibles	N/A	5.5 million (a)	
$U(0)$	Initial condition for HIV Undiagnosed	230	230 (b)	
$D(0)$	Initial condition for HIV Diagnosed	94	94 (b)	
$A(0)$	Initial condition for AIDS	3	3 (b)	
ω	Rate for a susceptible individual to become infected by an individual with AIDS	N/A	$8.5 \cdot 10^{-8}$ (c)	
α	Rate for a susceptible individual to become infected by an undiagnosed HIV+ individual	$9.3267 \cdot 10^{-8}$	$9.3267 \cdot 10^{-8}$ (b)	
α'	Rate for a susceptible individual to become infected by an diagnosed HIV+ individual	$5.4 \cdot 10^{-9}$	$5.4 \cdot 10^{-9}$ (b)	
β	Rate at which HIV+ individuals develop AIDS	0.10788	0.14 (d)	
μ	Mortality rate for HIV positive individuals	0.75	0.75 (b)	
μ'	Mortality rate for individuals with AIDS	0.0053	0.0053 (b)	
$k_1(t)$	'Random' testing rate performed by doctors	0.3743	1986-1991	0.3850 (e)
			1992-2000	0.2929 (e)
$k_2(t)$	Testing rate due to contact tracing	$2.27 \cdot 10^{-5}$	1986-1989, 1992-2000	$3.26 \cdot 10^{-5}$ (e)
			1990-1991	$5.89 \cdot 10^{-4}$ (e)

(a) UN (2005)
(b) Arazoza & Lounes (2002)
(c) Estimate based on α and α'
(d) Ahlgren *et al.* (1990)
(e) Estimate to fit data

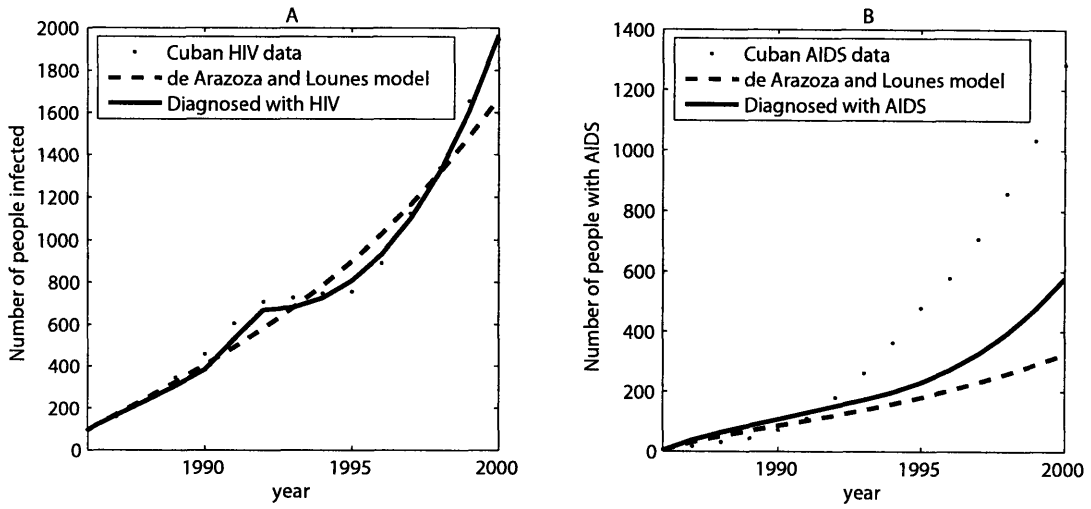

Figure 4-3: Comparison of model (4.2), and Arazoza & Lounes (2002) model with data for HIV positive cases in Cuba.

were chosen to be the same as those used in de Arazoza and Lounes (Arazoza & Lounes, 2002) and $S(0)$ was estimated to be 5.5 million (assuming half of the 11 million population (UN, 2005) are of a sexually active age). The resulting curves for both the diagnosed HIV cases and AIDS cases is shown in Fig. 4-3. We compared our model results with de Arazoza and Lounes model. As seen in Fig. 4-3, our model is a better fit to the data.

4.3.4 Basic reproduction ratio

The basic reproduction ratio, $\mathcal{R}_0$, is a dimensionless parameter that gives the expected number of secondary cases per primary case of infection in an entirely susceptible population. As a result, $\mathcal{R}_0$ has a threshold value equal to one, i. e., infection will spread and result in epidemic if $\mathcal{R}_0 > 1$, whereas the infection will die out if $\mathcal{R}_0 < 1$.

Model (4.2) has a disease free equilibrium (DFE), ε_0, given by

$$\varepsilon_0 : (S, U, D, A) = (S_0, 0, 0, 0). \tag{4.4}$$

$\mathcal{R}_0$ is calculated for constant values of k_1 and k_2, that is, there is an $\mathcal{R}_0$ for each time period. We are interested in looking at the stability of a simpler model of (4.2) with each k constant throughout. We are interested in the final period, with each k set to their final value.

From Diekmann *et al.* (1990), $\mathcal{R}_0$ is the spectral radius (ρ) of the next generation

matrix (see also van den Driessche & Watmough, 2002), $\mathbb{K}$,

$$\mathcal{R}_0 = \rho(\mathbb{K}), \tag{4.5}$$

where $\mathbb{K} = \mathbf{F}\mathbf{V}^{-1}$. $\mathbf{F}$ and $\mathbf{V}$ come from the Jacobian matrix of the linearization of (4.2) about the DFE. Here, non-negative matrix $\mathbf{F}$ shows new infections, and the inverse of the non-singular matrix $\mathbf{V}$ gives the expected times that individuals spend in each of the compartments. $\mathbf{F}$ and $\mathbf{V}$ are respectively given by

$$\mathbf{F} = \begin{pmatrix} \alpha S & \alpha' S & \omega S \\ 0 & 0 & 0 \\ 0 & 0 & 0 \end{pmatrix} \quad \text{and} \quad \mathbf{V} = \begin{pmatrix} k_1+\mu+\beta+k_2 D & 0 & 0 \\ -k_1-k_2 D & \mu+\beta & 0 \\ -\beta & -\beta & \mu' \end{pmatrix} \tag{4.6}$$

The basic reproduction ration for model (4.2) is then given by

$$\mathcal{R}_0 = \frac{S(0)}{\beta+\mu}\left(\frac{\alpha(\beta+\mu)+\alpha' k_1}{k_1+\mu+\beta} + \frac{\beta\omega}{\mu'}\right). \tag{4.7}$$

An advantage of considering $\mathcal{R}_0$ on a generation basis, is that we obtain expression (4.7) for $\mathcal{R}_0$ in terms of parameters of the model, which provides implications for the control of the epidemic which we discuss in Section 4.4.

Since we are interested in the simpler model where k's are constant throughout, our system becomes an autonomous system. The equilibrium ε_0 is locally asymptotically stable if $\mathcal{R}_0 < 1$ (van den Driessche & Watmough, 2002), and the population is not vulnerable to the outbreak of the disease. In the case when $\mathcal{R}_0 > 1$, the DFE is unstable so the disease can invade the population, eventually leading to an endemic equilibrium. These two types of dynamics are illustrated by simulations of model (4.2) in Figure 4-4.

4.4 Discussion

In this paper we present a new model for studying HIV/AIDS epidemic in Cuba, based on the de Arazoza and Lounes model (4.1). We modified their model in three ways. First, we allow for "random" testing rate (k_1) and contact tracing rate (k_2) to vary in time, in order to reflect the fluctuating socioeconomic situation in the country. Second, we assume that persons who developed AIDS can infect the susceptible individuals. Even though the people in the AIDS class have fewer sexual contacts

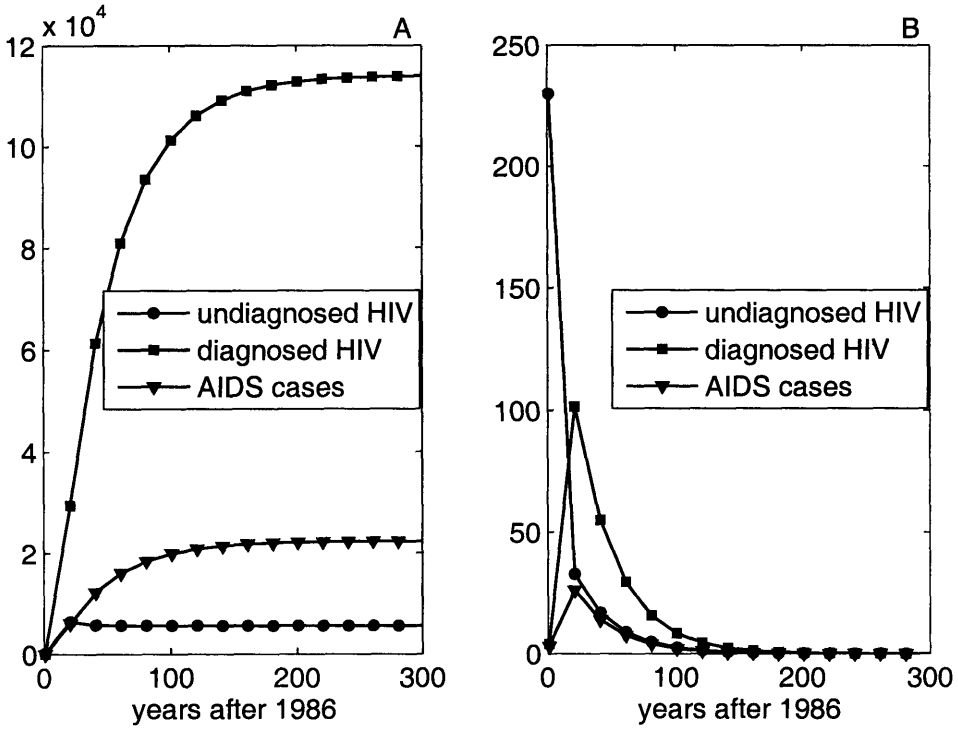

Figure 4-4: A) $\mathcal{R}_0 > 1$, the system reaches endemic equilibrium, B) $\mathcal{R}_0 > 1$, disease free equilibrium.

than the asymptomatic, HIV-positive individuals, symptomatic individuals are highly infectious. The viral load in the symptomatic (AIDS) stage can be up to 150 times higher than in the asymptomatic stage (Rapatski *et al.*, 2005), so the probability of transmission of HIV remains substantial in the symptomatic stage and we include it in the model (parameter ω). Lastly, since total population in Cuba is much greater (more than four orders of magnitude) than the number of people affected by HIV and AIDS, Arazoza & Lounes (2002) assume that the susceptible population is constant in time, and thereby reduce a dimension in their system. We, on the other hand, model the changes in the susceptible class as well.

To test our model we have used the yearly HIV-positive, AIDS cases, and deaths due to AIDS in Cuba in the period 1986-2000 (Table 1 from Arazoza & Lounes (2002)). Data includes newly HIV-infected people, the number of people who developed AIDS symptoms, and the number of people who died from complications of AIDS. From the data we cannot infer the time of HIV-infection.

The current state of the HIV/AIDS epidemic in Cuba is described with the parameter values given in Table 4.2. For these values, $\mathcal{R}_0 > 1$, so the number of new, diagnosed and undiagnosed, HIV infections in Cuba is increasing. However, compared with $\mathcal{R}_0$ values for sub Saharan Africa (9.62 Rapatski *et al.*, submitted), and India (31 Rapatski *et al.*, submitted), $\mathcal{R}_0$ for the Cuban epidemic is very small.

As long as $\mathcal{R}_0$ remains greater than one, the HIV/AIDS epidemic will continue to spread in Cuba. Mechanisms that decrease the value of $\mathcal{R}_0$ in (4.7) below the threshold are the mechanisms that can put the epidemic under control. Equation (4.7) suggest two different ways of controlling the epidemic: increasing the rate at which unknown HIV-infected persons are detected (k_1), and decreasing the rate of infection (α).

Let us look at the two possible mechanisms of control more closely. Increasing the testing rate requires more effective, precise and affordable HIV-detection tests, and a thorough and systematic testing organized by the public health system. As increasing the detection rate depends on advances in biotechnology and the structure of the public health system, increasing testing rate enough to bring $\mathcal{R}_0$ below the threshold is unlikely at the moment. On the other hand, there are widely-available, affordable methods that decrease the infection rate, α. The proper usage of condoms has been shown to reduce the risk of transmission of HIV in two ways. Condom usage reduces the risk of transmission of HIV itself, but it also significantly reduces

the risk of transmission of other sexually transmitted infections (STIs). Since many STIs can cause abrasion of the genital skin and membranes, STIs may facilitate both transmission and acquisition of HIV (Moss *et al.*, 1987). Given that less than a third of people use condoms with their non-regular partners (Gardner *et al.*, 1999), increased condom usage is a promising measure against future spread of HIV/AIDS epidemic in Cuba.

References

2005 (March). *Denial of food and medicine: the impact of the US embargo on health and nutrition in Cuba. Executive summary, American Association of World Health (AAWH).* Available from: http://www.cubasolidarity.net/aawh.html.

2005. *World Population Prospects: The 2004 Revision and World Urbanization Prospects.* Population Division of the Department of Economic and Social Affairs of the United Nations Secretariat. Accesed on 12 March, 2005.

Ahlgren, D. J., Gorny, M. K., & Stein, A. C. 1990. Model-Based Optimization of Infectivity parameters: A Study of the Early Epidemic in San Francisco. *J Acqr Immune Defic Syndr*, **3**, 631–643.

Anderson, R. M. 1996. *AIDS in the World II: Global Dimensions, Social Roots, and Responses. The Global AIDS Policy Coalition.* Oxford University Press. Chap. The spread of HIV and sexual mixing patterns, pages 71–86.

Arazoza, H. De, & Lounes, R. 2002. A non-linear model for sexually transmitted disease with contact tracing. *IMA Journal of Mathematics Applied in Medicine and Biology*, **19**, 221–234.

Burr, C. 1997. Assessing Cuba's approach to contain AIDS and HIV. *The Lancet*, **350**, 647.

Clark, S.J., Saag, M.S., Decker, W.D., Campbell-Hill, S., Roberson, J.L., Veldkamp, P.J., Kappes, J.C., Hahn, B.H., & Shaw, G.M. 1991. High titers of cytopathic virus in plasma of patients with symptomatic primary HIV-1 infection. *N Engl J Med*, **324**, 954–960.

Darr, E. S., Moudgil, T., Meyer, R. D., & Ho, D. D. 1991. Transient high levels of viremia in patients with primary human immunodeficiency virus type 1 infection. *N Engl J Med*, **324**, 961–964.

de Arazoza, H., Lounes, R., Perez, J., & Hoang, T. 2003. What percentage of the Cuba HIV-AIDS epidemic is known? *Revista Cubana de Medicina Tropical*, **55**, 30–37.

Diekmann, O., Hesterbeek, J. A. P., & Metz, J. A. J. 1990. On the definition and the computation of the basic reproduction ratio R_0 in models for infectious diseases in heterogeneous populations. *J. Math. Biol.*, **28**, 365–382.

Feinsilver, J. 1989. Cuba as a 'world medical power': the politics of symbolism. *Lat Ame Res Rev*, **24**, 1–34.

Gardner, R., Blackburn, R. D., & U. D. Upadhyay, et. al. 1999. *Population Reports.* Tech. rept. The Population Information Program, Center for Communication Programs, The Johns Hopkins School of Public Health.

Gray, R., Wawer, M. J., Brookmeyer, R., Sewankambo, N.K., Serwadda, D., Wabwire-Mangen, F., Lutalo, T., Li, X., vanCott, T., Quinn, T. C., & the Rakai Project Team. 2001. Probability of HIV-1 transmission per coital act in monogamous heterosexual, HIV-1-discordant couples in Rakai, Uganda. *The Lancet*, **357**, 1149–1153.

Holtz, T. *Summary of issue of HIV-AIDS in Cuba.* Avaliable from: http://www.cubasolidarity.net/cubahol2.html. Accessed on June 23, 2004.

Hsieh, Y.H., C.W.S., Chen, Lee, S., & de Arazoza, H. 2001. On the recent sharp increase in HIV detections in Cuba. *AIDS*, **15**, 426–428.

Hsieh, Y.H., de Arazoza, H., & Lounes, R. 2004. A class of methods for HIV contact tracing in Cuba: implications for intervention and treatment. *In press.*

Kirkpatrick, A. F. 1997. The US Attack on Cuba's health. *Canadian Medical Association Journal*, **157**, 281–284.

Moss, A. R., Osmond, D., Bachetti, P., Chermann, J.-C., Barre-Sinoussi, F., & Carlson, J. 1987. Risk factors for AIDS and HIV seropositivity in homosexual men. *American Journal of Epidemiology*, **125**, 1035–1047.

Pantaleo, G., Graziosi, C., & Fauci, A. S. 1993. Review article: the immunopathogenesis of human immunodeficiency virus infection. *N Engl J Med*, **328**, 327–335.

Perez-Stable, E. 1991. Cuba's response to the HIV epidemic. *American Journal of Public Health*, **81**, 563–567.

Piatak, M., Jr., Saag, M.S., Yang, L.C., Clark, S.J., Kappes, J.C., Luk, K.C., Hahn, B.H., Shaw, G.M., & Lifson, J.D. 1993. High levels of HIV-1 in plasma during all stages of infection determined by competitive PCR. *Science*, **259**, 1749–1754.

Rapatski, B. L., Suppe, F., & Yorke, J. A. 2005. HIV Epidemics Driven by Late Disease-Stage Transmission. *J Acqr Immune Defic Syndr*, **38**, 241–253.

Rapatski, B. L., Suppe, F., & Yorke, J. A. submitted. Determining the Virulence of HIV-1 Epidemics. *AIDS.*

Santana, S., Fass, L., & Wald, K. 1991. Human immunodeficiency virus in Cuba: the public health response of a third world country. *Internal Journal of Health Services*, **21**, 511–537.

Saracco, A., Musicco, M., Nicolosi, A., Angarano, G., Arici, C., Gavazzeni, G., Costigliola, P., Gafa, S., Gervasoni, C., Luzzati, R., Piccinino, F., Puppo, F., Salassa, B., Sinicco, A., Stellini, R., Tirelli, U., Turbess, G., Vigevani, G., Visco, G., Zerboni, R., & Lazzarin, A. 1993. Man-to-woman sexual transmission of HIV: Longitudinal study of 343 steady partners of infected men. *J Acqr Immune Defic Syndr*, **6**, 497–501.

UNAIDS. 2004 (December). *UNAIDS/WHO AIDS epidemic update.* Available online at http://www.unaids.org/wad2004/report.html.

van den Driessche, P., & Watmough, J. 2002. Reproduction numbers and subthreshold endemic equilibria for compartmental models of disease transmission. *Math. Biosci.*, **180**, 32–34.

Vincenzi, I. De. 1994. A longitudinal study of human immunodeficiency virus transmission by heterosexual partners. *The New England Journal of Medicine*, **331**, 341–346.

Waitzkin, H., Wald, K., & Kee, R. 1997. Primary care in Cuba: low and high technology developments pertinent to family medicine. *Journal of Family Practice*, **45**, 250–258.

Chapter 5

Stabilizing dispersal delays in predator–prey metapopulation models

Michael G. Neubert, Petra Klepac and P. van den Driessche

Neubert, M., Klepac, P., and P. van den Driessche. 2002. Stabilizing dispersal delays in predator–prey metapopulation models. *Theoretical Population Biology* **61**:339–347.

Contribution: Analysis of the Lotka-Volterra model with discrete delay.

Abstract

Time delays produced by dispersal are shown to stabilize Lotka-Volterra predator-prey models. The models are formulated as integrodifferential equations that describe local predator-prey dynamics and either intrapatch or interpatch dispersal. Dispersing individuals may (or may not) differ in the duration of their trip; these differences are captured via a distributed delay in the models. Our results include those of previous studies as special cases, and show that the stabilizing effect continues to operate when the dispersal process is modelled more realistically.

5.1 Introduction

Interest in the stability of predator-prey and host-parasitoid systems has continued unabated since the theoretical work of Lotka (1926), Volterra (1931), and Nicholson and Bailey (1935) and the experimental work of Gause (1934). The central question raised by their work is this: how do predator-prey systems apparently persist stably in nature when the most basic models and experiments predict instability? The answer most often given is that the models and experiments omit processes that affect stability in natural systems. To support this answer, theoreticians and experimentalists have proceeded to investigate the stability mediating effects of a long list of such processes (for examples see May 1973, Hassell 1978, Crawley 1992, and Mueller and Joshi 2000).

The basic theoretical tool in these investigations is the system of Lotka-Volterra equations for a prey with population density $N(T)$ and a predator with population density $P(T)$:

$$\frac{dN}{dT} = (R - AP)N, \tag{5.1a}$$

$$\frac{dP}{dT} = (BN - M)P. \tag{5.1b}$$

In the absence of predators, the prey population grows exponentially at the rate R, and in the absence of prey, the predator population decays exponentially at the rate M. The predator-prey interaction is captured by linear functional and numerical responses, scaled by the parameters A and B. The parameters R, A, B, and M are assumed to be positive.

The Lotka-Volterra predator-prey model is often criticized because its single, positive, equilibrium point is a center, i. e., a "neutrally stable" equilibrium surrounded

by a family of periodic orbits whose amplitudes depend on the initial population sizes. The slightest change to the model's structure typically results in qualitatively different behavior. For example, if R decreases linearly with prey density the equilibrium point is stable; on the other hand, introducing a saturating (Type II) functional response turns the equilibrium into an unstable spiral point (Gotelli 1995). This structural instability, the critics argue, means that the model cannot make any predictions that are robust enough to be tested. After all, we know that model (5.1) does not adequately describe even the most highly-controlled experiments.

Structural instability can, however, be used to our advantage. In effect, it allows us to use the Lotka-Volterra model as an exquisitely sensitive balance, with which we can determine the effects of the processes that it ignores. So, when we say that a Type II functional response is destabilizing, we mean that it destabilizes the equilibrium point in model (5.1). Similarly, when we say that the presence of carrying capacity for the prey tends to be stabilizing, we mean that it stabilizes the equilibrium point. There is a long tradition of using the Lotka-Volterra equations in this way (Murdoch and Oaten 1975), and we continue that tradition here.

Among the many processes that the Lotka-Volterra equations ignore, those with a spatial component have always attracted attention (Mueller and Joshi 2000). In particular, the presence of a metapopulation structure (i. e., locally interacting populations coupled via dispersal) can have interesting and variable effects (Hanski 1999). Taylor (1990) and Mueller and Joshi (2000) briefly review this topic.

The simplest metapopulation model consists of two habitat patches. A simple two-patch extension of the Lotka-Volterra model (5.1) is given by:

$$dN_i/dT = (R - AP_i)\,N_i + D_N[N_j - N_i], \tag{5.2a}$$

$$dP_i/dT = (BN_i - M)\,P_i + D_P[P_j - P_i], \tag{5.2b}$$

for $i = 1, 2$ and $j \neq i$ (Comins and Blatt 1974). The subscripts indicate the patch number; D_N and D_P are the prey and predator emigration rates.

Because predators are often more mobile than their prey, many authors have studied a simplified version of model (5.2) with $D_N = 0$. Jansen and de Roos (2000) provide a concise review of the dynamics of this model (also see Murdoch and Oaten 1975, Murdoch et al. 1992, Nisbet et al. 1992, Jansen 1995). When $D_P > 0$, there is a constant per capita predator migration rate between the patches. This coupling does not change the equilibrium values; there is a spatially homogeneous equilibrium with

population sizes in each patch equal to their sizes in the uncoupled case. Furthermore, coupling the two populations via predator dispersal does not change the stability of the equilibrium point. The equilibrium is surrounded by a planar family of unstable periodic solutions on the subspace defined by $N_1 = N_2$ and $P_1 = P_2$. Any initial differences in prey or predator population sizes between the two patches eventually disappear, so orbits converge to this plane. Large amplitude cycles in this plane are unstable to perturbations off the plane, while small amplitude orbits are stable to off-plane perturbations. There appear to be heteroclinic orbits connecting the large amplitude solutions to the small amplitude solutions. Thus perturbations to periodic orbits tend to result in periodic orbits of smaller amplitude. Only in this weak sense can predator dispersal (as described in model (5.2) with $D_N = 0$) be thought of as stabilizing. None of the periodic orbits is asymptotically stable (perturbations in the plane do not decay) and unless the initial condition is set exactly at the equilibrium value in each patch, the populations will ultimately cycle in synchrony.

So, predator dispersal by itself seems to be insufficient to stabilize the Lotka-Volterra predator-prey interaction. But the description of dispersal in model (5.2) is artificial in an important way: dispersers leaving one patch immediately appear in the other patch. In nature, dispersers take a finite amount of time to complete their trip. During this time, migrating individuals are typically not participating in the predator-prey interaction because the two species are in different places (Weisser and Hassell 1996, Weisser et al. 1997).

In this paper, we develop a general way to explicitly account for individual travel times, and show that dispersal is almost always stabilizing when an explicit travel-time is incorporated in the model. We are not the first to demonstrate this effect. Holt (1984) and Weisser and Hassell (1996) studied the effect of dispersal on the stability of a predator-prey system in a single patch. They coupled this patch to itself via constant per capita emigration (at rate E) and immigration (at rate I) into and out of a pool of dispersers (with density $Q(T)$). When predators disperse, the model has the form

$$\frac{dN}{dT} = (R - AP)N, \tag{5.3a}$$

$$\frac{dP}{dT} = (BN - M)P - EP + IQ, \tag{5.3b}$$

$$\frac{dQ}{dT} = EP - IQ - SQ. \tag{5.3c}$$

The term SQ accounts for mortality during dispersal. They found that this pool of dispersers was always stabilizing, and that the stabilizing effect was also produced by a pool of dispersing prey. Holt (1984) and Weisser et al. (1997) extended these results to a system of multiple patches coupled through such a dispersal pool.

Model (5.3) captures the essential fact that some fraction of the predator population is dispersing, and therefore not consuming prey in habitat patches. However, like the linearly coupled Lotka-Volterra model (5.2), model (5.3) makes some peculiar assumptions about the way dispersal occurs. In effect, it implies that there is an exponential distribution of trip durations. Thus there is no minimum travel time, no maximum travel time, and the peak of the travel-time distribution is at zero. Indeed, no matter how long the trip, there is a finite probability that a given predator will survive an even longer trip, dispersing without sustenance.

Although the properties of the dispersal process described by model (5.3) are unrealistic, they are no more unrealistic than other assumptions imbedded in the Lotka-Volterra model. Nevertheless, it is important to see if the above stabilizing effects discovered by Holt and Weisser et al. hold when dispersal is described more realistically.

In the next section, we formulate a model similar to (5.3) that allows for an arbitrary distribution of trip durations. We show that when only one species disperses, the equilibrium is almost always stabilized by including a finite travel time. The exception occurs when every trip has exactly the same duration. In this case there is a set of parameters values with zero-measure for which it is not possible to determine stability via the linearization method we use. In Section 3, we formulate a two patch version similar to model (5.2), and derive similar results. In Section 4 we consider multiple patches with two connection configurations. We have relegated some of the technical mathematics required to prove our results to the Appendix. We conclude with a brief discussion.

5.2 Dispersal Delays in 1 Patch Models

Because of the differences between individuals and the vagaries of travel, it is reasonable to assume that dispersal time varies among individuals and between trips for a single individual. To incorporate this variability, we define a probability density function, $G(S) \geq 0$, for the time it takes an individual to disperse, given that the in-

dividual survives the trip. The product $G(S)\,dS$ is the probability that a successfully dispersing individual departing at time T completes its trip between time $T+S$ and time $T+S+dS$. Because each such disperser has a nonnegative travel time,

$$\int_0^\infty G(S)\,dS = 1. \tag{5.4}$$

If there is a constant probability per unit time (M_d) for the disperser to perish while travelling, then $\exp(-M_d S)$ is the probability of surviving a trip of duration S.

Incorporating a distribution of travel times in a single-patch model where both prey and predators disperse gives:

$$\frac{dN}{dT} = (R-AP)N + D_N\left[\int_0^\infty G_N(S)\,e^{-M_N S}\,N(T-S)\,dS - N\right], \tag{5.5a}$$

$$\frac{dP}{dT} = (BN-M)P + D_P\left[\int_0^\infty G_P(S)\,e^{-M_P S}\,P(T-S)\,dS - P\right]. \tag{5.5b}$$

Here, and below, when the time dependence of a variable is not explicitly indicated we follow the convention that the variable is evaluated at the current (undelayed) time. We assume that the parameters D_N, D_P, M_N and M_P are nonnegative.

The analysis of model (5.5a) is simplified by rescaling variables and parameters via

$$t = RT,\quad s = RS,\quad \mu = M/R,\quad \mu_n = M_N/R,\quad \mu_p = M_P/R, \tag{5.6a}$$

$$p = AP/R,\quad n = BN/R,\quad d_n = D_N/R,\quad d_p = D_P/R. \tag{5.6b}$$

Using these new variables converts model (5.5a) to the dimensionless form

$$\dot{n} = (1-p)\,n + d_n\left[\int_0^\infty g_n(s)\,e^{-\mu_n s}\,n(t-s)\,ds - n\right], \tag{5.7a}$$

$$\dot{p} = (n-\mu)\,p + d_p\left[\int_0^\infty g_p(s)\,e^{-\mu_p s}\,p(t-s)\,ds - p\right], \tag{5.7b}$$

where $g_n(s)$ and $g_p(s)$ are the rescaled versions of $G_N(S)$ and $G_P(S)$. The dot is used to denote a derivative with respect to t. For the basic theory of delay differential equations that applies to model (5.7) see Cushing (1977) and Kuang (1993).

When both species are mobile, with their own characteristic emigration rate, travel-time distribution, and mortality rate during transit, the analysis of model (5.7)

is difficult. For simplicity, we therefore restrict attention to the special cases in which only one species disperses.

5.2.1 Predator Dispersal ($d_n = 0$, $d_p > 0$)

When prey do not disperse ($d_n = 0$), model (5.7) has two equilibria. The first, at $(0, 0)$, is always unstable to prey invasion. The second equilibrium is at

$$n^* = \mu + d_p(1 - \tilde{g}_p(\mu_p)), \quad p^* = 1, \tag{5.8}$$

where $\tilde{g}_p$ is the (one-sided) Laplace transform of the travel-time distribution g_p. That is,

$$\tilde{g}_p(x) \equiv \int_0^\infty g_p(s)\, e^{-xs}\, ds. \tag{5.9}$$

For real x, $\tilde{g}_p(x)$ is a positive, decreasing function with $\tilde{g}_p(0) = 1$.

We now show that the equilibrium point (5.8) is locally asymptotically stable for any finite travel-time distribution $g_p(s)$ that has measurable support. We begin by linearizing model (5.5a) in the neighborhood of the equilibrium point (5.8). Let $u(t)$ and $v(t)$ be small perturbations to the equilibrium point. That is, let

$$n(t) = n^* + u(t), \quad p(t) = p^* + v(t), \tag{5.10}$$

with $|u| << n^*$ and $|v| << p^*$. The dynamics of u and v are approximately given by the linear system

$$\dot{u} = -n^* v, \tag{5.11a}$$

$$\dot{v} = p^* u + d_p \left[\int_0^\infty e^{-\mu_p s} g_p(s)\, v(t-s)\, ds - \tilde{g}_p(\mu_p) v \right], \tag{5.11b}$$

to which we look for exponential solutions of the form

$$\begin{pmatrix} u \\ v \end{pmatrix} = \mathbf{w} e^{\lambda t}. \tag{5.12}$$

Using (5.12) in system (5.11) we obtain the system of equations $\mathbf{J}\mathbf{w} = 0$, where

$$\mathbf{J} = \begin{bmatrix} \lambda & n^* \\ -p^* & \lambda + d_p[\tilde{g}_p(\mu_p) - \tilde{g}_p(\mu_p + \lambda)] \end{bmatrix}. \tag{5.13}$$

The existence of a nontrivial solution $\mathbf{w}$ requires that $\det(\mathbf{J}) = 0$, which in turn gives the characteristic equation

$$H(\lambda) = K(\lambda), \tag{5.14}$$

where

$$H(\lambda) = \lambda[\lambda + d_p \tilde{g}_p(\mu_p)] + n^* p^*, \tag{5.15}$$

and

$$K(\lambda) = \lambda\, d_p\, \tilde{g}_p(\mu_p + \lambda). \tag{5.16}$$

We next show that all roots of the characteristic equation (5.14) have negative real parts, and hence that the equilibrium (5.8) is locally asymptotically stable. To do so we first eliminate the possibility of roots with positive real parts by assuming the existence of such roots and deriving a contradiction. Secondly, we eliminate the possibility of purely imaginary roots, again by deriving a contradiction. Finally, note that $\lambda = 0$ is not a root, since $H(0) > 0$ and $K(0) = 0$. The only possibility that then remains is that the real parts of all of the roots are negative.

Let $\lambda = x + iy$, with x and y real. Assuming that $x > 0$, the characteristic equation gives

$$\begin{aligned} |H(\lambda)|^2 &= |K(\lambda)|^2, && (5.17a)\\ &= |(x+iy)\, d_p\, \tilde{g}_p(\mu_p + x + iy)|^2, && (5.17b)\\ &\leq |(x+iy)\, d_p\, \tilde{g}_p(\mu_p)|^2, && (5.17c) \end{aligned}$$

which, after a little algebra, reduces to

$$x^4 + 2x^2(n^*p^* + y^2) + 2x d_p(x^2 + n^*p^* + y^2)\tilde{g}_p(\mu_p) + (y^2 - n^*p^*)^2 \leq 0. \tag{5.18}$$

Since we have assumed $x > 0$, each term on the left-hand side of expression (5.18) is nonnegative and at least one term is positive, thus the left-hand side is positive, violating the inequality. As a result, the roots of the characteristic equation cannot have positive real parts, thus $x \leq 0$.

Now assume $x = 0$. Setting $x = 0$ in the characteristic equation (5.14), and separating the equation into its real and imaginary parts, shows that y must be a

solution to the system

$$n^*p^* - y^2 = d_p\, y \int_0^\infty g_p(s)\, e^{-\mu_p s} \sin(ys)\, ds, \tag{5.19a}$$

$$d_p\, y\, \tilde{g}_p(\mu_p) = d_p\, y \int_0^\infty g_p(s)\, e^{-\mu_p s} \cos(ys)\, ds. \tag{5.19b}$$

But in the Appendix, we prove that for travel-time distributions $g_p(s)$ that are finite and have support on a measurable set, there is no real solution to system (5.19). Thus $x \neq 0$, and since $x \leq 0$, it must be that $x < 0$, and hence the equilibrium is locally asymptotically stable.

Discrete Delays

For our proof that system (5.19) has no real solution, we must assume that the travel-time distribution is finite. This requirement is satisfied by most biologically reasonable distributions, including the exponential distribution implicitly assumed by models that use a pool of dispersers (Holt 1984, Weisser and Hassell 1996, Weisser et al. 1997), or the gamma distribution that is often used as a convenient distribution because it makes numerical simulation easy (MacDonald 1989).

However, if every trip of every individual is of exactly the same duration τ, the travel-time distribution is a delta function: $g_p(s) = \delta(s - \tau)$. In this case, the distribution is not finite and our proof does not apply. The assumption of identical trips is certainly unrealistic. Nevertheless, we will analyze this case below because there is a long tradition of using discrete delays in population biology to account for individual development (Hutchinson 1948; Wangersky and Cunningham 1956, 1957a, 1957b; Caswell 1972; and many others), and we would like to compare the results of discrete-delays in our model with these results. Furthermore, the analysis sheds light on the reasons why dispersal delays are stablizing.

We now show that, except on a parameter set of measure zero, the equilibrium point remains locally asymptotically stable when all trips are of the same duration. The argument we have already laid out, up to and including the characteristic equation (5.14) holds with $\tilde{g}_p(\mu_p) = \exp(-\mu_p \tau)$. In addition, our proof that there are no roots with positive real part carries over to this case. For imaginary roots $\lambda = iy$,

equations (5.19) simplify to

$$n^*p^* - y^2 = d_p\, y\, e^{-\mu_p \tau} \sin(y\tau), \tag{5.20a}$$

$$d_p\, y\, e^{-\mu_p \tau} = d_p\, y\, e^{-\mu_p \tau} \cos(y\tau). \tag{5.20b}$$

By (5.20a), $y \neq 0$. Equation (5.20b) is satisfied only when $\cos(y\tau) = 1$, in which case equation (5.20a) gives $y = \pm\sqrt{n^*p^*}$ and equation (5.20b) gives,

$$\tau = \tau_k \equiv \frac{2k\pi}{\sqrt{n^*p^*}}, \text{ for } k = 0, 1, 2, \ldots, \tag{5.21}$$

with n^* and p^* given by (5.8). Note that in (5.8), n^* depends upon τ so that (5.8) and (5.21) must be solved simultaneously to find τ_k for any set of parameters.

When $\tau \neq \tau_k$ the equilibrium is locally asymptotically stable. If $\tau = \tau_k$, then the characteristic equation has purely imaginary roots at $\pm i\sqrt{n^*p^*}$. For $k = 0$, the model reduces to a dimensionless form of the Lotka-Volterra equations (5.1), with a neutrally stable equilibrium surrounded by a family of periodic solutions. When $k > 0$ we cannot infer the stability (or instability) of the equilibrium point from the linearized analysis.

5.2.2 Prey Dispersal ($d_n > 0$, $d_p = 0$)

When only prey disperse, $d_p = 0$, and the nontrivial equilibrium of model (5.7) becomes

$$n^* = \mu, \quad p^* = 1 - d_n(1 - \tilde{g}_n(\mu_n)). \tag{5.22}$$

If either the prey emigration rate (d_n) or the prey mortality rate while dispersing (μ_n) is too large, both prey and predators are unable to persist, and the equilibrium at $(0, 0)$ becomes stable.

Linearizing about (n^*, p^*), with p^* assumed positive, gives the same characteristic equation (5.14) as in the predator dispersal case, with d_p, μ_p, and $\tilde{g}_p$ replaced by d_n, μ_n, and $\tilde{g}_n$. Thus the results of Section 2.1 hold for mobile prey and sedentary predators whenever $p^* > 0$.

5.3 Dispersal Delays in 2 Patch Models

Incorporating a distribution of travel times for both the predator and its prey in the 2-patch Lotka-Volterra model (5.2) gives

$$dN_i/dT = (R - AP_i)\,N_i + D_N\left[\int_0^\infty G_N(S)\,e^{-M_N S}\,N_j(T-S)\,dS - N_i\right], \tag{5.23a}$$

$$dP_i/dT = (BN_i - M)\,P_i + D_P\left[\int_0^\infty G_P(S)\,e^{-M_P S}\,P_j(T-S)\,dS - P_i\right], \tag{5.23b}$$

for $i, j = 1, 2$ and $j \neq i$. Using the rescaled variables (5.6), now subscripted, converts model (5.23) to the dimensionless form

$$\dot{n}_i = (1 - p_i)\,n_i + d_n\left[\int_0^\infty g_n(s)\,e^{-\mu_n s}\,n_j(t-s)\,ds - n_i\right], \tag{5.24a}$$

$$\dot{p}_i = (n_i - \mu)\,p_i + d_p\left[\int_0^\infty g_p(s)\,e^{-\mu_p s}\,p_j(t-s)\,ds - p_i\right]. \tag{5.24b}$$

Again, we analyze only the cases in which one species disperses. When only predators disperse (i. e., $d_n = 0$, $d_p > 0$), model (5.24) has a unique positive equilibrium that is spatially homogeneous with densities equal to the equilibrium densities in the 1-patch model with predator dispersal: $n_1^* = n_2^* = n^*$ and $p_1^* = p_2^* = p^*$ with n^* and p^* given by (5.8). Linearizing model (5.24) in the neighborhood of this equilibrium gives, in analogy with (5.13)

$$\mathbf{J} = \begin{bmatrix} \mathbf{A} & \mathbf{B} \\ \mathbf{B} & \mathbf{A} \end{bmatrix}, \tag{5.25}$$

with

$$\mathbf{A} = \begin{bmatrix} \lambda & n^* \\ -p^* & \lambda + d_p\tilde{g}_p(\mu_p) \end{bmatrix} \text{ and } \mathbf{B} = \begin{bmatrix} 0 & 0 \\ 0 & -d_p\tilde{g}_p(\mu_p + \lambda) \end{bmatrix}. \tag{5.26}$$

Setting $\det(\mathbf{J}) = 0$ yields the following characteristic equation:

$$H^2(\lambda) = K^2(\lambda), \tag{5.27}$$

with $H(\lambda)$ and $K(\lambda)$ as in the single patch model (i. e., given by (5.15) and (5.16)).

The arguments in Section 2 can now be applied almost unchanged. For any finite travel-time distribution with support on a measurable set, the equilibrium is stabilized. The only change comes in the discrete-delay case, when the travel-time distribution is a delta function. In this case equations (5.20) must be modified, because any $\lambda = iy$ that satisfies $H(\lambda) = K(\lambda)$ or $H(\lambda) = -K(\lambda)$ is a purely imaginary eigenvalue. Thus equations (5.20) become

$$n^*p^* - y^2 = \pm d_p\, y\, e^{-\mu_p \tau} \sin(y\tau), \tag{5.28a}$$

$$d_p\, y\, e^{-\mu_p \tau} = \pm d_p\, y\, e^{-\mu_p \tau} \cos(y\tau), \tag{5.28b}$$

which now give $y = \pm\sqrt{n^*p^*}$ and $\tau = \tau_k/2$ (cf. equation (5.21)). When τ is equal to one of these special values, the eigenvalues are purely imaginary, and thus linearization cannot be used to determine the stability of the equilibrium point.

When only prey disperse (i. e., $d_n > 0$, $d_p = 0$), the unique nontrivial equilibrium is also spatially homogeneous and equal to the equilibrium densities of the 1-patch, prey-dispersal model (equations (5.22)), which we assume to be positive. The linearization still gives the matrix (5.25), but with $\mathbf{B}$ now given by

$$\mathbf{B} = \begin{bmatrix} -d_n \tilde{g}_n(\mu_n + \lambda) & 0 \\ 0 & 0 \end{bmatrix}. \tag{5.29}$$

Setting $\det(\mathbf{J}) = 0$ again gives the characteristic equation (5.27), but with all subscripts changed from p to n. All of the just derived two-patch predator-dispersal results therefore carry over to the prey-dispersal case.

5.4 Multiple Patches

We are also able to prove that one-species dispersal delays are stabilizing in configurations of an arbitrary number of patches that admit a spatially homogeneous equilibrium. In such configurations every patch is identical to every other patch. A ring of $m \geq 3$ patches is perhaps the simplest example. In the predator dispersal

case, the ring model is given by:

$$\dot{n}_i = (1 - p_i)\, n_i \tag{5.30a}$$

$$\dot{p}_i = (n_i - \mu)\, p_i + \frac{d_p}{2}\left[\int_0^\infty g_p(s)\, e^{-\mu_p s}\, (p_{i-1}(t-s) + p_{i+1}(t-s))\, ds - 2p_i\right], \tag{5.30b}$$

for $i = 1, \ldots, m$. To close the ring, define $p_0 = p_m$ and $p_{m+1} = p_1$.

The equilibrium (5.8) remains unchanged. Linearizing around it and substituting an exponential solution gives the characteristic equation $\det(\mathbf{J}_{(m)}) = 0$, with the $2m \times 2m$ matrix $\mathbf{J}_{(m)}$ given by

$$\mathbf{J}_{(m)} = \begin{bmatrix} \mathbf{A} & \frac{1}{2}\mathbf{B} & 0 & \cdots & 0 & \frac{1}{2}\mathbf{B} \\ \frac{1}{2}\mathbf{B} & \mathbf{A} & \frac{1}{2}\mathbf{B} & 0 & \cdots & 0 \\ 0 & \frac{1}{2}\mathbf{B} & \mathbf{A} & \frac{1}{2}\mathbf{B} & \cdots & 0 \\ & & \vdots & & & \\ 0 & \cdots & 0 & \frac{1}{2}\mathbf{B} & \mathbf{A} & \frac{1}{2}\mathbf{B} \\ \frac{1}{2}\mathbf{B} & 0 & \cdots & 0 & \frac{1}{2}\mathbf{B} & \mathbf{A} \end{bmatrix}. \tag{5.31}$$

with blocks $\mathbf{A}$ and $\frac{1}{2}\mathbf{B}$ given by (5.26).

$\mathbf{J}_{(m)}$ is an example of a block-circulant matrix with 2×2 blocks. That is, it has the form

$$\mathbf{C} = \begin{bmatrix} \mathbf{A}_0 & \mathbf{A}_1 & \cdots & \mathbf{A}_{m-1} \\ \mathbf{A}_{m-1} & \mathbf{A}_0 & \cdots & \mathbf{A}_{m-2} \\ \vdots & \vdots & & \vdots \\ \mathbf{A}_1 & \mathbf{A}_2 & \cdots & \mathbf{A}_0 \end{bmatrix}, \tag{5.32}$$

where the $\mathbf{A}_i$ are 2×2 matrices. The determinant of such matrices is given by

$$\det \mathbf{C} = \prod_{\ell=0}^{m-1} \det \mathbf{T}_\ell, \tag{5.33}$$

with

$$\mathbf{T}_\ell = \sum_{j=0}^{m-1} e^{2\pi i j \ell / m} \mathbf{A}_j \tag{5.34}$$

(see, for example, Friedman (1961, Theorem 6)). Applying these formulae to $\mathbf{J}_{(m)}$

gives

$$\det \mathbf{J}_{(m)} = \prod_{\ell=0}^{m-1} \left(H(\lambda) - \cos\left(\frac{2\pi\ell}{m}\right) K(\lambda) \right). \tag{5.35}$$

If λ is an eigenvalue, at least one term in the product (5.35) will vanish, i. e.,

$$H(\lambda) = \cos\left(\frac{2\pi\ell}{m}\right) K(\lambda) \tag{5.36}$$

for some $\ell < m$. But taking absolute values of both sides and squaring gives $|H(\lambda)|^2 \leq |K(\lambda)|^2$, which brings us back to equation (5.17) and the single patch case. Distributed dispersal delays are always stabilizing in this "ring" model.

For discrete delays of duration τ, the real and imaginary parts of equation (5.36) give, in analogy to equations (5.20),

$$n^* p^* - y^2 = \cos\left(\frac{2\pi\ell}{m}\right) d_p\, y\, e^{-\mu_p \tau} \sin(y\tau), \tag{5.37a}$$

$$d_p\, y\, e^{-\mu_p \tau} = \cos\left(\frac{2\pi\ell}{m}\right) d_p\, y\, e^{-\mu_p \tau} \cos(y\tau). \tag{5.37b}$$

While $y = 0$ is always a solution to (5.37b), it is never a solution to (5.37a). We therefore take $y \neq 0$. If the number of patches in the ring (m) is odd, there is only one value of ℓ with $\ell < m$ for which (5.37b) has a solution; it is $\ell = 0$. In this case purely imaginary eigenvalues occur at $\tau = \tau_k$, with τ_k given by equation (5.21). If the number of patches is even, imaginary eigenvalues occur at $\tau = \tau_k/2$. For k even they arise from (5.37b) with $\ell = 0$. For k odd, they come from (5.37b) with $\ell = m/2$. Linearization is uninformative for these delays.

Another configuration with all patches identical is obtained if each patch is coupled to every other patch in exactly the same way (e. g., through a pool of dispersers). The resulting model in this case is

$$\dot{n}_i = (1 - p_i)\, n_i \tag{5.38a}$$

$$\dot{p}_i = (n_i - \mu)\, p_i + \frac{d_p}{m-1} \cdot \left\{ \sum_{j=1, j\neq i}^{m} \left[\int_0^\infty g_p(s)\, e^{-\mu_p s}\, p_j(t-s)\, ds \right] - (m-1) p_i \right\}, \tag{5.38b}$$

for $i = 1, \ldots, m$. For $m = 2$, this model reduces to the two-patch model of Section 2.1; for $m = 3$ it is the same as model (5.30). We therefore take $m \geq 4$.

Linearization around the equilibrium (again given by (5.8)) gives

$$\mathbf{J}_{(m)} = \begin{bmatrix} \mathbf{A} & \frac{1}{m-1}\mathbf{B} & \cdots & \cdots & \frac{1}{m-1}\mathbf{B} \\ \frac{1}{m-1}\mathbf{B} & \mathbf{A} & \frac{1}{m-1}\mathbf{B} & \cdots & \frac{1}{m-1}\mathbf{B} \\ & & \vdots & & \\ \frac{1}{m-1}\mathbf{B} & \cdots & \cdots & \frac{1}{m-1}\mathbf{B} & \mathbf{A} \end{bmatrix}, \tag{5.39}$$

and the resulting characteristic equation is

$$\det(\mathbf{J}_{(m)}) = \prod_{\ell=0}^{m-1} \left[H(\lambda) - \frac{1}{m-1} \left(\sum_{j=1}^{m-1} \exp\left(\frac{2\pi i j \ell}{m} \right) \right) K(\lambda) \right]. \tag{5.40}$$

By the argument used on the determinant (5.35), it follows that, for a distributed delay, the conclusions are the same as in the single-patch case. A discrete-delay of duration τ is also stabilizing, unless $\tau = \tau_k$.

5.5 Discussion

The predator-prey models we formulated above, wherein one species disperses between habitat patches while the other does not, all show that a dispersal delay almost always stabilizes the spatially homogeneous positive equilibrium. It is well known that the inclusion of a delay can lead to a qualitative change in the dynamics of a model, but it is typically the case that an increase in the delay produces instability and gives rise to stable periodic solutions (see, e. g., MacDonald 1989, p. 8, 15). In this sense, our results can be seen as counterintuitive, although some models with delay-dependent parameters exhibit stability switches from stable to unstable and back to stable again as the delay increases (see, e. g. Beretta and Kuang 2001).

What is the mechanism by which dispersal delays act to stabilize these systems? First let us say that certain mechanisms are *not* responsible. The stabilizing effect is not (strictly speaking) a metapopulation effect. After all, it is evident in the one-patch model. It is not an effect of a cost of dispersal (in terms of increased mortality). After all, the mechanism operates when μ_p or μ_n vanish. Finally it is not a result of spatial heterogeneity; every patch is identical to every other patch in our models.

The stabilizing mechanism that does operate is evident in the one-patch predator-dispersal model. In particular, consider the case where $\mu_p = 0$. In this case, the term

that accounts for predator dispersal can be rewritten as

$$p(t)\left\{d_p\left[\frac{\int_0^\infty g_p(s)\,p(t-s)\,ds}{p(t)}-1\right]\right\}. \tag{5.41}$$

The term between the curly brackets represents the instantaneous per capita net migration rate (i.e., immigration minus emigration). It is density dependent. If the population in the patch is high relative to historically average values (the average being taken with respect to the weighting function $g_p(s)$), then net migration is negative; if the current population size is low relative to historical averages, then the net migration rate is positive. This term therefore has the effect of damping oscillations and enhancing stability. The same mechanism also works in the multiple-patch scenario.

Murdoch et al. (1992) also showed that "temporal density-dependence" in immigration rates can stabilize predator-prey metapopulation dynamics. The fundamental difference between their results and ours is the mechanism by which the density-dependence is generated. In their model, spatial heterogeneity in the demographic parameters generates asynchronous population dynamics between connected habitat patches, which leads to a decoupling of local immigration rates from local population density. In our model, no such spatial heterogeneity is required to generate the decoupling. Instead, dispersal tends to synchronize the dynamics between patches, while the delay decouples immigration rates from local density.

When the delay is discrete, there is a set of delays for which we have not been able to determine the stability of the equilibrium. Because this set of delays has zero measure, these cases are biologically irrelevant. Nevertheless, an understanding of the dynamics in these cases would complete the mathematical analysis. We conjecture that for these special values of the delay, dispersal does not stabilize the equilibrium.

The models we have analyzed, while more complex than the Lotka-Volterra model, are still simple in the extreme. An important simplification we have made is that every patch is identical to every other patch—including being connected via dispersal to the same number of equidistant patches. In real systems, this assumption is violated. When the distance between patches is not constant, the travel time distribution will differ for different pairs of patches. Models of this type are notoriously difficult to analyze, but it is important to know the extent to which our results rely on this assumption. The interaction between more realistic population dynamics and dispersal

delays is a topic that we are currently investigating and will report elsewhere.

References

Beretta, E. and Kuang, Y. 2001. Geometric stability switch criteria in delay differential systems with delay-dependent parameters. *SIAM Journal on Mathematical Analysis.* To appear.

Caswell, H. 1972. A simulation study of a time lag population model. *Journal of Theoretical Biology* **34**:419–439.

Comins, H.N. and Blatt, D.W.E. 1974. Prey-predator models in spatially heterogeneous environments. *Journal of Theoretical Biology* **48**:75–83.

Crawley, M. J., ed. 1992. *Natural Enemies: The Population Biology of Predators, Parasites and Diseases.* Blackwell Scientific, London.

Cushing, J. M. 1977. *Integrodifferential Equations and Delay Models in Population Dynamics.* Springer-Verlag, Berlin.

Friedman, B. 1961. Eigenvalues of composite matrices. *Proceedings of the Cambridge Philosophical Society* **57**:37-49.

Gause, G. F. 1934. *The Struggle for Existence.* Williams and Wilkins, Baltimore.

Gotelli, N. J. 1995. *A Primer of Ecology.* Sinauer, Sunderland.

Hanski, I. 1999. *Metapopulation Ecology.* Oxford University Press, Oxford.

Hardy, G., Littlewood, J. E., and Pólya, G. 1952. *Inequalities.* Cambridge University Press, Cambridge.

Hassell, M. P. 1978. *The Dynamics of Arthropod Predator-Prey Systems.* Princeton University Press, Princeton.

Holt, R. D. 1984. Spatial heterogeneity, indirect interaction, and the coexistence of prey species. *American Naturalist* **124**:377–406.

Hutchinson, G. E. 1948. Circular causal systems in ecology. *Annals of the New York Academy of Sciences* **50**:221–246.

Jansen, V.A.A. 1995. Regulation of predator-prey systems through spatial ineractions: a possible solution to the paradox of enrichment. *Oikos* **74**:384–390.

Jansen, V.A.A. and de Roos, A. M. 2000. The role of space in reducing predator-prey cycles. Pages 183–201 in, *The Geometry of Ecological Interactions: Simplifying Spatial Complexity.* Cambridge University Press, Cambridge.

Kuang, Y. 1993. *Delay Differential Equations with Applications in Population Dynamics.* Academic Press, Boston.

Lotka, A. J. 1926. *Elements of Physical Biology.* Williams and Wilkins, Baltimore.

MacDonald, N. 1989. *Biological Delay Systems: Linear Stability Theory.* Cambridge University Press, Cambridge.

May, R. M. 1973. *Stability and Complexity in Model Ecosystems.* Princeton University Press, Princeton.

Mueller, L. D. and Joshi, A. 2000. *Stability in Model Populations.* Princeton University Press, Princeton.

Murdoch, W. W., Briggs, C. J., Nisbet, R. M., Gurney, W. S. C., and Stewart-Oaten, A. 1992. Aggregation and stability in metapopulation models. *American Naturalist* **140**:41–58.

Murdoch, W. W., and Oaten, A. 1975. Predation and population stability. *Advances in Ecological Research* **9**:1–131.

Nicholson, A. J. and Bailey, V. A. 1935. The balance of animal populations. *Proceedings of the Zoological Society of London* **1**:551–598.

Nisbet, R. M., Briggs, C. J., Gurney, W. S. C., Murdoch, W. W. and Stewart-Oaten, A. 1992. Two-patch metapopulation dynamics. In Levin, S. A., Steele, J. H. and Powell, T. (editors). Patch dynamics in terrestrial, freshwater, and marine ecosystems. Lecture Notes in Biomathematics **96**. Springer-Verlag, Berlin.

Taylor, A. D. 1990. Metapopulations, dispersal, and predator-prey dynamics: an overview. *Ecology* **71**:429–436.

Volterra, V. 1931. *Leçons sur la Théorie Mathématique de la Lutte Pour la Vie.* Gauthier-Villars, Paris.

Wangersky, P. J. and Cunningham, W. J. 1956. On time lags in equations of growth. *Proceedings of the National Academy of Science USA* **42**:699-702.

Wangersky, P. J. and Cunningham, W. J. 1957a. Time lag in population models. *Cold Spring Harbor Symposia on Quantitative Biology* **22**:329–338.

Wangersky, P. J. and Cunningham, W. J. 1957b. Time lag in prey-predator population models. *Ecology* **38**:136–139.

Weisser, W. W., and Hassell, M. P. 1996. Animals 'on the move' stabilise host-parasitoid systems. *Proceedings of the Royal Society of London B* **263**:749–754.

Weisser, W. W., Jansen, V. A. A., and Hassell, M. P. 1997. The effects of a pool of dispersers on host-parasitoid systems. *Journal of Theoretical Biology* **189**:413–425.

Chapter 6

Dispersal Delays, Predator-Prey Stability, and the Paradox of Enrichment

Petra Klepac, Michael G. Neubert, and P. van den Driessche

This article has been accepted for publication and is in press in Theoretical Population Biology.

Abstract

It takes time for individuals to move from place to place. This travel time can be incorporated into metapopulation models via a delay in the interpatch migration term. Such a term has been shown to stabilize the positive equilibrium of the classical Lotka-Volterra predator–prey system with one species (either the predator or the prey) dispersing.

We study a more realistic, Rosenzweig-MacArthur, model that includes a carrying capacity for the prey, and saturating functional response for the predator. We show that dispersal delays can stabilize the predator–prey equilibrium point despite the presence of a Type II functional response that is known to be destabilizing. We also show that dispersal delays reduce the amplitude of oscillations when the equilibrium is unstable, and therefore may help resolve the paradox of enrichment.

6.1 Introduction

The basic models of predator–prey and host–parasitoid systems predict unstable equilibria, often accompanied by large-amplitude oscillations in both species. These oscillations drive the populations to low densities, and have been interpreted as potential causes of extinction. In contrast, natural predator–prey systems seem to persist for long periods. Theoreticians and experimentalists have suggested a number of potential processes that might resolve this conflict between models and data (see, for example, May, 1973; Hassell, 1978; Crawley, 1992; Mueller & Joshi, 2000). Spatial processes, and in particular metapopulation structure, have garnered significant attention (Taylor, 1990; Briggs & Hoopes, 2004).

Dispersal, the process that distinguishes spatial models from their nonspatial counterparts, has been added to predator–prey models in many different ways, with varying effects on stability (Briggs & Hoopes, 2004). One way to include dispersal is to distinguish a class of dispersing individuals, that, while dispersing, do not participate in the predator–prey interaction. A number of authors have shown that including such a pool of dispersers (be they predators or prey) in a Lotka–Volterra model stabilizes coexistence at an equilibrium point. The models of Holt (1984), Weisser & Hassell (1996) and Weisser *et al.* (1997) include the dispersal pool explicitly, and couple it to the dynamics within a patch via constant per capita immigration and emigration rates. These models implicitly assume an exponential distribution of the time that an individual spends dispersing.

Exponential travel-time distributions, however, have some biological peculiarities.

For example, there is no maximum travel time, and the modal travel-time is zero. To see if these implicit assumptions play a role in stabilizing the equilibrium, Neubert *et al.* (2002) relaxed this assumption by prescribing an arbitrary distribution of dispersal times. They showed that, except in cases so rare as to be biologically irrelevant, the stabilizing effect of such "dispersal delays" remains.

All of these analyses are based upon the Lotka–Volterra predator–prey model

$$\frac{dN}{dT} = (R - AP)N, \tag{6.1a}$$

$$\frac{dP}{dT} = (BN - M)P, \tag{6.1b}$$

where N is the population density of the prey and P is the population density of the predator. The prey population has a constant per capita growth rate R, and the predator population has a constant per capita mortality rate M. The predator-prey interaction is captured by linear functional and numerical responses, scaled by the parameters A and B. The parameters R, A, B, and M are assumed to be positive.

Model (6.1) has a unique coexistence equilibrium point (i. e., an equilibrium point at which both species have positive densities) at $N = M/B$, $P = R/A$. This equilibrium point is a center, surrounded by a family of periodic orbits whose amplitudes depend on the initial population sizes. Adding either predator or prey dispersal to this model stabilizes the equilibrium point if dispersal delays are accounted for (Neubert *et al.*, 2002). In the absence of delays, predator dispersal reduces the amplitude of the oscillations but does not stabilize the equilibrium point (Jansen, 1995; Jansen & de Roos, 2000). Increasing the number of patches in this model gives rise to other equilibria in which the prey are absent from one or more patches (see, for example, Feng & Hinson, 2005) that we do not consider here.

Model (6.1), and its spatial extensions, have been criticized as being oversimplified for two reasons. First, in the absence of the predators, the prey grow exponentially without bound. Second, the per capita rate of consumption of prey by predators grows in proportion to the prey population size, implying that individual predators can process prey items infinitely fast. These faults are eliminated in the Rosenzweig-

MacArthur model (Rosenzweig & MacArthur, 1963)

$$\frac{dN}{dT} = RN\left(1-\frac{N}{K}\right) - \frac{ANP}{C+N}, \tag{6.2a}$$

$$\frac{dP}{dT} = \frac{BNP}{C+N} - MP, \tag{6.2b}$$

which includes a carrying capacity for the prey (K) and a finite prey handling time for the predators that results in a saturating functional response. Here, A is the maximum rate at which an individual predator can consume prey and C is the prey density at which an individual predator's consumption rate equals $A/2$. The ratio B/A gives the fraction of consumed prey that are converted into predators.

The dynamics of model (6.2) are more complicated than those of model (6.1) (Kot, 2001). For small values of carrying capacity, the coexistence equilibrium point is locally asymptotically stable. As the carrying capacity increases beyond some threshold value, the equilibrium point becomes unstable, and trajectories are drawn onto a single stable limit cycle. The amplitude of predator-prey oscillations increases with increasing prey's carrying capacity, reaching vanishingly small densities at which natural populations cannot persist. This destabilization by increasing prey carrying capacity is known as the 'paradox of enrichment' (Rosenzweig, 1971; May, 1972; Gilpin, 1972).

Here we present three major findings. First, we show that dispersal delays can stabilize the coexistence equilibrium point of model (6.2) (as they did in model (6.1)) by delineating the stability region in parameter space. Second, we show that for many parameter values, stability persists in a so-called "Type II model" wherein prey growth is density independent (i. e. model (6.2) in the limit of infinite carrying capacity K). We thus establish that delayed dispersal can overcome a destabilizing Type II functional response even in the absence of stabilizing prey density-dependence. Finally, we show that dispersal delays help resolve the paradox of enrichment by reducing the amplitude of oscillations when the equilibrium is unstable, thereby preventing the small population sizes that might lead to extinction.

We begin, in the next section, by constructing a Rosenzweig-MacArthur model that incorporates dispersal delays. Using the methods outlined in Neubert *et al.* (2002), it can be shown that if dispersal delays stabilize the single patch model they also stabilize a spatially homogeneous equilibrium of a model with an arbitrary number of identical patches. Therefore, we limit our investigation to a single habitat

patch from which only predators disperse. We then present results for two types of dispersal delay: a discrete delay that implies that all individuals spend exactly the same amount of time away from the patch, and a distributed delay that accounts for differences in, for example, dispersal ability between individuals. For discrete-delays our results are derived from numerical simulations. In the case of a distributed delay with Erlang distribution, we analytically derive a polynomial characteristic equation. whose roots we find numerically. We conclude with a brief discussion.

6.2 Model

The model that we analyze,

$$\frac{dN}{dT} = RN\left(1-\frac{N}{K}\right) - \frac{ANP}{C+N}, \tag{6.3a}$$

$$\frac{dP}{dT} = \frac{BNP}{C+N} - MP + D\left[\int_0^\infty G(S)\,e^{-M_P S}P(T-S)\,dS - P\right], \tag{6.3b}$$

describes the dynamics of a sedentary prey and a mobile predator in a single habitat patch. Individual predators emigrate from the patch at the constant per capita rate D, and return S units of time after their departure.[1] To account for the differences in dispersal abilities between predators, we define a distribution of dispersal delays, $G(S) \geq 0$, for the time a predator takes to disperse, given that it survives the trip (Neubert *et al.*, 2002). Because all dispersal times are nonnegative it follows that $\int_0^\infty G(S)\,dS = 1$ (see also Azer & van den Driessche, 2006). We assume that the probability of surviving a trip of duration S is $e^{-M_P S}$, where M_p is the mortality rate during the migration.

Model (6.3) takes the form of a delay differential equation with distributed delay. For examples of how such equations have been used in other types of ecological models, and for how they may be analyzed, see the books by Kuang (1993) and MacDonald (1989).

In order to reduce the number of parameters, and simplify our analyses, we scale

[1]For notational convenience, a variable with no time dependence explicitly given is to be evaluated at the current (undelayed) time.

the variables and parameters of the model (6.3) according to

$$t = RT, \quad s = RS, \quad \mu = M/R, \quad d = D/R, \quad \mu_p = M_P/R, \tag{6.4a}$$

$$p = AP/RC, \quad n = BN/RC, \quad \varepsilon = R/B, \quad \kappa = KB/RC. \tag{6.4b}$$

Substitution into system (6.3) gives the dimensionless form

$$\dot{n} = n\left(1 - \frac{n}{\kappa}\right) - \frac{np}{1+\varepsilon n}, \tag{6.5a}$$

$$\dot{p} = \frac{np}{1+\varepsilon n} - \mu p + d\left[\int_0^\infty g(s)\, e^{-\mu_p s} p(t-s)\, ds - p\right], \tag{6.5b}$$

where $g(s)$ is the scaled version of $G(S)$.

In Sec. 3, we focus on the effects of κ (the dimensionless carrying capacity) and d (the dimensionless emigration rate) on the stability of the unique coexistence equilibrium for model (6.5):

$$n^* = \frac{\mu + d\,(1 - \tilde{g}\,(\mu_p))}{1 - \varepsilon\,[\mu + d\,(1 - \tilde{g}(\mu_p))]}, \qquad p^* = \left(1 - \frac{n^*}{\kappa}\right)(1 + \varepsilon\, n^*)\,. \tag{6.6}$$

Here, $\tilde{g}(x)$ is the (one-sided) Laplace transform of the travel-time distribution $g(s)$, i. e.,

$$\tilde{g}(x) \equiv \int_0^\infty g(s)\, e^{-xs} ds. \tag{6.7}$$

The equilibrium (6.6) is positive only if

$$d < \frac{\kappa\,(1 - \varepsilon\mu) - \mu}{(\kappa\varepsilon + 1)\,[1 - \tilde{g}(\mu_p)]}. \tag{6.8}$$

If d is too large, and inequality (6.8) is violated, the predators do not spend sufficient time feeding on the prey patch to maintain a positive growth rate and are extirpated as a result.

To determine the stability of the coexistence equilibrium point (6.6) of model (6.5) we must determine the fate of small perturbations, $u(t)$ and $v(t)$, to the coexistence equilibrium. Set

$$n(t) = n^* + u(t), \quad p\,(t) = p^* + v(t). \tag{6.9}$$

For $|u|$ and $|v|$ sufficiently small, the dynamics of these perturbations are approxi-

mated by the linear system

$$\dot{u} = u\left[1 - \frac{2n^*}{\kappa} - \frac{p^*}{(1+\varepsilon n^*)^2}\right] + v\left(-\frac{n^*}{1+\varepsilon n^*}\right), \tag{6.10a}$$

$$\dot{v} = u\left(\frac{p^*}{1+\varepsilon n^*}\right) + v\left(\frac{n^*}{1+\varepsilon n^*} - \mu - d\right) + d\int_0^\infty g(\tau)e^{-\mu_p \tau} v(t-\tau)d\tau. \tag{6.10b}$$

Looking for solutions to (6.10) of the form

$$\begin{pmatrix} u \\ v \end{pmatrix} = \mathbf{w}e^{\lambda t}, \quad \mathbf{w} \neq 0, \tag{6.11}$$

we find that λ and $\mathbf{w}$ must satisfy

$$(\mathbf{J} - \lambda \mathbf{I})\,\mathbf{w} = 0, \tag{6.12}$$

where $\mathbf{J}$ is the Jacobian matrix

$$\mathbf{J}\begin{bmatrix} 1 - \frac{2n^*}{\kappa} - \frac{p^*}{(1+\varepsilon n^*)^2} & -\frac{n^*}{1+\varepsilon n^*} \\ \frac{p^*}{(1+\varepsilon n^*)^2} & d[\tilde{g}(\mu_p + \lambda) - \tilde{g}(\mu_p)] \end{bmatrix} \tag{6.13}$$

Equation (6.12) has solutions with $\mathbf{w} \neq 0$ only if $\det(\mathbf{J} - \lambda \mathbf{I}) = 0$, which translates to

$$H(\lambda) = K(\lambda), \tag{6.14}$$

with

$$H(\lambda) = \left[\lambda + \frac{2n^*}{\kappa} + \frac{p^*}{(1+\varepsilon n^*)^2} - 1\right][\lambda + d\,\tilde{g}(\mu_p)] + \frac{n^* p^*}{(1+\varepsilon n^*)^3}, \tag{6.15a}$$

$$K(\lambda) = \left[\lambda + \frac{2n^*}{\kappa} + \frac{p^*}{(1+\varepsilon n^*)^2} - 1\right] d\,\tilde{g}(\mu_p + \lambda). \tag{6.15b}$$

The roots of this "characteristic" equation are the eigenvalues; they are, in general, complex numbers.

The real parts of the eigenvalues determine the stability of the equilibrium point. If all of the eigenvalues have negative real parts, u and v will vanish in the limit $t \to \infty$, and the equilibrium point is therefore locally stable. If any eigenvalue has a positive real part, the perturbations grow, and the equilibrium is unstable. Note that

(6.14) and (6.15) together imply that $\lambda = 0$ is not an eigenvalue since n^* and p^* are positive.

In the absence of dispersal, $d = 0$. In this case, local stability of the equilibrium point is guaranteed from (6.8) and (6.14) if

$$\frac{\mu}{1-\varepsilon\mu} < \kappa < \frac{1+\varepsilon\mu}{\varepsilon(1-\varepsilon\mu)}. \tag{6.16}$$

For finite κ, if the left-hand inequality is violated the predator is extirpated, since for this parameter range there is no positive steady state; see inequality (6.8). Violation of the right-hand inequality results in a Hopf bifurcation and a predator-prey limit cycle (Kot, 2001). Note that in the limit $\kappa \to \infty$, the equilibrium point is never stable.

6.3 Results

6.3.1 Discrete travel time

If the duration of every dispersal event of every individual is exactly τ, then the dispersal delay distribution is a delta function: $g(s) = \delta(s-\tau)$ and $\tilde{g}(x) = \exp(-\tau x)$. We have been unable to analytically infer the local stability of the coexistence equilibrium in this case, as the characteristic equation (6.14) is a transcendental equation with infinitely many solutions. Therefore, we illustrate our results (in Fig. 6-1) using numerically generated stability diagrams in the (τ, d) parameter plane for various values of κ. For each combination of the parameters, we (i) calculated the equilibrium point (6.6), (ii) for coexistence equilibria we chose a random initial condition for the prey and the predator uniformly distributed between 50% and 150% of the equilibrium values, (iii) using the Simulink package in Matlab, we simulated the model (6.5) and discarded the transient dynamics. We then distinguished three sets in (τ, d) parameter plane: (a) a set of parameters for which the coexistence equilibrium does not exist (because inequality (6.8) is violated), (b) a set for which the coexistence equilibrium exists but it is unstable, and (c) a set for which the coexistence equilibrium is stable.

We start (Figure 6-1A) with a case that is stable in the absence of the dispersal delay (i. e., satisfying (6.16)). As expected, the coexistence equilibrium is stable everywhere it exists. In Figures 6-1B-D the values of κ violate the right-most inequality in (6.16). For these values of the carrying capacity, the equilibrium point of

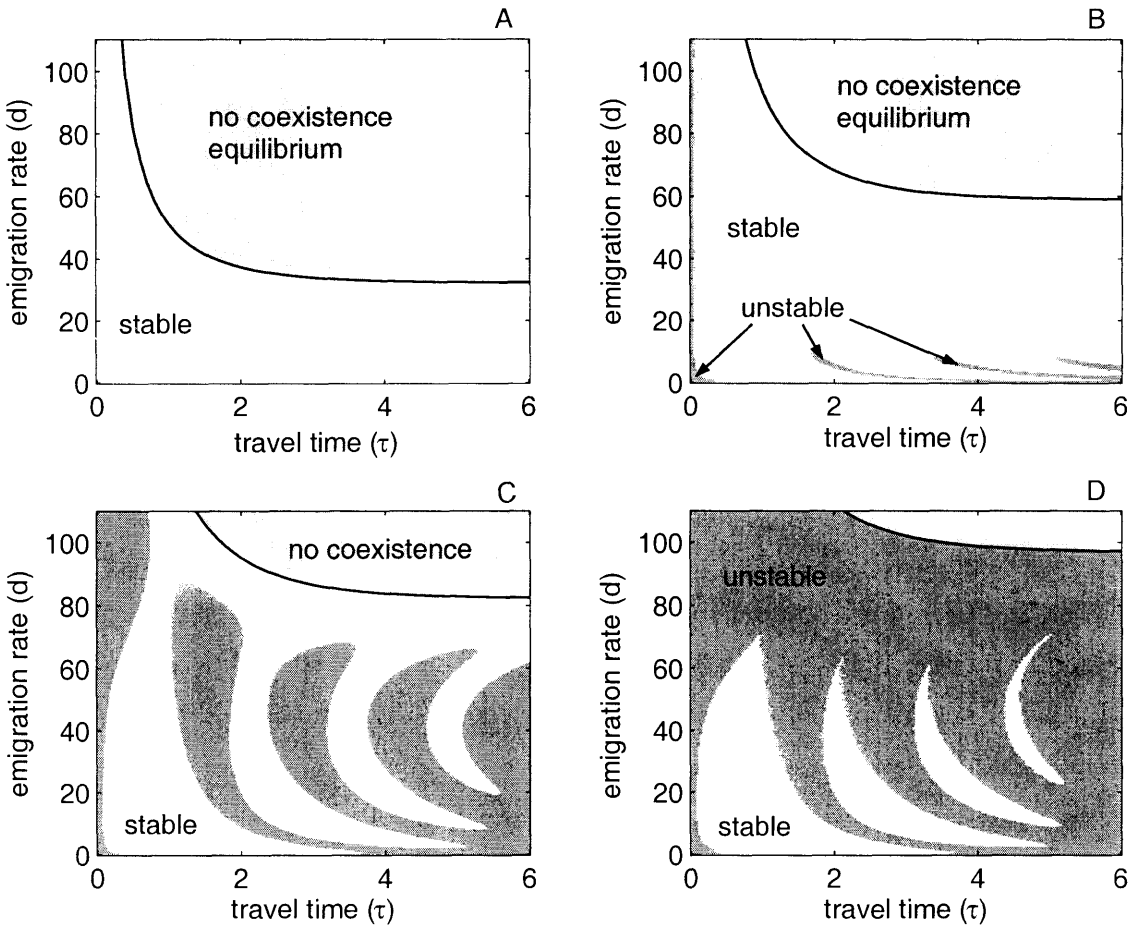

Figure 6-1: Stability diagrams from simulations of model (6.5) with discrete dispersal delay for various values of κ, $\varepsilon = 0.01$, $\mu = \mu_p = 1$: A) $\kappa = 50$; B) $\kappa = 150$; C) $\kappa = 500$; D) $\kappa = 5000$. White areas designate a stable equilibrium point, dark gray stands for an unstable equilibrium point and an area where there is no positive coexistence equilibrium is shown in light gray, bounded by the black curve, i.e., the case of equality (6.8).

the Rosenzweig-MacArthur model (6.2) is unstable, surrounded by a predator-prey cycle. Dispersal delay dampens the predator-prey oscillation resulting in the area of stable equilibrium shown in white. For $\kappa \gtrsim 1000$, the stability region reduces to four "islands".

Since stability diagrams do not reveal the details of the unstable behavior, we generated bifurcation diagrams for different values of parameters, for both predator and prey densities. All diagrams exhibit qualitatively similar behavior, so we show only one bifurcation diagram for prey density with τ as the bifurcation parameter (Fig. 6-2).

For each value of τ we simulated model (6.5), discarded the transient dynamics, and present only the final behavior by plotting only the local maxima and minima of the trajectory. Stable equilibria therefore appear as a single point. Oscillations with one peak appear as two points, and oscillations with two peaks appear as four points, et cetera. Quasi-periodic and aperiodic oscillations appear as "smears."

In addition to quasi-periodic and aperiodic behavior, the bifurcation diagrams also reveal the coexistence of multiple attractors. In Fig. 6-2A, we increased τ from 0 to 7 in small steps, using the end of the simulation for one value of τ as the initial condition of the simulation for the following value of τ. We followed the same procedure in Fig. 6-2B, except that we decreased τ from 7 to 0. For values of τ in the shaded regions of Fig. 6-2, solutions converge to different attractors depending on initial conditions.

In Fig. 6-3 we categorize the dynamics of the Type II model,

$$\dot{n} = n - \frac{np}{1+\varepsilon n}, \tag{6.17a}$$

$$\dot{p} = \frac{np}{1+\varepsilon n} - \mu p + d\left[\int_0^\infty g(s)\, e^{-\mu_p s} p(t-s)\, ds - p\right], \tag{6.17b}$$

in the (τ, d) parameter space over a range of ε. In Fig. 6-3A, the predator's functional response is strong (ε is relatively large) and the equilibrium cannot be stabilized by dispersal delays. As ε decreases, however, stable islands grow in number and in size. In the limit $\varepsilon \to 0$, Neubert *et al.* (2002) showed the equilibrium is stable everywhere except for a set of measure zero in the (τ, d) plane. Comparing Fig. 6-3C with Fig. 6-1D shows that the stability properties of the Type II model are essentially the same as the Rosenzweig-MacArthur model with large carrying capacity.

The stability in the Type II model implies that dispersal delays can help resolve

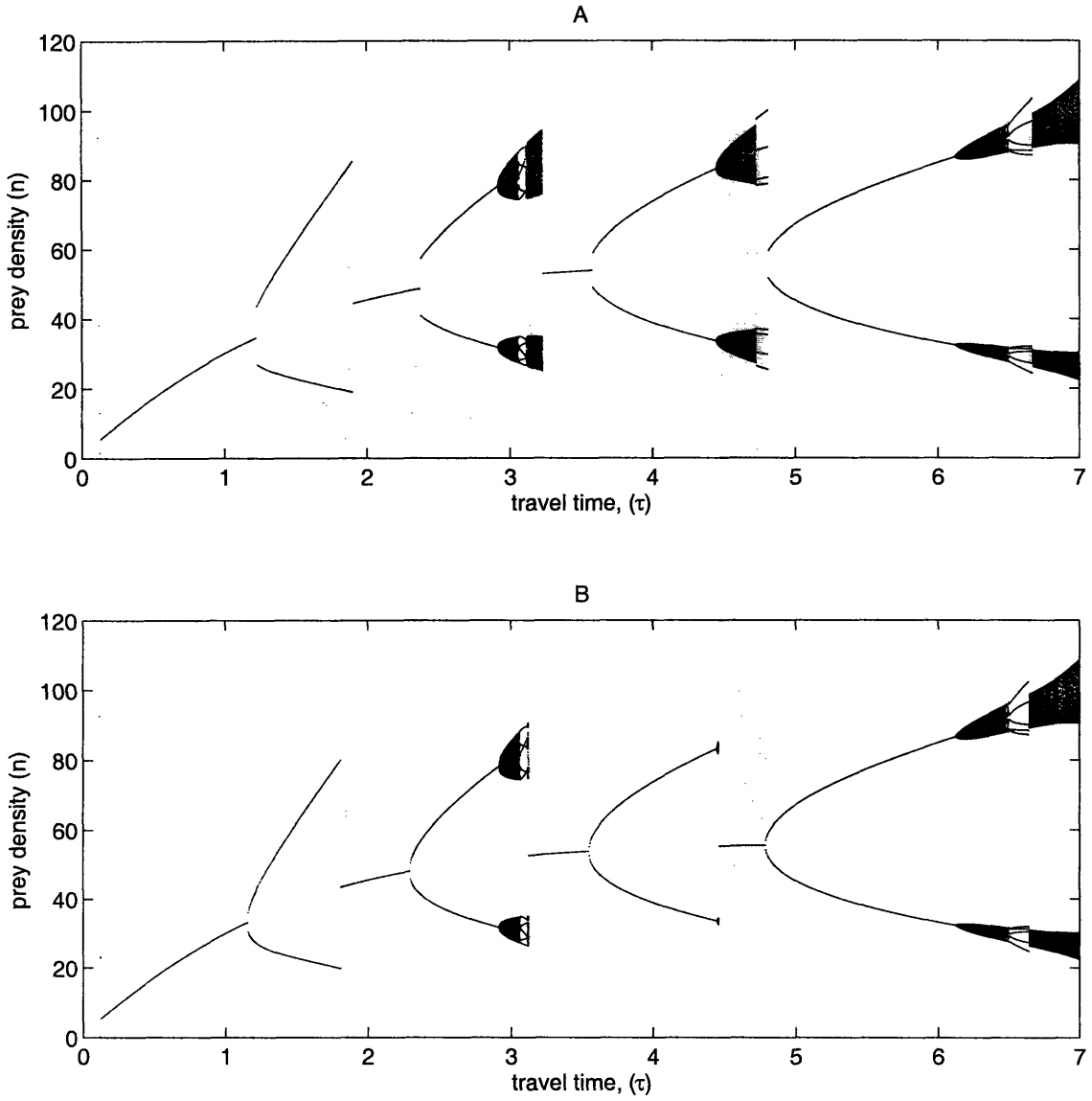

Figure 6-2: Bifurcation diagrams for the prey population density of model (6.5) with discrete dispersal delay (minimum and maximum population densities), $d = 35$, $\varepsilon = 0.01$, $\kappa = 5000$, $\mu = \mu_p = 1$. A) τ is changed forwards; B) τ is changed backwards. Shaded regions depict the coexistence of multiple attractors. Detailed explanation in the text.

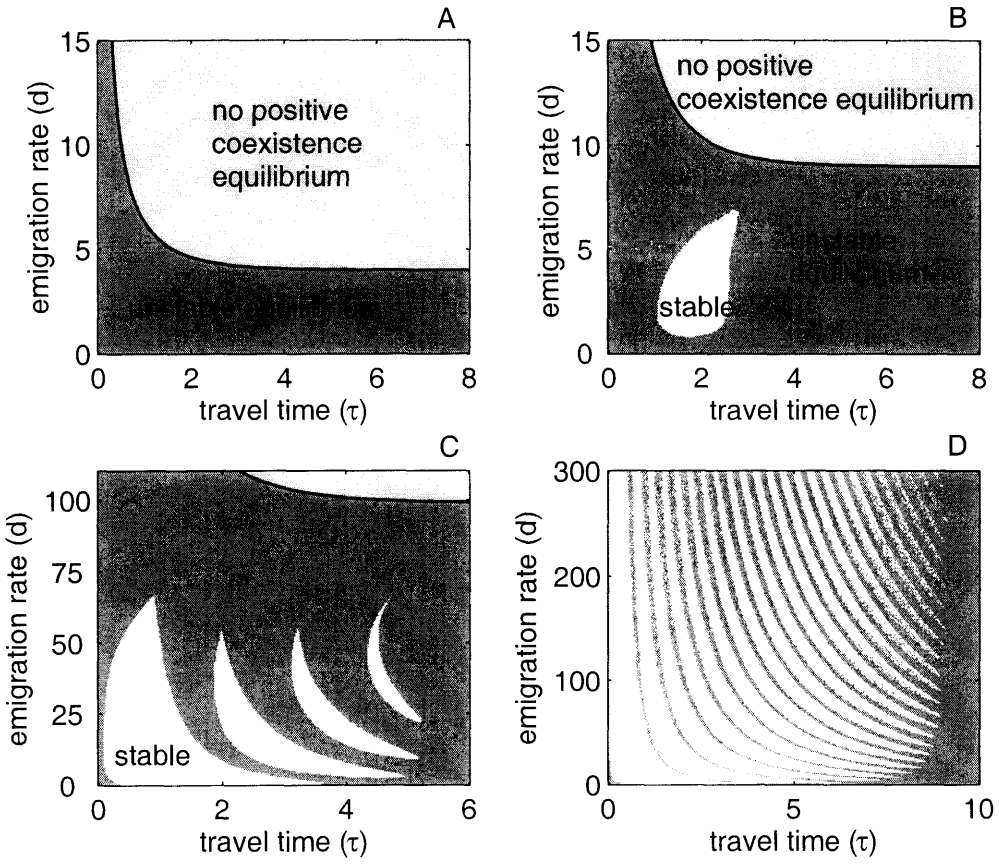

Figure 6-3: Stability area of the Type II model (6.17) with discrete dispersal delay for various ε: A) $\varepsilon = 0.2$; B) $\varepsilon = 0.1$; C) $\varepsilon = 0.01$; and D) $\varepsilon = 0.0002$. Other parameter values are as in Fig. 1.

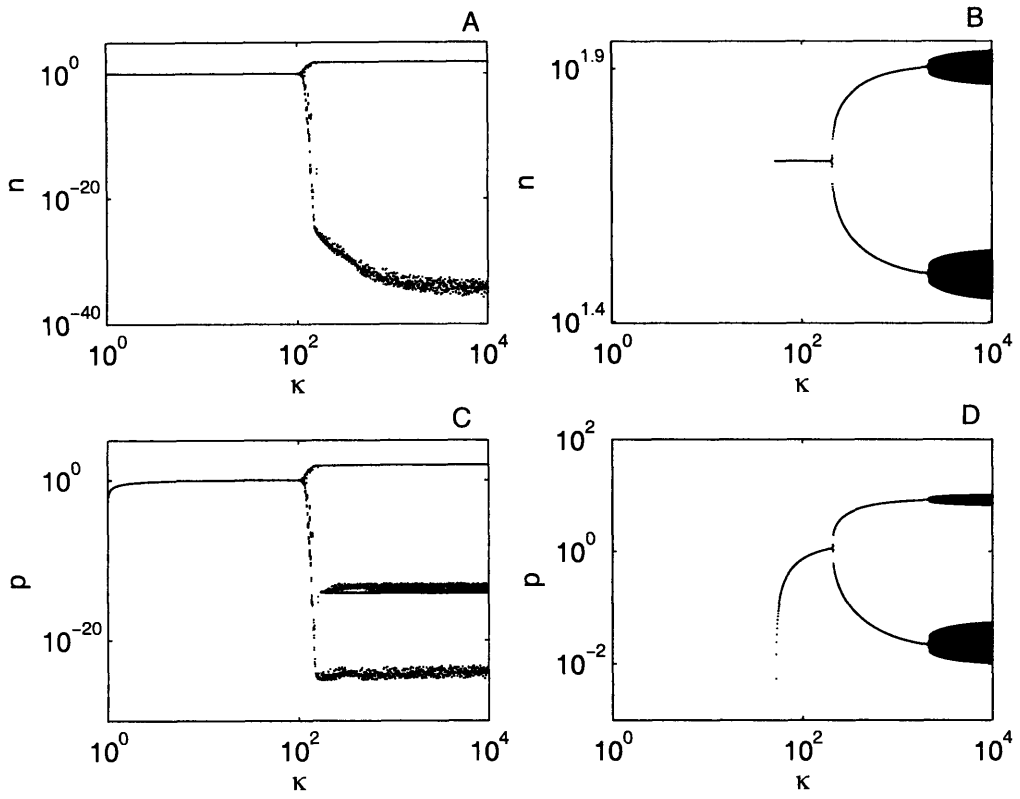

Figure 6-4: Bifurcations diagram for model (6.5) with κ as bifurcation parameter show that the amplitude of oscillation is significantly smaller in the presence of dispersal delays; $d = 35$, $\varepsilon = 0.01$, $\mu = \mu_p = 1$. A) prey population, no dispersal ($\tau = 0$); B) prey population, $\tau = 3$; C) predator population, no dispersal ($\tau = 0$); D) predator population, $\tau = 3$.

the paradox of enrichment. In the MacArthur-Rosenzweig model without dispersal, the amplitude of oscillation increases with increasing carrying capacity and the population soon reaches vanishingly small densities. We illustrate this with a bifurcation diagram with κ as a bifurcation parameter (Fig. 6-4A, C). We again present only the long-term dynamics by plotting local minima and maxima of the trajectory. The minimal population density decreases rapidly with increasing κ and eventually becomes dominated by numerical round-off errors, so the graphs in Fig. 6-4A and C appear blurred. For comparison, in Fig. 6-4 B and D we show how the amplitude of the oscillation changes with increasing capacity in the presence of discrete dispersal delays. In this case, large values of κ give rise to quasi-periodic and aperiodic behavior, but minimal population densities remain well above zero for both prey (Fig. 6-4B) and predator (Fig. 6-4D).

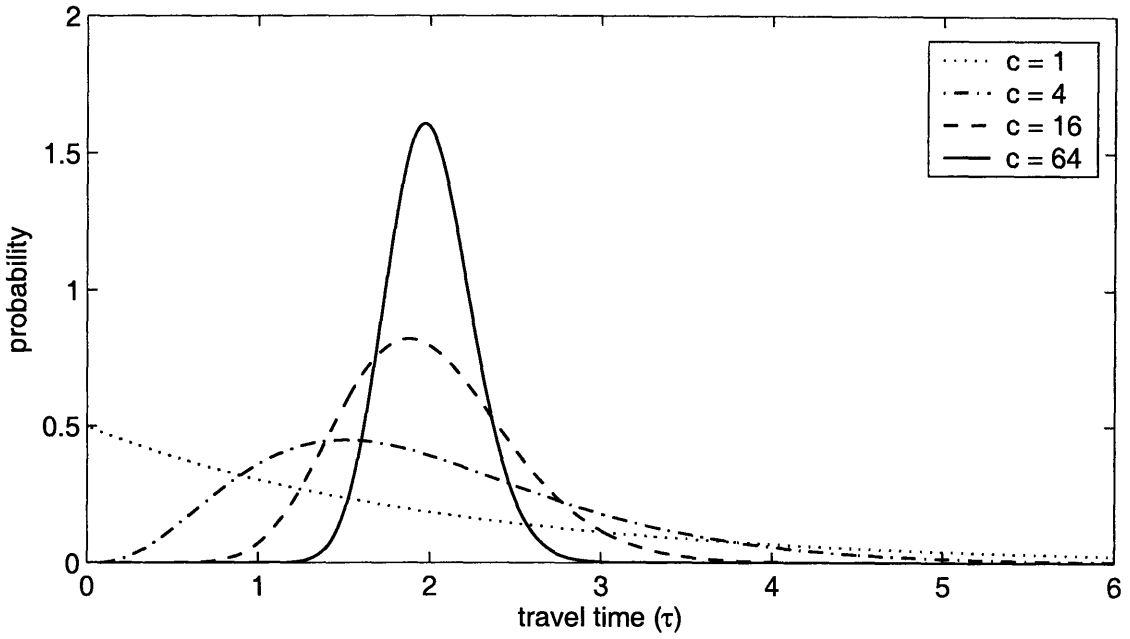

Figure 6-5: Shape of the Erlang distribution for increasing values of c. The mean of each distribution is fixed at $\tau_{av} = 2$; thus $b = c/2$ for each curve. Notice that distribution of travel times is narrower for larger c.

6.3.2 Distributed travel time

When the movement abilities of the predators differ, or the vagaries of dispersal affect individuals differently, individual travel-times form some distribution. For mathematical convenience we study a case where the delay distribution is an Erlang distribution

$$g(s) = g_{b,c}(s) = \frac{b^c\, s^{c-1}\, e^{-bs}}{(c-1)!}, \tag{6.18}$$

with shape parameter c and scale parameter b (Fig. 6-5). For $c = 1$ the distribution is exponential, and the dispersal model is equivalent to one that includes an explicit pool of dispersers with constant per capita emigration and immigration rates, à la Weisser & Hassell (1996) and Weisser *et al.* (1997). For $c > 1$ the mode of the distribution, at $(c-1)/b$, is positive. For large c, the mode approaches the mean, $\tau_{av} = c/b$, and the distribution resembles a delta function.

For this special family of distributions, we can determine the local stability of the equilibrium point (6.6) by linearizing system (6.5) and using the Laplace transform

$$\tilde{g}(x) = \tilde{g}_{b,c}(x) = \frac{b^c}{(x+b)^c}. \tag{6.19}$$

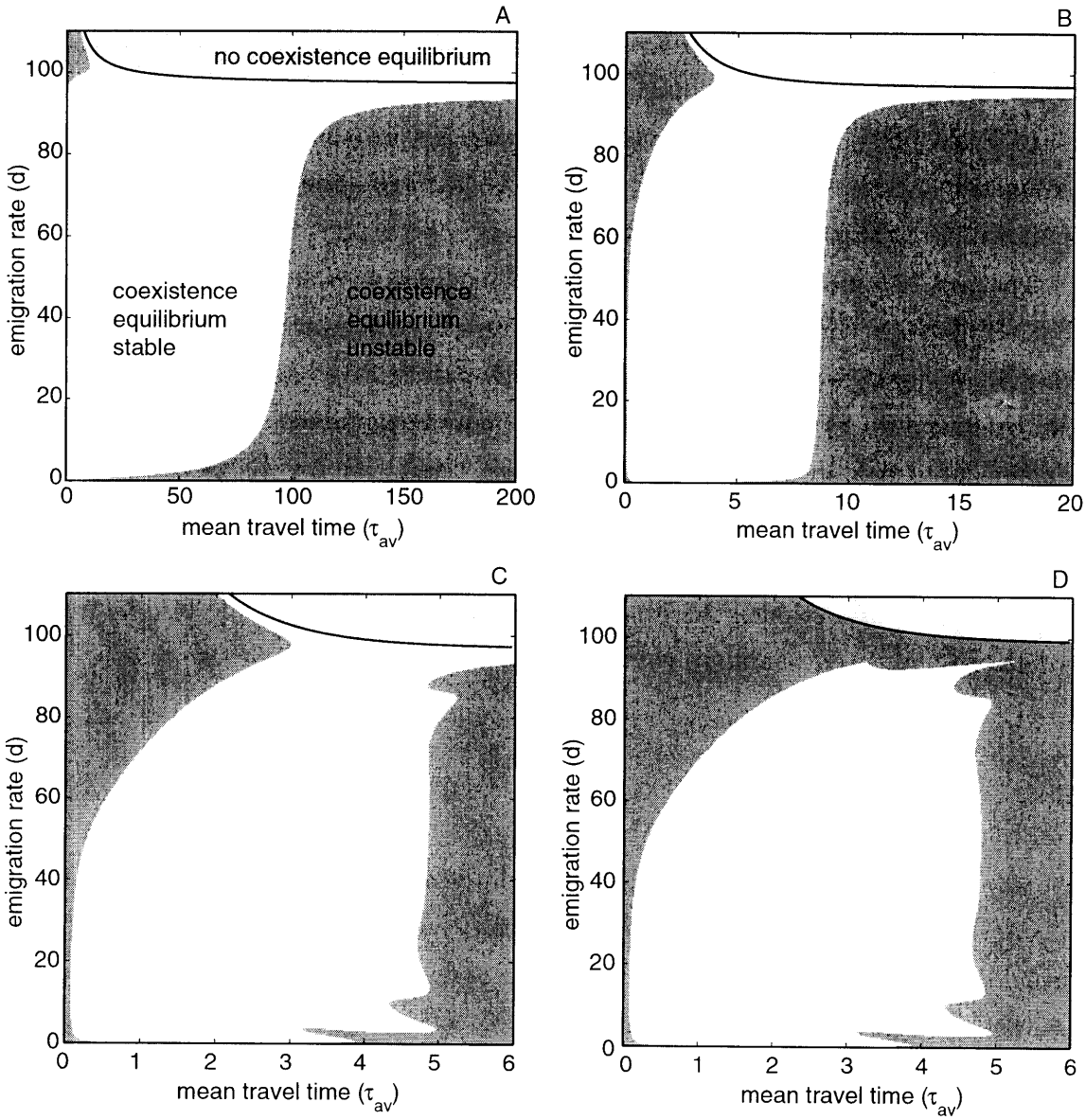

Figure 6-6: A-C) Stability diagrams for model (6.5) with Erlang distributed dispersal-delays computed from (6.20); $\varepsilon = 0.01$, $\mu = \mu_p = 1$,$\kappa = 1000$. A) $c = 1$. B) $c = 4$. C) $c = 64$. D) Stability diagram for the Type II model (6.17) with Erlang distributed delay; $c = 64$. Note the changing scale of the τ_{av}-axis.

The characteristic equation (6.14) then reduces to a polynomial of degree $c+2$:

$$[(\lambda+\mu+d)(\lambda p^*-\varepsilon n^*)+n^*(1-\lambda)]\left(\frac{b+\mu_p+\lambda}{b}\right)^c = d(\lambda p^*-\varepsilon n^*). \qquad (6.20)$$

To construct the stability diagrams in Fig. 6-6, we found the roots of equation (6.20) numerically using the Matlab function `roots()`.

In Figs. 6-6A-C we show stability diagrams for increasing values of the shape parameter c, with the other parameters fixed at levels that produce an unstable equilibrium in the absence of dispersal delays.

The area in the parameter space where the equilibrium point is stable is largest for $c=1$ (Fig. 6-6A), implying that the stabilizing effect of dispersal delays is strongest when individual travel times are exponentially distributed. As c increases, the stability region shrinks and its borders become more convoluted. The area of stability remains large even in the limit as $\kappa \to \infty$ (Fig. 6-6D). We expect that as c becomes even larger the stability diagram would look even more like the discrete-delay case. Unfortunately, for c much larger than 64, the characteristic polynomial (6.20) is extremely poorly conditioned, with coefficients differing in magnitude by hundreds of orders; we have been unable to construct a stability diagram for these cases.

6.4 Discussion

We have shown that the coexistence equilibrium point of the single-patch Rosenzweig-MacArthur model (6.2) can be stabilized when predator dispersal includes a dispersal delay. Stabilization occurs because the dispersal delays introduce density dependence into the dispersal process (Murdoch *et al.*, 1992; Neubert *et al.*, 2002). If the predator population on the patch is abundant compared to earlier times, emigration from the patch will exceed immigration, and the abundance on the patch decreases. If, on the other hand, the current population on the patch is small, immigration will exceed emigration, thereby increasing the population size. In this way, population oscillations are reduced and species abundances eventually reach their equilibrium levels.

The stabilizing effect of a dispersal delay is strongest when the individual travel times are exponentially distributed, as they are in models that include a pool of dispersers. The stabilizing effect weakens as the delay distribution becomes more concentrated around its mode. In the weakest case, when the delay distribution

is a delta function and the carrying capacity is infinite, the stability region takes the shape of an archipelago (Fig. 6-3B-D). The same structure, dubbed "islands of amplitude death," has been observed in mathematical studies of coupled oscillators (Reddy *et al.*, 1998, 1999). These studies find that the amplitude of two coupled limit-cycle oscillators can be "quenched" when the coupling is time delayed.

Dispersal delays are less effective at stabilizing the equilibrium as the carrying capacity of the prey increases. Nevertheless, for a significant set of parameter values, the model with dispersal delays has a stable coexistence equilibrium even for an infinite carrying capacity (see Fig. 6-3 and Fig. 6-6D). Thus dispersal delays alone are capable of inducing stability in the face of a destabilizing Type II functional response.

Even when the equilibrium is unstable, the amplitude of the predator-prey oscillation does not grow with increasing carrying capacity, and the minimum population densities remain well above zero (Fig. 6-4B, and D). In this sense, our results can be added to those of Jansen (1995) (see also de Roos *et al.*, 1991; Scheffer & de Boer, 1995; Nisbet *et al.*, 1998; Jansen & de Roos, 2000; Jansen, 2001) who also proposed dispersal (without delay) as a potential resolution of the paradox of enrichment. The stabilizing effect of dispersal in these studies is weaker than it is in our model, however, as it only produces a decrease in the amplitude of the limit cycle, rather than stabilizing the equilibrium point.

Spatial structure is by no means the only factor that has been proposed to resolve the paradox (Abrams & Walters, 1996). Other factors include heterogeneity within the prey population and complex food web structure. Enrichment of the prey can reduce the amplitude of population cycles when prey have different profitability (Genkai-Kato & Yamamura, 1999) or when a single predator attacks two prey species, one of which is inedible (Kretzschmar *et al.*, 1993). Enrichment can even lead to stability in systems that have a prey refuge (Abrams & Walters, 1996; Gurney & Veitch, 2000) or inducible defences in prey (Vos *et al.*, 2004). Enhanced system persistence and stability in intricate food webs has been attributed to weak trophic interactions that dampen oscillations between consumers and resources and maintain population densities further away from zero (McCann *et al.*, 1998).

Our analysis has several limitations. We focussed on a single habitat patch from which only predators dispersed. Using methods outlined Neubert *et al.* (2002), one can show that if dispersal delays stabilize the single patch model they also stabilize a

spatially homogeneous equilibrium of a model with an arbitrary number of identical patches. Many real metapopulations, however, are composed of numerous patches that differ in several attributes. In particular, the distance between two patches, and therefore the distribution of dispersal delays between them, will not be the same for all pairs of patches. Furthermore, both prey and predators may disperse. Our analysis does not apply to these more complicated scenarios.

Finally, we note that our results may depend upon the exact way in which we modeled the dispersal process. Another approach uses so called "patch occupancy models," which keep track of the number of habitat patches that are in various states, e. g., empty, or occupied by prey, or occupied by predators. In contrast to our results, Sabelis *et al.* (1991) showed that while the addition of a pool of dispersing prey was stabilizing in a simple patch occupancy model, dispersing predators could be destabilizing. When it comes to the effects of dispersal on predator-prey dynamics, the details of how dispersal is incorporated appear to be important.

References

Abrams, P. A., & Walters, C. J. 1996. Invulnerable prey and the paradox of enrichment. *Ecology*, **77**, 1125–1133.

Azer, N., & van den Driessche, P. 2006. Competition and dispersal in patchy environments. *Mathematical Biosciences and Engineering*, **3**(2), 283–296.

Briggs, C. J., & Hoopes, M. F. 2004. Stabilizing effects in spatial parasitoid–host and predator–prey models: a review. *Theor. Pop. Biol.*, **65**, 299–315.

Crawley, M. J. 1992. *Natural Enemies: The Population Biology of Predators, Parasites and Diseases.* London: Blackwell Scientific.

de Roos, A. M., McCauley, E., & Wilson, W. G. 1991. Mobility versus density-limited predator–prey dynamics on different spatial scales. *Proc. R. Soc. Lond. B*, **246**, 117–122.

Feng, W., & Hinson, J. 2005. Stability and pattern for two-patch predator–prey population dynamics. *Discrete and Continuous Dynamical Systems*, **Supplement Volume 2005**, 268–279.

Genkai-Kato, M., & Yamamura, N. 1999. Unpalatable prey resolves the paradox of enrichment. *Proc. R. Soc. Lond. B*, **266**, 1215–1219.

Gilpin, M. E. 1972. Enriched predator–prey systems: Theoretical stability. *Science*, **177**, 902–904.

Gurney, W. S. C., & Veitch, A. R. 2000. Self-organization, scale and stability in a spatial predator–prey interaction. *Bull. Math. Biol.*, **62**, 61–86.

Hassell, M. P. 1978. *The Dynamics of Arthropod Predator–Prey Systems.* Princeton, NJ: Princeton University Press.

Holt, R. D. 1984. Spatial heterogeneity, indirect interactions, and the coexistence of prey species. *Am. Nat.*, **124**, 377–406.

Jansen, V. A. A. 1995. Regulation of predator–prey systems through spatial interactions: a possible solution to the paradox of enrichment. *Oikos*, **74**, 384–390.

Jansen, V. A. A. 2001. The dynamics of two diffusively coupled predator–prey populations. *Theor. Pop. Biol.*, **59**, 119–131.

Jansen, V. A. A., & de Roos, A. M. 2000. *The Geometry of Ecological Interactions: Simplifying Spatial Complexity.* Cambridge, U.K.: Cambridge University Press. Chap. The role of space in reducing predator–prey cycles, pages 183–201.

Kot, M. 2001. *Elements of Mathematical Ecology.* Cambridge, UK: Cambridge University Press.

Kretzschmar, M., Nisbet, R. M., & McCauley, E. 1993. A predator–prey model for zooplankton grazing on competing algal populations. *Theor. Pop. Biol.*, **44**, 32–66.

Kuang, Y. 1993. *Delay Differential Equations with Applications in Population Dynamics.* Academic Press, Boston.

MacDonald, N. 1989. *Biological Delay Systems: Linear Stability Theory.* Princeton, NJ: Cambridge University Press.

May, R. M. 1972. Limit cycles in predator–prey communities. *Science*, **177**, 900–902.

May, R. M. 1973. *Stability and Complexity in Model Ecosystems.* Princeton, NJ: Princeton University Press.

McCann, K., Hastings, A., & Huxel, G. R. 1998. Weak trophic interactions and the balance of nature. *Nature*, **395**, 794–798.

Mueller, L. D., & Joshi, A. 2000. *Stability in Model Populations.* Princeton, NJ: Princeton University Press.

Murdoch, W. W., Briggs, C. J., Nisbet, R. M., Gurney, W. S. C., & Stewart-Oaten, A. 1992. Aggregation and stability in metapopulation models. *Am. Nat.*, **140**, 41–58.

Neubert, M. G., Klepac, P., & van den Driessche, P. 2002. Stabilizing dispersal delays in predator–prey metapopulation models. *Theor. Pop. Biol.*, **61**, 339–347.

Nisbet, R. M., de Roos, A. M., Wilson, W. G., & Snyder, R. 1998. Discrete consumers, small scale resource heterogeneity, and population stability. *Ecology Letters*, **1**, 34–37.

Reddy, D. V. R., Sen, A., & Johnson, G. L. 1998. Time delay induced death in coupled limit cycle oscillators. *Phys. Rev. Lett.*, **80**, 5109–5112.

Reddy, D. V. R., Sen, A., & Johnson, G. L. 1999. Time delay effects in coupled limit cycle oscillators at Hopf bifurcation. *Physica D*, **129**, 15–34.

Rosenzweig, M. L. 1971. Paradox of enrichment: destabilization of exploitation ecosystems in ecological time. *Science*, **171**, 285–387.

Rosenzweig, M. L., & MacArthur, R. H. 1963. Graphical representation and stability conditions of predator–prey interactions. *Am. Nat.*, **97**, 209–223.

Sabelis, M. W., Diekmann, O., & Jansen, V. A. A. 1991. Metapopulation persistence despite local extinction: predator-prey patch models of the Lotka–Volterra type. *Biol. J. Linn. Soc.*, **42**, 267–283.

Scheffer, M., & de Boer, R. J. 1995. Implications of spatial heterogeneity for the paradox of enrichment. *Ecology*, **76**, 2270–2277.

Taylor, A. D. 1990. Metapopulations, dispersal, and predator–prey dynamics: an overview. *Ecology*, **71**, 429–433.

Vos, M., Kooi, B. W., DeAngelis, D. L., & Mooij, W. M. 2004. Inducible defences and the paradox of enrichment. *Oikos*, **105**, 471–480.

Weisser, W. W., & Hassell, M. P. 1996. Animals 'on the move' stabilize host–parasitoid systems. *Proc. R. Soc. Lond. B*, **263**, 749–754.

Weisser, W. W., Jansen, V. A. A., & Hassell, M. P. 1997. The effects of a pool of dispersers on host–parasitoid systems. *J. Theor. Biol.*, **189**, 413–425.

Chapter 7

Future directions: Matrix population models for epidemics and demography

7.1 Introduction

Infectious diseases often affect host individuals of different (st)ages in a different way. For example, children aged 6–59 months, pregnant women, and persons aged 50 years or more are at much higher risk for influenza-related complications and severe disease than persons between ages 5 and 50. Different stages can have different susceptibility to a disease also in the case of wildlife infections. In case of the phocine distemper virus, different groups have different behavior, influencing their probability of getting infected.

The demographic time-scale is usually very different from the epidemic time-scale, so most models focus either on demographic or epidemic questions. But, in order to know how recurring epidemics, or epidemics that have long infectious period, such as HIV/AIDS, affect the population, the model should incorporate both realistic demographic and epidemic detail. One way to incorporate age structure into epidemic models has been by using integro-differential equations (*e. g.*, Diekmann & Heesterbeek, 2000; Hethcote, 2000; Dietz & Heesterbeek, 2002; Thieme, 2003). Another way is to use matrix models. Apart the applications in the analysis of age-prevalence data (Saporu, 1990, 1996), and description of the contact and transmission processes (*e. g.*, Pugliese, 1991; Keeling & Grenfell, 1997), the matrix approach hasn't commonly been

used in epidemiology.

I want to construct a matrix model that accounts for both epidemic and demographic detail, and look at its dynamics.

7.2 Epidemic model with demography

To allow for demographic detail in each of the epidemic compartment I will follow the approach formulated by Hunter & Caswell (2005) to model spatial matrix population models. The authors constructed matrix models from a manageable block-diagonal formulation of the dispersal and demographic processes, using a special permutation matrix called a vec-permutation matrix.

Even though the spatial spread of infectious diseases is an important area of research today, here I am not interested in spatial aspect of an epidemic. Instead, I want to apply the vec-permutation approach to study epidemic processes in a demographic setting.

Let the host population be divided into s stages and c epidemic categories. The total number of population compartments is then $s \times c$. The state of the epidemic in the population at time t can then be described by the matrix

$$\mathbf{N}(t) = \begin{pmatrix} n_{11} & n_{12} & \cdots & n_{1c} \\ n_{21} & n_{22} & \cdots & n_{2c} \\ \vdots & \vdots & \ddots & \vdots \\ n_{s1} & n_{s2} & \cdots & n_{sc} \end{pmatrix}(t), \tag{7.1}$$

where $n_{ij}(t)$ is the number of individuals in stage i and in epidemic category j at time t. Row i $(n_{i\cdot})$, for example, has individuals of the same stage but in different epidemic categories, where column j $(n_{\cdot j})$ gives individuals in the same epidemic category, but in different stages. Forming a population vector by stacking the rows of this matrix, will give us all the individuals in stage 1, followed by all the individuals in stage 2, etc.

$$\mathbf{n}_{\text{stages}} = \begin{pmatrix} n_{1\cdot}^{\top} \\ \hline \vdots \\ \hline n_{s\cdot}^{\top} \end{pmatrix}. \tag{7.2}$$

Accordingly, we can stack the population vector according to the epidemic categories,

$$\mathbf{n}_{\text{epidemic}} = \left(\begin{array}{c} n_{\cdot 1} \\ \hline \vdots \\ \hline n_{\cdot c} \end{array}\right). \tag{7.3}$$

The population vector n can be easily organized into epidemic or demographic stages by the use of the vec operator, $\text{vec}(\cdot)$, that stacks the columns of a matrix on top of each other,

$$\mathbf{n}_{\text{stages}} = \text{vec}(N^{\top}), \tag{7.4}$$

$$\mathbf{n}_{\text{epidemic}} = \text{vec}(N). \tag{7.5}$$

The vectors (7.4) and (7.5) are related by a special matrix called the *vec-permutation matrix* $\mathbf{P}$ so that

$$\text{vec}(N^{\top}) = \mathbf{P}\,\text{vec}(N). \tag{7.6}$$

Since $\mathbf{P}$ is a permutation matrix, it holds that

$$\mathbf{P}^{\top} = \mathbf{P}^{-1}. \tag{7.7}$$

Imagine a case where a population reproduces at the beginning of the projection interval. As we want to keep track of both the demographic stages and epidemic categories of the individuals, upon birth newly born individuals are assigned to their epidemic compartments. An infection occurs at the end of the projection interval, and let the matrix $\mathbb{A}[\mathbf{n}(t)]$ describe the epidemic transitions that occur during this outbreak. Let the matrix $\mathbb{R}$ describe reproductive events, and the matrix $\mathbb{M}$ move the newborn individuals to appropriate epidemic categories. Using the vec-permutation configuration and a population vector organized into epidemic categories, we can describe the transitions that occur in one projection interval by

$$\left(\begin{array}{c} n_{\cdot 1} \\ \hline \vdots \\ \hline n_{\cdot c} \end{array}\right)(t+1) = \mathbf{P}^{\top}\mathbb{A}[\mathbf{n}(t)]\,\mathbb{M}\,\mathbf{P}\,\mathbb{R}\left(\begin{array}{c} n_{\cdot 1} \\ \hline \vdots \\ \hline n_{\cdot c} \end{array}\right)(t). \tag{7.8}$$

Alternatively, an outbreak of infection may occur at the beginning of the projection interval, followed by the reproduction, and 'movement'. In this case, it is more

convenient to organize the population according to its demographic compartments,

$$\begin{pmatrix} \frac{n_{1\cdot}^{\top}}{\vdots} \\ \hline n_{s\cdot}^{\top} \end{pmatrix}(t+1) = \mathbb{M}\,\mathbf{P}\,\mathbb{R}\,\mathbf{P}^{\top}\,\mathbb{A}[\mathbf{n}(t)] \begin{pmatrix} \frac{n_{1\cdot}^{\top}}{\vdots} \\ \hline n_{s\cdot}^{\top} \end{pmatrix}(t). \tag{7.9}$$

7.2.1 A (not so) simple example

To see how to formulate epidemic and demographic transition matrices, consider a population that consists of only juveniles and adults – 2 demographic stages, $s = 2$. Further assume that the disease that invades this population follows the standard SIR-type dynamics, so at any given time an individual can be either susceptible (S), infectious (I), or recovered (R) – 3 epidemic categories, $c = 3$. In this example, the total number of compartments in the population is $s \times c = 6$. The population matrix can be described as

$$N = \begin{array}{c} \begin{array}{ccc} S & I & R \end{array} \\ \begin{pmatrix} n_{11} & n_{12} & n_{13} \\ n_{21} & n_{22} & n_{23} \end{pmatrix} \end{array} \begin{array}{l} \\ \text{juveniles} \\ \text{adults} \end{array} \tag{7.10}$$

Epidemic part

Let the transmission rate β vary between groups, so that β_{ij} is the transmission rate between a susceptible individual in demographic stage i and an infectious individual in demographic stage j. The probability that a susceptible in stage 1 has no infectious contacts with infectives in stage 1 during the time interval $(t, t+1)$ is $\exp\left(-\beta_{11} n_{12}(t)\right)$. Accordingly, the probability that a susceptible in stage 1 has no contacts with infectives in stage 2 is $\exp\left(-\beta_{12} n_{22}(t)\right)$. The total force of infection $\Lambda_1[\mathbf{n}(t)]$ for stage 1 (juveniles) at time t is then

$$\Lambda_1[\mathbf{n}(t)] = 1 - \exp\left(-\sum_j \beta_{1j}\, n_{j2}(t)\right). \tag{7.11}$$

After getting infected, a individual in stage i remains infectious for an average duration of $1/\gamma_i$, after which it recovers with the probability r_i. We can summarize the

epidemic transition with the matrix $\mathbb{A}[\mathbf{n}(t)]$

$$\mathbb{A}[\mathbf{n}(t)] = \left(\begin{array}{ccc|ccc} 1-\Lambda_1[\mathbf{n}(t)] & 0 & 0 & & & \\ \Lambda_1[\mathbf{n}(t)] & 1-\gamma_1 & 0 & & 0 & \\ 0 & r_1\gamma_1 & 1 & & & \\ \hline & & & 1-\Lambda_1[\mathbf{n}(t)] & 0 & 0 \\ & 0 & & \Lambda_2[\mathbf{n}(t)] & 1-\gamma_2 & 0 \\ & & & 0 & r_2\gamma_2 & 1 \end{array}\right) \tag{7.12}$$

and we can project the epidemic via

$$\mathbf{n}(t+1) = \mathbb{A}[\mathbf{n}(t)]\,\mathbf{n}(t). \tag{7.13}$$

When we don't account for the demographic detail, an outbreak of disease quickly grows into an epidemic, and finally disappears from the population (see Figure 7-4). Without the reproduction, there is no influx of susceptibles, so hosts are quickly exhausted and the disease disappears from the population without the possibility of reaching an endemic equilibrium.

Demographic part

The population at any time-step consists of juveniles ($\mathbf{n}_{1\cdot}$) and adults ($\mathbf{n}_{2\cdot}$) that can either be susceptible ($\mathbf{n}_{\cdot 1}$), infectious ($\mathbf{n}_{\cdot 2}$), or recovered ($\mathbf{n}_{\cdot 3}$). Individuals in the stage i and epidemic category j suffer mortality m_{ij} from natural, non-disease related causes. Juveniles in the epidemic category i survive and grow to adults (in the same epidemic category) with the probability g_i. Adults in the epidemic category i have the per-capita fertility f_i, and they produce newborns that are temporarily in three new demographic stages, $\mathbf{n}_{3\cdot}$ (see Figure 7-2 for an illustration). The temporary stage n_{31} consists of newborns produced by susceptibles, n_{32} are newborns produced by infecteds, and recovered individuals give birth to n_{33}.

If we summarize the transitions of epidemic category i with the matrix $\mathbf{R}_i$,

$$\mathbf{R}_i = \begin{pmatrix} (1-g_i)(1-m_{1i}) & 0 \\ g_i(1-m_{1i}) & 1-m_{2i} \\ 0 & f_i \end{pmatrix} \tag{7.14}$$

The reproduction, survival, and growth can be written using the block-diagonal form

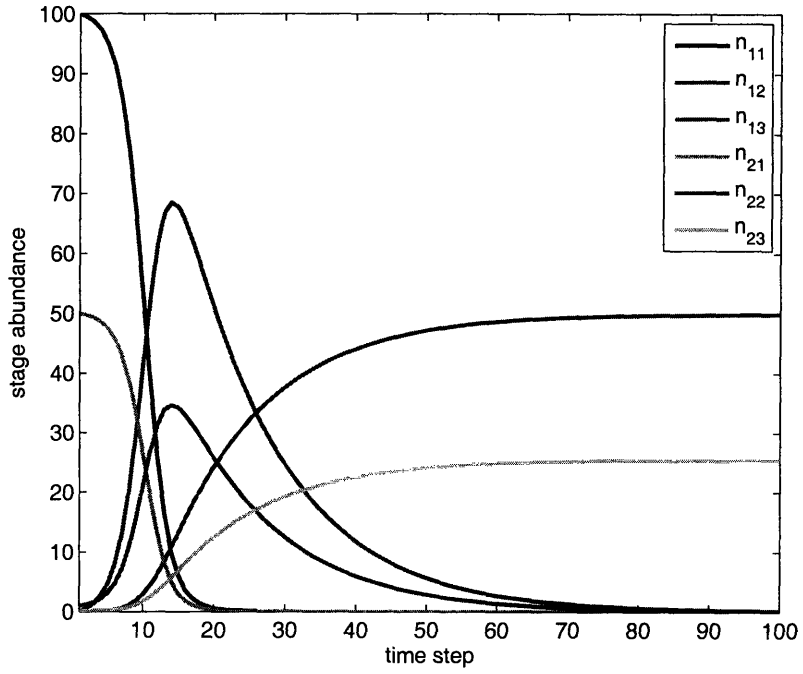

Figure 7-1: Dynamic of the epidemic in a structured population without demography. Parameter values: $\beta_{ij} = 0.005$, $\gamma_1 = \gamma_2 = 1/14$, $r_1 = r_2 = 0.5$, initial conditions: $\mathbf{n}_{\text{stages}} = \begin{pmatrix} 100 & 0 & 0 & 50 & 1 & 0 \end{pmatrix}^\top$.

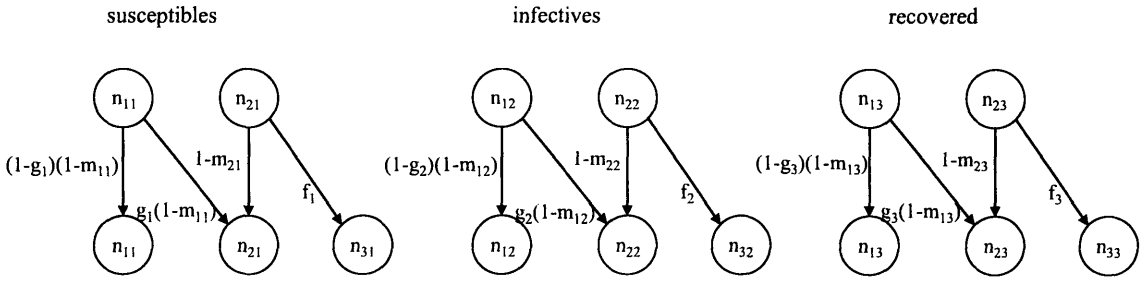

Figure 7-2: Reproduction matrix $\mathbb{R}$ accounts for the reproduction, survival and growth. New individuals temporarily show up in extra states ($\mathbf{n}_{3\cdot}$) before they are assigned to their epidemic categories.

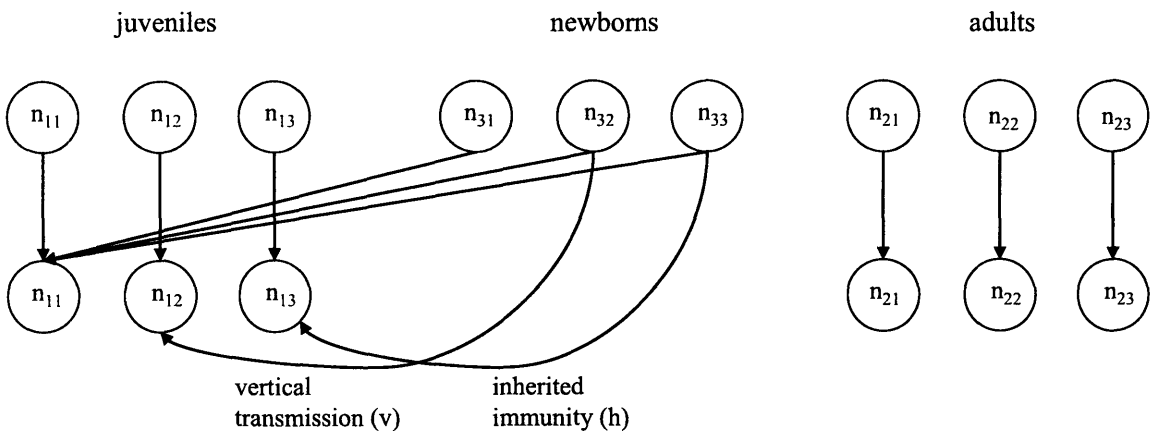

Figure 7-3: After reproduction, newborn individuals are assigned to their epidemic categories by the matrix $\mathbb{M}$. If there is no vertical transmission or inherited immunity ($v = 0$, $h = 0$) then all newborn individuals will be susceptible.

as

$$\begin{pmatrix} n_{11} \\ n_{21} \\ n_{31} \\ \hline n_{12} \\ n_{22} \\ n_{32} \\ \hline n_{13} \\ n_{23} \\ n_{33} \end{pmatrix} = \underbrace{\left(\begin{array}{c|c|c} \mathbf{R}_1 & 0 & 0 \\ \hline 0 & \mathbf{R}_2 & 0 \\ \hline 0 & 0 & \mathbf{R}_3 \end{array}\right)}_{\mathbb{R}} \begin{pmatrix} n_{11} \\ n_{21} \\ \hline n_{12} \\ n_{22} \\ \hline n_{13} \\ n_{23} \end{pmatrix}, \tag{7.15}$$

where $\mathbb{R}$ is a 9×6 matrix that consists of 3×2 blocks $\mathbf{R}_i$ on the diagonal and zeros elsewhere.

Newly born individuals do not have to be in the same epidemic category category as their parents. If there is no vertical transmission of a disease, new individuals born to infectious parents will be susceptible. In case that newborns don't have maternal antibodies (*i. e.*, inherited immunity) against an infection, even though they are born to immune (recovered) parents, they will be susceptible. Figure 7-3 summarizes those possibilities.

Assignment of newborn individuals to epidemic categories can be summarized by the 'movement' matrix $\mathbb{M}$ and the following equation.

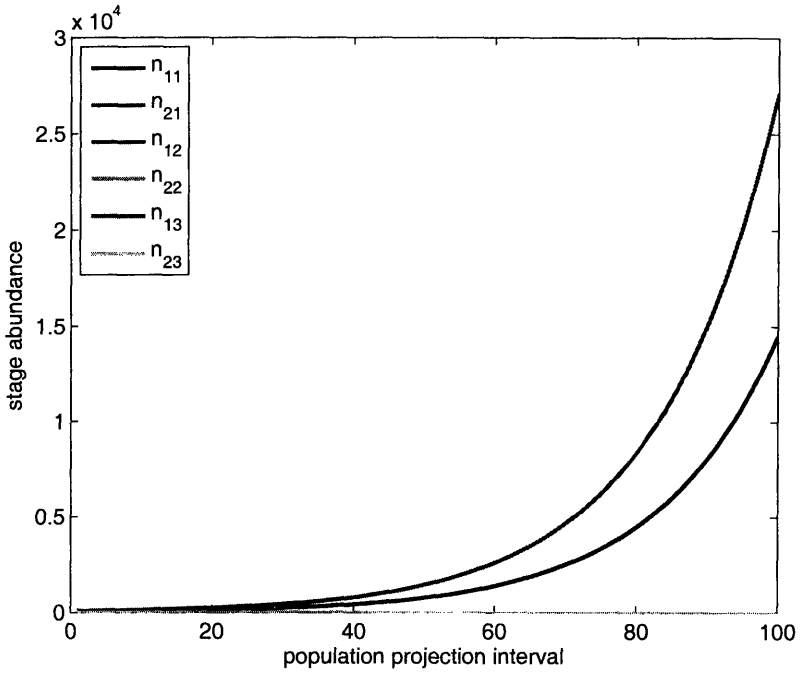

Figure 7-4: Without the epidemic, the structured population grows exponentially. Parameter values: $g_i = 0.3$, $m_{1\cdot} = 0.2$, $m_{2\cdot} = 0.1$, $f_i = 0.3$, initial conditions: $\mathbf{n}_{\text{epidemic}} = \begin{pmatrix} 100 & 50 & 0 & 0 & 0 & 0 \end{pmatrix}^\top$.

$$\begin{pmatrix} n_{11} \\ n_{12} \\ n_{13} \\ \hline n_{21} \\ n_{22} \\ n_{23} \end{pmatrix} = \underbrace{\left(\begin{array}{cccccc|ccc} 1 & 0 & 0 & 1 & 1-v & 1-h & & & \\ 0 & 1 & 0 & 0 & v & 0 & & 0 & \\ 0 & 0 & 1 & 0 & 0 & h & & & \\ \hline & & & & & & 1 & 0 & 0 \\ & & & 0 & & & 0 & 1 & 0 \\ & & & & & & 0 & 0 & 1 \end{array}\right)}_{\mathbb{M}} \begin{pmatrix} n_{11} \\ n_{12} \\ n_{13} \\ n_{31} \\ n_{32} \\ n_{33} \\ \hline n_{21} \\ n_{22} \\ n_{23} \end{pmatrix} \tag{7.16}$$

In the absence of infections, the dynamics of the population is given by

$$\mathbf{n}(t+1) = \mathbf{P}_6^\top \mathbb{M} \mathbf{P}_9 \mathbb{R} \mathbf{n}(t) \tag{7.17}$$

where P_6 and P_9 are permutation matrices described in (7.6). Without the epidemic, the population grows exponentially, without any infectious individuals. The population growth rate is given by the dominant eigenvalue λ_1 of the square matrix

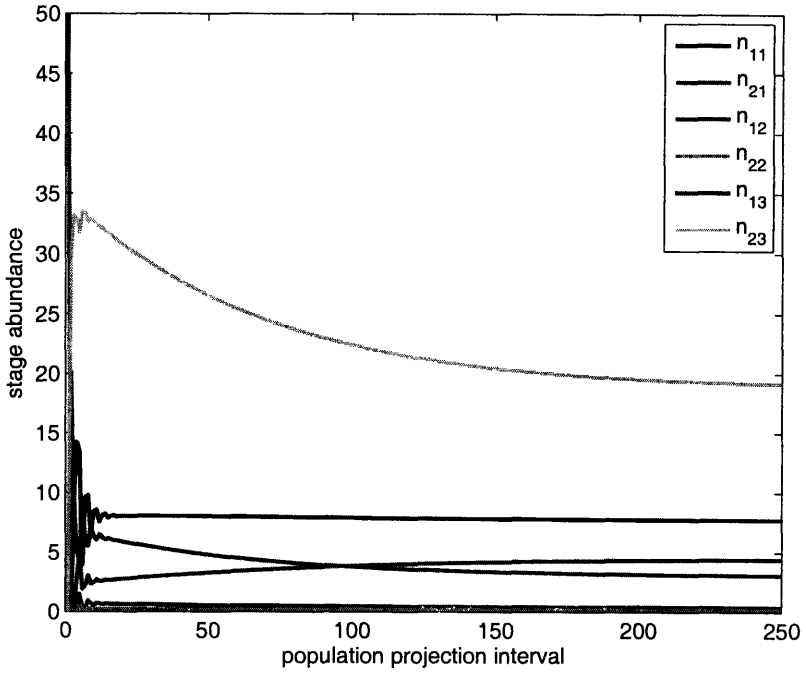

Figure 7-5: Endemic equilibrium of model (7.18) that includes both demographic and epidemic detail. Parameter values: $g_i = 0.3$, $m_{1\cdot} = 0.2$, $m_{2\cdot} = 0.1$, $f_i = 0.3$, $\beta_{ij} = 0.005$, $\gamma_1 = \gamma_2 = 1/14$, $r_1 = r_2 = 0.5$, $h = 0$, $v = 0$, initial conditions: $\mathbf{n}_{\text{epidemic}} = \begin{pmatrix} 50 & 50 & 1 & 0 & 0 & 0 \end{pmatrix}^\top$.

$\mathbb{B} = \mathbf{P}_6^\top \mathbb{M} \mathbf{P}_9 \mathbb{R}$.

Model with demography and epidemics

Combining demographic and epidemic detail can be done in several ways. For example, the reproduction can be followed by an outbreak of a disease as in (7.8), or there can be an outbreak at the beginning of the population projection interval, followed by the reproduction as in (7.9).

Consider a case where an epidemic occurs at the end of the population projection interval.

$$\mathbf{n}(t+1) = \mathbf{P}_6^\top \, \mathbb{A}[\mathbf{n}(t+k\Delta t)] \cdots \mathbb{A}[\mathbf{n}(t+\Delta t)]\mathbb{A}[\mathbf{n}(t)] \, \mathbb{M} \mathbf{P}_9 \mathbb{R} \, \mathbf{n}(t) \tag{7.18}$$

The epidemic introduces nonlinearity into the model that brings this, otherwise exponentially growing, population to an equilibrium. The demographic part, on the other hand, introduces an influx of susceptibles into the population, which allows the disease to become endemic. Combining a standard SIR dynamic with simple

demographic model allows a new type of behavior - endemic equilibrium - which was not possible in models (7.13) and (7.17).

7.3 Future analyses

Combining epidemic and demographic detail into a single model, gives rise to the dynamics not present in the building blocks of this model. In the future I want to explore the dynamics of this model in more detail and look at the endemic equilibria and the stability of this system. What epidemic and what demographic parameters can drive this system to instability? I'm interested to see under what conditions can a disease persist in this model, and what factors lead to disease extinction.

References

Diekmann, O., & Heesterbeek, J. A. P. 2000. *Mathematical epidemiology of infectious diseases: model building, analysis and interpretation.* John Wiley & son, LTD.

Dietz, Klaus, & Heesterbeek, J. A. P. 2002. Daniel Bernoulli's epidemiological model revisited. *Mathematical Biosciences*, **180**, 1–21.

Hethcote, H.W. 2000. The mathematics of infectious diseases. *SIAM Review*, **42**(4), 599–653.

Hunter, Christine M., & Caswell, Hal. 2005. The use of the vec-permutation matrix in spatial matrix population models. *Ecological Modelling*, **188**, 15–21.

Keeling, M. J., & Grenfell, B.T. 1997. Disease extinction and community size: modeling the persistence of measles. *Science*, **275**, 65–67.

Pugliese, Andrea. 1991. Contact Matrices for Multipopulation Epidemic Models: How to Build a Consistent Matrix Close to Data. *Math Med Biol*, **8**(4), 249–271.

Saporu, F. W. O. 1990. Introducing Leslie Matrix Techniques Into the Analysis of Age-Prevalence Data. *The Statistician*, **39**(1), 67–77.

Saporu, F. W. O. 1996. On the Use of the Leslie Matrix in the Analysis of Prevalence Data for General Epidemic Processes. *The Statistician*, **45**(2), 207–221.

Thieme, Horst R. 2003. *Mathematics in Population Biology.* Princeton Series in Theoretical and Computational Biology. Princeton Univeristy Press.

Appendix A

Proof that system (5.19) has no real solution

To rule out imaginary roots for the characteristic equation (5.14) we prove that system (5.19) has no real solution. To complete the proof we use a theorem by Hardy et al. (1952). To use the this theorem we first need the following definitions.

Definition 1 Max f, *the 'effective upper bound' of* f, *is defined to be the largest* ξ *which has the following property: if* $\epsilon > 0$, *there is a set* $e(\epsilon)$ *of positive measure in which* $f > \xi - \epsilon$. *If there is no such* ξ, *we write* $\text{Max} f = \infty$. *For functions continuous on a closed interval,* Max f *is the ordinary maximum.*

Definition 2 *The mean of* f *with respect to the weight function* ϕ *on a measurable set* E *is defined as*

$$\mathcal{U}(f) = \frac{\int_E \phi(s)\, f(s)\, ds}{\int_E \phi(s)\, ds} \tag{A1}$$

With these definitions, we can now state the theorem.

Theorem 1 (Hardy et al. 1952, Theorem 183) *Let the measurable function* f *be finite almost everywhere on a measurable set* E *and non-negative. Let the measurable function* ϕ *be finite and positive everywhere in* E, *and integrable over* E. *Then, if* $\mathcal{U}(f)$ *is finite and positive,*

$$\mathcal{U}(f) < \text{Max}\, f, \tag{A2}$$

unless $f = C$ *(*C *a constant) almost everywhere.*

We now prove the following lemma.

Lemma 1 *If d_p, μ, n^* and p^* are positive, μ_p is nonnegative, and the probability density function $g_p(s)$ is finite and has support on a measurable set, then system (5.19) has no real solution y.*

Proof. One solution of equation (5.19b) is $y = 0$. But $y = 0$ is not a solution of (5.19a), so $y \neq 0$. Dividing equation (5.19b) by $d_p y \tilde{g}_p(\mu_p)$ gives

$$\frac{\int_0^\infty g_p(s)\, e^{-\mu_p s}\, \cos(ys)\, ds}{\int_0^\infty g_p(s)\, e^{-\mu_p s}\, ds} = 1, \tag{A3}$$

which implies

$$\frac{\int_0^\infty g_p(s)\, e^{-\mu_p s}\, |\cos(ys)|\, ds}{\int_0^\infty g_p(s)\, e^{-\mu_p s}\, ds} \geq 1. \tag{A4}$$

But Theorem 1, with $\phi(s) = g_p(s)e^{-\mu_p s}$, $f(s) = |\cos(ys)|$, $E = \{s > 0 : g_p(s) > 0\}$ and $y \neq 0$, implies that the left hand side of equation (A4) is less than one. Thus system (5.19) does not have a solution. □

References

Hardy, G., Littlewood, J. E., and Pólya, G. 1952. *Inequalities.* Cambridge University Press, Cambridge.